2008

Mesoporous silica nanoparticles as vehicles for intracellular trafficking and controlled release

Igor Iván Slowing
Iowa State University

Mesoporous silica nanoparticles as vehicles for intracellular trafficking and controlled release

by

Igor Iván Slowing

A dissertation submitted to the graduate faculty

in partial fulfillment of the requirements for the degree of

DOCTOR OF PHILOSOPHY

Major: Organic Chemistry

Program of Study Committee:
Victor Shang-Yi Lin, Major Professor
Mark S. Gordon
Mark S. Hargrove
William S. Jenks
Nicola L. Pohl

Iowa State University

Ames, Iowa

2008

To Flor de Maria, Soledad and Anika,
the other words I use to call my life…

"A world is given to man,
it is not his glory to bear or to despise this world,
but to enrich it by creating other universes."
Mario Bunge

"Through doubting we come to questioning,
and through questioning we arrive to thruth."
Peter Abelard (ca. 1200 A.D.)

TABLE OF CONTENTS

ACKNOWLEDGMENTS

I would like to express my gratitude to a number of wonderful people that have provided me with so much support during these years.

To my advisor Professor Victor Shang-Yi Lin, for his guidance and counseling, for teaching me the balance between creativity and self-criticism that leads to results that can be both bright and solid at a time.

To the members of my POS committee, Prof. Dr. Nicola Pohl, Prof. Dr. Mark Gordon, Prof. Dr. Mark Hargrove and Prof. Dr. William Jenks, for sharing their time and knowledge to help me over the course of these years.

To the staff of the cell, hybridoma, confocal microscopy and image analysis facilities of Iowa State University for their help and guidance in a field that was new to me.

To the University of San Carlos of Guatemala, for the financial support during my stay at Iowa State University.

To the U.S. National Science Foundation and the U.S. Department of Energy, Ames Laboratory for the funding of the projects in this dissertation.

To my mother Olga Umaña for all the efforts she has put all over my life to help me reach this goal, for her unconditional love and support, which has sealed forever my life.

To my sisters Karin and Olga, my brother Otto, and my family-in-law for staying so close, reminding me that solidarity can show up only when it is based upon love.

To my wife Flor de Maria –the light within my heart and mind- and my daughters Soledad and Anika, the reasons for which each and every effort is worth, for tolerating all this time of hardships and for sharing all dreams, all laughs and all tears.

ABSTRACT

Mesoporous silica nanoparticles (MSN) are introduced as potential agents for the intracellular delivery and controlled release of drugs and biomolecules. A general review of the current state of the knowledge in the field is presented, including a description of the synthesis and control of the structural and functional properties of the material, a report of the interactions with living cells, and an enumeration of a variety of stimuli-responsive properties that have been recently developed for the material.

The ability to functionalize the external surface of MSN was exploited as a way to control the cellular uptake of the material. The results obtained demonstrate that the modification of the surface of MSN with small organic groups can not only determine the efficiency of their endocytosis by mammalian cells, but also the mechanism by which the material is taken up and the possibility to escape from endosomal entrapment.

A modification of the synthetic procedure of MSN was developed in order to obtain a material with a similar particle size but larger pores than the ones of MSN. The pore-enlarged MSN were shown to be able to deliver large cargoes into cells such as the membrane-impermeable protein cytochrome *c*.

The unique structural properties of MSN were shown to provide an additional benefit for the biological application of this material. It was demonstrated that, as opposed to amorphous silica -whose hemolytic properties are well documented-, MSN do not exhibit significant cytotoxic properties towards red blood cells at biologically relevant concentrations. This discovery along with the abovementioned abilities to control membrane

trafficking and to adjust the inner space of the material to the characteristics of the cargo molecules, allow us to propose MSN as a material with a great potential for the safe and controlled delivery of drugs and biomolecules into living cells.

CHAPTER 1. OVERVIEW

This dissertation is presented as a contribution to establish the fundamental requirements of design for using mesoporous silica nanoparticles (MSN) as devices for intracellular trafficking of biologically relevant species.

The dissertation is organized in six chapters. The first chapter describes the organization of the dissertation. Chapters 2 to 5 are journal articles, some of which have been already published and others have been submitted for publication, and chapter 6 finishes the dissertation with general conclusions and an overview of the work that is expected to follow.

Chapter 2 is a literature review describing the properties and preparation of MSN and the current state of the application of these materials to the field of intracellular drug and gene delivery. Since the biomedical applications of nanostructured silica are still in their infancy, this chapter contributes to put together the recent advances in the area in order to have a clear picture of this emerging field and to show the directions that research is expected to take in the following years. The contribution of the author to this article represents approximately a 40% of the work.

A preliminary condition for using MSN as controllable intracellular carriers is to understand the mechanism by which they are internalized by cells, and the factors that regulate the efficiency of their uptake. Chapter 3 is a study that addresses these questions. The effect of grafting a variety of functional groups on the external surface of the particles

upon the efficiency and mechanism of uptake was investigated. The author contributed with approximately 90% of the presented research.

Given the moderate pore size of MSN, their application as intracellular carriers has been limited to relatively small and simple molecules. Chapter 4 describes the modification of the synthesis conditions of MSN to yield nanoparticles with larger pores, which were then successfully applied as agents for the delivery of membrane impermeable proteins into cells. The contribution of the author corresponds to approximately 90% of the presented research.

Silica dust has been long recognized as a material highly toxic to red blood cells, causing membrane rupture in a process known as hemolysis. Such a property represents a serious drawback to the proposal of using MSN as *in vivo* drug delivery agents. In chapter 5 it is demonstrated, however, that the unique structural properties of MSN inhibit the hemolytic properties of their constitutive material, thus eliminating a serious hurdle in the road to employ MSN for biomedical purposes.

The dissertation is finished in chapter 6 with a general conclusion and an outline of the directions that this area of research is expected to take in the future.

CHAPTER 2. MESOPOROUS SILICA NANOPARTICLES AS CONTROLLED RELEASE DRUG DELIVERY AND GENE TRANSFECTION CARRIERS

A paper accepted for publication in ***Advanced Drug Delivery Reviews***

Igor I. Slowing, Juan L. Vivero-Escoto, Chia-Wen Wu, and Victor S.-Y. Lin

Abstract

In this review, we highlight the recent research developments of a series of surface-functionalized mesoporous silica nanoparticle (MSN) materials as efficient drug delivery carriers. The synthesis of this type of MSN materials is described along with the current methods for controlling the structural properties and chemical functionalization for biotechnological and biomedical applications. We summarized the advantages of using MSN for several drug delivery applications. The recent investigations of the biocompatibility of MSN in vitro are discussed. We also describe the exciting progress on using MSN to penetrate various cell membranes in animal and plant cells. The novel concept of gatekeeping is introduced and applied to the design of a variety of stimuli-responsive nanodevices. We envision that these MSN–based systems have a great potential for a variety of drug delivery applications, such as the site-specific delivery and intracellular controlled release of drugs, genes, and other therapeutic agents.

1. Introduction

Over the past few decades, research breakthroughs made in designing pharmaceutical drugs for various diseases have greatly advanced the knowledge of physicochemical properties of drug molecules as well as mechanisms of cellular uptake leading to numerous effective therapeutic strategies. However, in some cases, such as chemotherapy for cancer, the current treatment methods primarily rely on the use of conventional cytotoxic drugs that have adverse side effects and only limited effectiveness. Many studies have indicated that these problems could be attributed to the lack of target specificity of the current state-of-the-art antitumor drugs. To overcome this hurdle, a widely pursuit strategy is to design a target-specific drug delivery system (DDS) that can transport an effective dosage of drug molecules to the targeted cells and tissues.

Obviously, the success of this approach hinges upon the ability to construct a biocompatible carrier that allows high loading of drug molecules without any premature release of the cargo before reaching the destination. As outlined below, several perquisites need to be incorporated into such a material in order to serve as an efficient DDS.

1. The carrier material should be biocompatible.
2. High loading/encapsulation of desired drug molecules.
3. Zero premature release, i.e., no leaking, of drug molecules.
4. Cell type or tissue specificity and site directing ability.
5. Controlled release of drug molecules with a proper rate of release to achieve an effective local concentration.

At first glance, it seems impossible to find a material that could have high affinity for absorbing certain drug molecules, yet it would willingly release the same cargo upon reaching the designated site of cells or tissues. To circumvent this catch-22 situation, several biodegradable materials, such as polymeric nanoparticles, dendrimers, and liposomes, have been used as "smart" drug delivery systems that can controllably release pharmaceutical drugs in aqueous solution upon the structural degradation of the carrier triggered by various chemical factors, such as pH, under physiological conditions. While several exciting DDS systems have been prepared following this approach, it is difficult to achieve "zero" premature release of drugs in these structurally unstable "soft" materials[1]. In many cases, the matrix-entrapped drug molecules would start leaking out the biodegradable carrier as soon as the system was introduced in water.

This premature release problem not only limits the usage of these biodegradable DDS materials for effective cancer treatment, but also presents a major challenge for the site-selective delivery of protein- and nucleotide-based drugs via oral administration. The precious pharmaceutical cargo of enzymes, DNAs, and RNAs would decompose in the highly acidic environment of stomach if the carrier cannot offer the necessary protection. For these applications, it is critical that the drug carrier would not degrade or leak until it reaches its intended destination, securing the release of high local concentrations of the drug at the target.

Due to the rapidly increasing importance of these applications, recent research has focused on developing structurally stable drug delivery systems that are able to deliver a relatively large amount of drug molecules without any premature release problem to targeted tissues or

even intracellular organelles. Among many structurally stable materials that have been investigated for drug delivery, silica materials with defined structures and surface properties are known to be biocompatible. Silica is often the material of choice to enable the biological use of inorganic nanoparticles[2-4]. For example, silica-coated semiconductor quantum dots, such as cadmium sulfide and selenide, have been demonstrated to possess high stability, chemical versatility, and biocompatibility that are crucial for many biomedical applications[5,6]. Also, silica has been employed in the formulation of artificial implants because of the osteogenic properties of its composites[7]. For controlled release applications, it has been shown that silica is able to store and gradually release therapeutically relevant drugs like antibiotics[8,9], and others[10]. Furthermore, silica is used to enhance the biocompatibility of several drug delivery systems, such as magnetic nanoparticles[11-13], biopolymers[14], and micelles[15].

2. Mesoporous Silica Nanoparticles

2.1. Morphology Control

Mesoporous silicas, such as MCM-41 and SBA-15 silicas, are solid materials, which are comprised of a honeycomb-like porous structure with hundreds of empty channels (mesopores) that are able to absorb/encapsulate relatively large amounts of bioactive molecules. The unique properties, such as high surface area (> 900 m^2/g), large pore volume (> 0.9 cm^3/g), tunable pore size with a narrow distribution (2-10 nm), and good chemical and thermal stability, of these materials make them potentially suitable for various controlled release applications.

Since the discovery of surfactant-templated synthesis of mesoporous silica materials in 1992[16], many have explored the functionalization and utilization of these materials for various applications, such as catalysis[17], separation[18], and sensors[18]. Despite these exciting advancements, there was no report on the utilization of these materials for controlled release and delivery application until the early 2000's. One of the possible reasons is the lack of morphology control. The conventional synthetic methods for preparing mesoporous silica materials give rise to amorphous chunks and particles with different shapes and sizes. The polydispersity and the amorphous nature of the mesoporous silicas present a major challenge in understanding and controlling the mass-transport properties at the nano-level, which is of fundamental importance for drug delivery and controlled release in biological systems.

2.1.1. Particle Size

Mesoporous Silica Microspheres: Unger, Stucky, and Zhao were among the first groups that made micrometer-sized mesoporous silica spheres with a narrow size distribution[17,19,20]. Their goal was to control the particle size and monodispersity of mesoporous silica spheres for chromatographic applications[18]. Their synthesis of mesoporous silica microspheres was based on the well-established Stöber reaction for the synthesis of monodisperse non-porous silica spheres. The reaction involved the co-hydrolysis and subsequent condensation of tetraethoxysilane (TEOS) and an alkyltrialkoxysilane in a mixture of ethanol, water, and aqueous ammonia. Ethanol acted as a co-solvent to form a homogeneous solution, ammonia served as a morphological catalyst, and n-alkyltrialkoxysilane had the function of generating the porosity[17]. Other groups showed later the synthesis of mesoporous silica microspheres by

using surfactant-stabilized emulsion chemistry[21], static acidic conditions[20], and co-surfactant methods[22]. By fine-tuning the reaction conditions such as the relative amounts of reagents (alkoxysilane, water, and ammonia) and the reaction temperature, spheres with diameter of sub-micrometer to micrometer were successfully made. Furthermore, the surface area and pore size of the mesoporous silica microspheres were regulated either by choosing various kinds of n-alkyltrialkoxysilanes or surfactants at different concentrations[21].

Mesoporous Silica Nanosphere (MSN): While the mesoporous silica microspheres are potentially useful for many non-biological functions, they are not suitable for many important biotechnological and biomedical applications. For example, these materials cannot serve as efficient agents for gene transfection or carriers for intracellular drug delivery because mammalian cells cannot efficiently engulf large particles via endocytosis. Also, mesoporous silica microspheres are within the size window of bacteria and could potentially trigger acute immune response in vivo. To circumvent these problems, our group has developed a synthetic approach for preparing a series of mesoporous silica nanoparticle (MSN) materials. Our method took advantage of the well-known synthesis of MCM-41 type of mesoporous silica, where TEOS was used as a silica source, a cationic surfactant cetyltrimethylammonium bromide (CTAB) was used as a structure-directing agent, water was used as solvent, and sodium hydroxide was used as a morphological catalyst[23]. The template surfactant (CTAB) was then removed from as-synthesized material either by solvent extraction (HCl in methanol solution) or calcination to generate pores. A typical MSN has an average particle diameter around 100 nm, surface areas around 900 m^2/g, pore sizes around 2 nm, pore volumes around 0.9 cm^3/g, abundant surface silanol groups (around 30 mol%), and

a hexagonal porous channel structure (Figure 1). As will be discussed later, our group has developed several methods to control the morphology, pore size and surface functionalization of MSN.

The following unique properties of MSN have attracted a lot of research attention for various controlled release delivery applications.

1. *Tunable particle size.* The particle size of MSN can be tuned from 50 to 300 nm allowing a facile endocytosis by living animal and plant cells without any significant cytotoxicity.
2. *Stable and rigid framework.* Compared to other polymer-based drug carriers, MSN is more resistant to heat, pH, mechanical stress, and hydrolysis-induced degradations.
3. *Uniform and tunable pore size.* The pore size distribution of MSN is very narrow and the pore diameter can be tuned between 2 to 6 nm. These features allow one to adjust the loading of different drug molecules and to study the kinetics of drug release with high precision.
4. *High surface area and large pore volume.* As mentioned previously, the total surface area (> 900 m^2/g) and pore volume (> 0.9 cm^3/g) are very large, which allows high loadings of drug molecules.
5. *Two functional surfaces.* MSN have an internal surface (i.e., cylindrical pores) and an external surface (i.e. exterior particle surface). This characteristic allows the selectively functionalization of the internal and/or external surfaces of MSN with different moieties.

6. *Unique porous structure.* Many drug delivery materials have interconnecting porous structures, such as dendrimers with branching porous structure and liposomes with a large void core and a porous shell. A "perfect" capping is necessary in order to achieve the desired "zero premature release" of drug because the pore-encapsulated guest molecules can leak through the interconnecting porous matrix when some of the pores are not capped. In contrast, MSN is comprised of honeycomb-like, 2D hexagonal porous structure with cylindrical pores running from one end of the sphere to the other (Figure 1). There is no interconnectivity between individual porous channels. This unique feature renders the "no-leaking" capability even in the case of incomplete capping, meaning that the individual cylindrical pores can still serve as independent reservoirs for drug encapsulation and release, as long as both ends of a given channel are capped.

Other Mesoporous Silica Nanospheres: Ying and co-workers recently reported a fluorocarbon-surfactant-mediated synthesis for MSN[22]. The particle size of the material was tuned from 50 to 300 nm, and different types of mesostructures including 3D cubic, 2D hexagonal, foamlike, and disordered (named IBN series) were successfully produced. The Bein group recently reported on the synthesis of a colloidal mesoporous silica (CMS) material by introducing triethanolamine (TEA) to the condensation reaction of TEOS. By tuning the ratio of TEOS to TEA, they demonstrated that the particle size of CMS could be varied from 50 to 100 nm with a high surface area (> 1000 m^2/g) and a large pore volume (~1 cm^3/g). The pore geometry in CMS is unique, where the pores grow radially from the center

of the particle to the periphery[24]. Okubo and co-workers used ethylene glycol (EG) in their synthesis in order to improve structural order and to control particle size and morphology[25]. The pore size of their MSN is around 2 nm when using CTAB as the structure-directly agent. In contrast, we recently demonstrated that MSN with adjustable pore sizes ranging from 3 to 6 nm could be synthesized by including mesitylene as a pore-expander[26].

2.1.2. Particle Shape

Particle shape has been shown to have an effect on the agglomeration and circulation properties of several non-porous nanoparticles in vitro[27,28]. To investigate how the different particle shapes impact the MSN material, we have developed various methods to tune the particle morphology of these mesoporous silica materials. The first method involved the use of a series of antimicrobial room-temperature ionic liquids (RTIL's) with various alkyl chain lengths as templates for the synthesis of MSN[29]. Spheres, ellipsoids, rods, and tubes were successfully synthesized by using 1-alkyl-3-methylimidazolium with different alkyl chains. Interestingly, a rod-shaped MSN with a pseudo-moiré rotational pattern of mesopores was observed in the case of using an achiral 1-octadecyl-3-methylimidazolium as surfactant template, yet the parallel channels were twisted into a helical structure along the long axis of the MSN nanorods. This type of helical mesoporous structures were first observed by Tatsumi, Terasaki, and co-workers using chiral surfactants as templates[30]. It is notable that, in our case, an achiral RTIL template could also give rise to the helical porous structure. We also demonstrated that the antimicrobial activity of these RTIL containing MSNs could be tuned by modifying the morphology of these nanoparticles.

The second method was based a co-condensation reaction with TEOS and different organoalkoxysilanes. For example, when TEOS was co-condensed with 3-aminopropyltrimethoxy-silane (APTMS), a curved hexagonal tubular structure was produced. Interestingly, upon replacing the APTMS with other structurally similar organoalkoxysilanes, such as N-(2-aminoethyl)-3-aminopropyltrimethoxysilane (AAPTMS) and 3-[2-(2-aminoethylamino)ethylamino]propyltrimethoxy-silane (AEPTMS), the particle shapes transformed into twisted columns and micrometer-sized spheres, respectively. The effect of other co-condensing species on morphology was studied in detail, which enabled us to control the formation of MSN with different particle shapes[23].

The third method to control particle morphology was done by tuning the ratios of reactants. For example, by simply adding the double concentrations of the TEOS, CTAB and NaOH in the typical reaction mixture of regular MSN, the morphology of the nanoparticles changes from spheres to tubes while the pore structure and pore size remain the same. Another example is the change of the ratios of AEPTMS to TEOS in the synthesis. With the increase of AEPTMS/TEOS molar ratio from 1.28 to 12.8 mol%, a concurrent transformation of the particle morphology from small kidney-bean-shaped rods to spheres is observed, while elongated rods and ellipsoidal particles result at intermediate concentrations of AEPTMS[31].

2.2. Surface Functionalization

As outlined in Table 1, the surface of mesoporous silica materials can be modified by any of the following three methods: co-condensation (one-pot synthesis), grafting (post-synthesis modification), and imprint coating method[32,33]

Co-condensation of a tetraalkoxysilane and one or more organoalkoxysilanes has been widely used for producing inorganic-organic hybrid networks. The advantages of this method are: (a) it is applicable to a wide variety of organoalkoxysilanes; (b) it is suitable for a wide range of reaction conditions; (c) the coverage of functional groups is homogeneous; (d) the loading amount of functional groups is high without affecting dramatically the structural ordering of the pores. Phase separation of the precursors and the cleavage of Si-C bonds during the sol-gel reaction and during surfactant removal have to be avoided in the co-condensation reactions. We investigated the different electrostatic matching effects of various anionic organoalkoxysilanes, such as thiolate-, carboxylate- and sulfonate-containing organoalkoxysilane on the degree of organic functionalization of the MSN[34]. By co-condensation of two organoalkoxysilanes, we were able to introduce both acidic and basic functional groups into MSN[35]. This bifunctionalized MSN possess interesting chemical properties that suggest a variety of novel applications.

Grafting is commonly carried out by silylation on free (≡Si−OH) and geminal silanol (=$Si(OH)_2$) groups. If a high surface coverage with functional groups is desired, it is important to maintain a large amount of surface silanol groups after removal of the surfactant. Surfactant removal is usually carried out either by calcination or by appropriate extraction methods. Calcination promotes condensation of unreacted silanol groups, and many surface functional groups are lost at typical calcination temperatures (400-550°C). Extraction processes (*e.g.* with acid/alcohol mixtures for cationic surfactants or with alcohols for neutral surfactants) minimize loss of surface silanols. The most remarkable feature of the grafting method is the ability to selectively functionalize the external or the internal (pore) surfaces of

the MSN. For example, we have demonstrated that 1, 5, 6-epoxyhexyltriethoxysilane (EHTES) can be successfully grafted on the external surface of MSNs before the removal of surfactant CTAB. The externally grafted groups can be further reacted, for example in the case of EHTES we were able to polymerize lactic acid on the external surface of MSN [36]. Recently, Tamanoi and co-workers also modified the external surface of MSNs with trihydroxysilylpropyl methylphosphonate (THMP) after particle formation in order to reduce the aggregation and to increase the stability of the particles in aqueous solution[37] .

In the grafting processes above described, the silylation reagents were typically added under dry conditions to avoid hydrolysis and self-condensation of the reagents away from the surface of MSN. When silylating under anhydrous conditions the hydrophilic portion of the silica surface is preserved and the resulting functional groups are relatively isolated. By employing just enough water in the process to form a monolayer on the pore surface, more homogeneous coverage of organoalkoxysilanes can be obtained, leading to a higher concentration of functional groups in the final product[38].

Recently, Burleigh and co-workers reported a new imprint coating method[32]. They coated the mesoporous surface of MCM-41 with ligands that were already bound to metal ions rather than just with the free ligands. When the metal ions were removed, the ligands were already positioned for complexation with metal ions of the same type. The selectivity to binding the original metal ions in competitive binding experiments was greater than in randomly functionalized mesoporous materials.

3. Intracellular Uptake of MSN

In order for a material to be efficiently uptaken by non-phagocytic cells, the particle size of the material needs to be in the sub-micron scale[39,40]. For intracellular drug and gene delivery applications, this limitation has led to extensive research efforts on designing materials with precise control of the particle size. Furthermore, it is important for the drug carrier to have proper surface properties that can have favorable interactions with the drug molecules to achieve high loading. This would allow the release of drug with high local concentrations at the site of interest intracellularly. As mentioned previously, the particle size and surface property of MSN could be adjusted with precision for intracellular controlled release applications.

Cellular uptakes of molecules are often facilitated by the specific binding between these species and membrane-bound receptors (*e.g.* LDL or transferrin receptors). In contrast, materials for which cells do lack receptors can still be uptaken by constitutive "adsorptive" endocytosis or by fluid phase pinocytosis[39,41]. Silica particles are known to have a great affinity for the head-groups of a variety of phospholipids[42]. Therefore, the high affinity for adsorbing on cell surfaces that eventually leads to endocytosis is not surprising. We and others have demonstrated that MSN can be efficiently endocytosed *in vitro* by a variety of mammalian cells including cancer (HeLa, CHO, lung, PANC-1), non cancer (neural glia, liver, endothelial), macrophages, stem cells (3TL3, mesenchymal) and others[26,37,43-46] as depicted in Figure 2. The uptake of MSN is fast. Particles are often observed inside the cells within 30 minutes of introduction[43,47].

3.1. Biocompatibility

The biocompatibility of MSN with and without surface functionalization has been tested by different methods. Our studies on the viability and proliferation of various mammalian cells indicated that these properties were not affected by the internalization of MSN at concentrations below 100 μg/mL per 10^5 cells even after 7 cell cycles. Cell membrane integrity is conserved after uptake of MSN as determined by selective DNA staining followed by flow cytometry[43]. Microscopic analysis shows normal cell morphology upon uptake of MSN. Mitochondrial activity remains at normal levels as determined by colorimetric assay with 3-[4,5-dimethylthiazol-2-yl]-2,5-diphenyltetrazolium bromide (MTT)[45,48]. Growth rates for cells exposed to MSN are similar to the ones of cells grown in the absence of MSN[6,43]. The long-term biocompatibility and the biodegradation of MSN are not yet determined and understood, given the fact that this area of research is at its infancy. Nonetheless, a recent report[10] on the long-term biocompatibility of silica implants in animals has indicated that these materials did not present any toxic side effects for a period of 42 days. One would envision that MSN materials would have equal, if not better, biocompatibility than other silica-based materials.

3.2. Mechanism of cellular uptake

We and other groups have used several spectroscopy techniques, including flow cytometry, transmission electron microscopy, and confocal fluorescent microscopy, to determine the cellular uptake of MSN (Figure 2 and 3)[26,43-46,49]. In flow cytometry, the abundant washing of cells along with the use of extracellular fluorescence quenchers, such as

trypan blue, allow us to distinguish the endocytosed MSN particles from the cell membrane adsorbed ones. The ability of applying Z-stacking confocal microscopy to examine both fixed and live cells with MSNs eliminates any false conclusion on the endocytosis efficiency that could be derived from the artifactual, fixation-promoted uptake. The uptake of MSN has been shown to be energy-dependent by the use of metabolic inhibitors and by following the uptake at low temperatures[41,43,47].

Interestingly, even if there are no known cell surface receptors for silica, the uptake of MSN has been found to take place mainly through a clathrin-coated endocytosis pathway, and through pinocytosis, particularly for some of the surface-functionalized MSNs. We have shown that, by decorating the external surface of MSN with different functionalities, one can control the uptake efficiency of MSN as well as their ability to escape endosomal compartments. By manipulating the surface charge property (zeta potential) of MSN, we have demonstrated that ionic MSNs with high surface charges can easily escape endosomal entrapment as depicted in Figure 3. This phenomenon could be attributed to the osmotic pressure produced by the high density of ions surrounding the surface of highly charged MSN. We discovered that the uptake efficiency (EC_{50}) for MSN ranges from 1 to 50 μg/mL per million cells depending on the chemical nature of functional groups present on the surface of MSN. Also, a notable increase in the efficiency of uptake by cancer cells was observed upon grafting folic acid on the surface of MSN, competition experiments showed that the increase of uptake is associated with the participation of folic acid receptors in the surface of the cells. As described above, the functionalization of MSN has been shown to impact their route of entry into cells as determined by the effect of a variety of chemical

inhibitors on the uptake observed by flow cytometry. Clathrin pits have been identified as the main pathway of cell entry of non functionalized MSN and folic acid receptor mediated endocytosis of folic acid grafted MSN, interestingly amine and guanidinium functionalized MSN appear to enter cells by a clathrin and caveolae independent mechanism[43].

4. The Gatekeeping Concept

As mentioned previously, any drug/gene delivery system has to fulfill a list of desirable properties in order to achieve the release of the cargo in a suitable concentration at the desired target in a determined amount of time. MSN-based stimuli-responsive systems using a concept of gatekeeping were first developed in our group to achieve these goals[6]. These systems have the advantage of using a variety of chemical entities (like nanoparticles, organic molecules, or supramolecular assemblies) as "gatekeepers" to regulate the encapsulation and release of drug molecules (Figure 4). This type of DDS with "zero premature release" performance is particularly useful when the cargo to be delivered is toxic, like anti-cancer drugs. Furthermore, obtaining the ability to release drugs/genes "at will", *i.e.* precise control over the location and timing of the release of drug, would bring a major breakthrough to many site-specific delivery applications. These MSN-based stimuli-responsive controlled-release systems have real potential in achieving such an ambitious goal. As summarized in Table 2, several MSN-based nanodevices have been achieved through the development of photochemical, pH responsive, and redox active gatekeepers.

4.1. Nanoparticles as Gatekeepers

We have recently developed a redox-controlled drug delivery system that is based on MSN capped with cadmium sulfide nanoparticles (CdS)[6]. In this system, CdS was chemically attached to MSN through a disulfide linker, which is chemically labile and could be cleaved with various disulfide reducing agents, such as dithiothreitol (DTT) and mercaptoethanol (ME). As a proof of priciple, vancomycin and adenosine triphosphate (ATP) were used as guest molecules. The capping ability of CdS was tested by suspending the CdS-capped MSN in phosphate saline buffer (PBS). After 12 hours of suspending in aqueous solution, no leaching of guest molecules from the CdS-capped MSN was observed. The release properties of the CdS-MSN system were evaluated in vitro by using different concentrations of reducing agents. After addition of a disulfide reducing agent (DTT), the CdS-MSN systems released 54% of the loaded vancomycin, and only a 28% of the loaded ATP. This variation was attributed to the different electrostatic interactions between the linker-functionalized MSN, which at neutral pH is positively charged because of the 2-(propyldisulfanyl)ethylamine functionality, and the guest molecules, vancomycin (cationic at neutral pH) *versus* ATP (anionic at neutral pH). The biocompatibility and utility of the CdS-MSN release system was demonstrated by site-selective stimulation of astrocyte cells[6]. ATP is known to induce a receptor-mediated increase in the intracellular concentration of calcium in astrocytes. ATP-loaded CdS-MSN was added to an astrocyte culture in presence of Fura-2 AM, a Ca^{2+} sensitive fluorescent dye, followed by the addition of mercaptoethanol serving as a trigger for the uncapping of the CdS-MSN. After addition of the trigger, a pronounced increase in intracellular $[Ca^{2+}]_i$ was observed by fluorescence microscopy (Figure 5). In this

way, the use of CdS-MSN as a novel stimuli responsive controlled-release redox-controlled delivery system was demonstrated.

The magnetic motor effect is very attractive for the development of site-directing and site-specific drug delivery systems. To accomplish this goal, we have developed a redox-controlled drug delivery system that could be moved using a commercial magnet[46]. The system is comprised of a 3-(propyldisulfanyl)propionic acid-functionalized MSN (linker-MSN). The mesopores of this disulfide linker-MSN were capped by 3-aminopropyltriethoxysilyl-functionalized superparamagnetic iron oxide nanoparticles (Fe_3O_4). As a proof of principle, fluorescein was used as the guest molecule to be encapsulated inside the linker MSN material. As mentioned before, the disulfide linker binding the MSN and Fe_3O_4 nanoparticles is chemically labile and can be cleaved with various "cell-produced" and "artificial" antioxidants, such as dihydrolipoic acid (DHLA) and DTT, respectively. The release of fluorescein from the Fe_3O_4-MSN was tested in PBS solution. After 48 hours of incubation, 85% of the total release of fluorescein (40% of the total loading) was attained with DTT. With DHLA, the maximum percentage of fluorescein released was 31.4% of the total loading. The amount of fluorescein released after 72 hours showed a similar dependence on the concentration for both of the reducing agents. This result indicated that the rate of release was dictated by the rate at which the Fe_3O_4 nanoparticles were removed.

The endocytosis and biocompatibility of the system was investigated in HeLa cells. DAPI-stained HeLa cells were incubated with Fe_3O_4-MSN, confocal microscopy of the cells showed green fluorescence at the same focal plane as the blue fluorescence of the DAPI-

stained cellular nucleus; a clear indication that the Fe_3O_4-MSN were indeed endocytosed and the intracellular release of fluorescein was achieved. Furthermore, we were able to observe the magnetic motor effect moving the cells across the cuvette, propelled by a commercially available magnet. This combination of controlled-release properties with magnetic motor effects makes this system very attractive for site-specific drug delivery applications[46].

Gold nanoparticles (AuNP) have been widely used in biomedical and biotechnological applications[50]. Recently, we reported on the synthesis of a AuNP-MSN system to deliver plasmid DNA vector and chemicals into isolated plant cells and intact leaves[51]. The intracellular delivery in plant cells is limited because of their thick cell wall. Some strategies have been successfully applied to deliver DNA into plant cells, like "gene gun bombardment" using DNA-coated gold microparticles as "bullets", but this sort of systems have the limitation of only being able to deliver nucleic acids with small quantity due to the invasive nature of the bombardment, meaning many copies of DNA were damaged from the large sheer stress created during the cell penetration. In contrast, the porous nature of our AuNP-MSN system enables them to be used as a carrier of DNA and other chemicals at the same time. AuNP are biocompatible capping agents; furthermore, they increase the density of the MSN allowing it to be used in the "gene gun" system. We developed a redox-controlled gene and drug delivery system based on AuNP-MSN, which consists in the already mentioned disulfide linker strategy, which is used as bridge to bind the AuNP and MSN. We were able to prove the utility of this system loading β-oestradiol (transgene expression agent) inside of the channels and coating the system with an inducible GFP marker gene. The release of β-oestradiol was triggered by DTT, resulting in the expression of the GFP vector inside of the

cells. These results indicate that it was possible to deliver in a controlled manner DNA molecules carrying a marker gene and a chemical that is needed for its expression into plant cell simultaneously[51].

4.2. Organic Molecules as Gatekeepers

In addition to solid nanoparticles, flexible organic molecules have also been shown to be able to serve as gatekeepers for mesoporous silicas. Tanaka and co-workers first reported a reversible photo-triggered controlled release mesoporous silica (MCM-41) system that could function in organic solvents[52]. Their system took advantage of a photodimerization reaction of coumarin. The pores of MCM-41 were functionalized with 7-[(3-triethoxysilyl)propoxy]coumarin. Given that the size of the coumarinic group is around 1.3 nm, the dimerization of this coumarinic functionality yielded a cyclobutane coumarin dimer, which was large enough to close the mesoporous opening of MCM-41 silica. The authors showed that both cholestane and phenanthrene could be encapsulated and released in n-hexane solution[52].

Martínez-Mañez and co-workers developed an ionically-controlled mesoporous silica sensor[53]. Their system is comprised of a diaminoethylenepropylsilane derivative grafted at the openings of the pores and a mercaptopropyl group anchored inside of the porous channels of the mesoporous silica. The signal transduction mechanism is based on a colorimetric reaction between blue squaraine dye and the mercaptopropyl groups inside of the channels. The authors showed that the agglomeration/packing of the oligoamine-based "gatekeepers" could be manipulated by different pH's and anions. In the case of the pH-controlled gating,

an acidic solution of squaraine was introduced to the sensor. The blue color of the squaraine dye remained for hours, indicating no reaction with the thiols inside the oligo-amine-gated pores. The result suggested that the gate was closed because of the oligo-amines were protonated in the acidic solution causing a swelling between the gatekeepers. On the other hand, a color bleaching of squaraine was observed in a basic solution, indicating the gate was opened and the thiol groups inside were accessible to react with the dye molecules[53].

4.3. Supramolecular Assemblies as Gatekeepers

The combination of mesoporous silica materials as solid supports and supramolecular assemblies as gatekeepers has resulted in novel organic/inorganic hybrid materials with improved functionalities. Our group developed a dendrimer-capped MSN gene transfection system using a generation 2 poly(amidoamine) dendrimer (G2-PAMAM)[44]. We demonstrated that this system could be used as both drug delivery and gene transfection agent. We first tethered a G2-PAMAM on an isocyanatopropyl functionalized MSN to alter the surface charge property of the capped mesoporous silica. This positively charged system was able to bind electrostatically to a plasmid DNA vector encoding for enhanced green fluorescence protein (EGFP). We were able to demonstrate that G2-PAMAM-MSN protects efficiently the plasmid DNA against the digestion of a type-II restriction enzyme, BamHI (Figure 6). The transfection efficacy, uptake efficiency, and biocompatibility of the G2-PAMAM-capped MSN were investigated with neural glia, HeLa and Chinese Hamster Ovarian (CHO) cells. The G2-PAMAM-MSN transfection efficiency to express plasmid DNA EGFP was compared with other commercial transfection reagents (Table 3). Our

results indicated that gene transfection efficiency of G2-PAMAM-MSN was indeed better than those of other commercial reagents.

Cellular uptake of G2-PAMAM-MSN was also demonstrated by fluorescence confocal and transmission electron microscopy (TEM). Texas Red loaded G2-PAMAM-MSN was endocytosed by glia cells, fluorescence confocal micrographs showed red spots, corresponding to the Texas Red-loaded MSN, inside of the cells. TEM further confirmed the intracellular localizations of MSN particles. The biocompatibility of the G2-PAMAM-MSN system was evaluated by following cell proliferation during 6 days. The cell growth curves with and without G2-PAMAM-MSN were very similar, demonstrating the high biocompatibility of these silica nanoparticles in vitro.

To further investigate the controlled release properties of these capped-MSNs, our group was able to follow the ATP release kinetics by means of a real-time imaging system[54]. Two kinds of caps were used; CdS and PAMAM (G2.5 and G4.5) were chemically attached to MSN through the abovementioned disulfide linker. The method was based on luminescence by detecting the ATP-induced chemiluminescence of luciferase in situ. Two different reducing agents, DTT and tris-(2-carboxyethyl)phosphine (TCEP), were used to release ATP from either CdS or PAMAM-MSN. The results showed that DTT is a better trigger than TCEP to release ATP, which was rationalized in terms of the higher reducing power, the smaller size, and the lack of charge of DTT. Regarding to the type of cap, this work revealed that CdS caps require less time to release ATP than PAMAM dendrimers. Two main reasons could account for this difference. The first one is the different capping efficiency. Because of the lack of flexibility, CdS nanoparticles cannot form as many disulfide bonds as the

flexible PAMAM molecules. The other explanation could be attributed to the fact that the diffusion of the reducing agent to the locations of disulfide "hinges" would be slow in the case of PAMAM-MSN because the MSN was held tighter to PAMAM than to CdS.

Another example of supramolecular gates for mesoporous silica was developed by Stoddart, Zink and co-workers. Their system is comprised of a series of electrochemical redox-controlled pseudorotaxanes attached to mesoporous silica, which can be switched on and off[55]. In a typical case, [2]-pseudorotaxane $[DNPD\text{-}CBPQT]^{4+}$ was used as a gatekeeper, which includes 1,5-dioxynaphtalene derivative (DNPD) acting as the gate post, and cyclobis-(paraquat-p-phenylene) ($CBPQT^{4+}$) as the movable part of the molecule. By using $Ir(ppy)_3$ as a guest molecule in a toluene/ethanol (1:1) solution, the authors were able to demonstrate the redox-controlled release process using $NaCNBH_3$ as a reducing agent to open the nanovalve. Following the same redox-controlled release approach, the authors improved their system by developing a reversible nanovalve[56]. In this later work, the authors synthesized a [2]-rotaxane R^{4+} system, which consists of two different recognition sites in a dumbbell-type component. These recognition sites are tetrathiafulvalene (TTF) and 1,5-dioxynaphtalene (DNP), which are separated by an oligoethyleneglycol chain incorporating a rigid terphenylene spacer. As in their previous work, the authors used $CBPQT^{4+}$ as the movable part of the molecule. Ferric perchlorate and ascorbic acid were used to oxidize and reduce, respectively the [2]-rotaxane R^{4+} nanovalve system. In its ground state, $CBPQT^{4+}$ ring prefers to encircle the TTF recognition site rather than the DNP, which is far from the entrances to the pores, leaving thereby the gate open. A two electron-oxidation of the TTF with ferric perchlorate afforded TTF^{2+}, which destabilizes its interaction with the $CBPQT^{4+}$

ring. This produced the movement of the ring to the DNP recognition site, which is at the entrance of the pores closing in this way the gate. The nanovalve was reopened upon reduction of the TTF^{2+} with ascorbic acid, which caused the ring to shuttle back to the more distant location unblocking again the pores. As a proof of the concept the authors used luminescent compounds as guest molecules, which they were able to load and release by applying the mentioned redox triggers.

While these controlled-release nanovalves could indeed function effectively in non-aqueous environments, in order to apply these materials for drug delivery in vitro or in vivo, these systems would need to perform properly in aqueous environments, where some unfavorable electrostatic interaction and hydrogen bonding may inhibit the site recognition motifs.

Another pseudorotaxane-based MSN controlled release system was recently reported by Kim and co-workers[57]. In their work, the system consists of polyethyleneimine (PEI) as fixed motif and α- or γ-cyclodextrin as the movable ring. The authors used calcein as a guest molecule in PBS solution. The working principle is based on the fact that at pH 11 the cyclodextrin could thread into the PEI block, thereby closing the gate. Upon decreasing the pH to 5.5, the binding between PEI and cyclodextrin would be lost, which allowed the latter diffuse away, and thereby opening the gate. The authors were able to prove the principle following the release of calcein triggered by pH.

5. Controlled Release Drug Delivery

As it has been mentioned in the previous sections, MSN-based controlled release systems have been demonstrated to be able to deliver different kinds of guest molecule as summarized in Table 2. The loading is usually in the order of hundred milligrams per gram of MSN. The ones that have been used the most are imaging agents, such as fluorescein, Texas red, and rhodamine B, with the main goal of testing the working principle of the stimuli controlled-release drug/gene delivery system. Our group has used this kind of imaging agents to demonstrate the performance of our stimuli-responsive MSN systems. For instance, by using the aforementioned Texas Red-loaded G2-PAMAM-MSN material, we discovered that this system was indeed endocytosed by HeLa cells as determined by confocal fluorescent microscopy[44]. Fluorescein has also been very useful in demonstrating the controlled-release performance of our mesoporous silica nanoparticles in solution and in vitro as highlighted in our work with the Fe_3O_4-MSN system[46]. Also, with the help of these fluorescent dyes as pore-encapsulated molecules, we were able to determine the concentration effect of the gate-opening trigger on the release kinetics of guest molecules both inside and outside of cells.

To apply these systems for releasing biologically active molecules to living cells, we have investigated the CdS-MSN system for controlled release of drugs (vancomycin) and neurotransmitters (ATP) to live cells[6]. The controlled-release of ATP from CdS-MSN was used to artificially trigger a well-studied biological process, *i.e.* to promote the increase in intracellular calcium in astrocytes. We also used the controlled-release of ATP from CdS-MSN and PAMAM-MSN to prove the performance of a real-time imaging method based on Luciferase chemiluminescence[54].

Besides our group, others have also been able to release different kinds of drugs from mesoporous silica. Vallet-Regí and co-workers have demonstrated the release of ibuprofen[58], erythromycin[59], and alendronate[60] using different strategies to modify the control of drug release. Very recently, Tamanoi and co-workers demonstrated the release of camptothecin (CPT), a hydrophobic anticancer drug, from MSN[37]. Using confocal fluorescence microscopy, the authors confirmed the CPT release inside of various cancer-cell lines. Moreover, they were able to observe the growth inhibition and cell death, resulted from the delivery of CPT into the cancer cells.

The intracellular delivery of peptides and proteins is also relevant for therapeutic purposes. Recently, we demonstrated the use of pore expanded MSN to deliver a membrane-impermeable protein (cytochrome *c*) into HeLa cells, thereby showing that not only small drugs, but also macromolecules can be delivered with MSN based systems[26].

Gene therapy has caught a lot of attention in medicine because it provides great opportunities for treating diseases, infections and cancer. One of the main drawbacks for this technique is that there is not yet an efficient and safe system to deliver the therapeutic genes to a specific tissue or organ. To address this issue we have evaluated our stimuli-responsive mesoporous silica nanoparticles as gene transfection agents. Using our G2-PAMAM-MSN system, we demonstrated that our system can protect plasmid DNA vector (EGFP) against enzymatic cleavage and induce EGFP expression in HeLa cells[44]. The EGFP expression was not only observed in mammalian cells, but also observed in plant cells using AuNPs-MSN system as transfection agent, with the additional advantage of simultaneously deliver the corresponding transgene expression additive[51].

6. Conclusion and Future Directions

In this review, we have highlighted some exciting research progress on the utilization of mesoporous silica nanoparticles as intracellular controlled-release drug delivery agents. The mechanisms, by which non-functionalized MSN can be transformed into stimuli-responsive drug delivery agents, have already been established, although further improvements are expected in terms of increasing the inventory of gatekeepers and controlled release mechanisms. While these results are encouraging and show great potential for future applications, new breakthroughs are still needed for this type of drug delivery systems. For example, the system has not yet been studied in vivo and therefore essential information regarding circulation properties in blood, possible immunogenicity, and accumulation in liver or specific tissues need to be obtained and, eventual problems emerging from those studies will need to be addressed. Cell type specificity is a challenge that also needs to be overcome. Furthermore, the possibility of other therapeutic applications using MSN as an intracellular controlled release nanodevice could be envisioned. For instance, it is plausible that some functionalized MSNs would be able to perform specific tasks inside of cells, e.g., altering cellular processes by sequestration or immobilization of metabolites or other functional biomolecules. We look forward to seeing many exciting research accomplishments in this burgeoning field of nano-bio-materials.

Acknowledgement

The authors thank U.S. NSF (CHE-0239570), U.S. DOE, Office of Basic Energy Sciences (DE-AC02-07CH11358), and Plant Science Institute at Iowa State University for financial support.

REFERENCES

(1) Kwon, I. K.; Jeong, S. H.; Kang, E.; Park, K. *Cancer Nanotech.* **2007**, 333-344.

(2) Bottini, M.; D'Annibale, F.; Magrini, A.; Cerignoli, F.; Arimura, Y.; Dawson, M. I.; Bergamaschi, E.; Rosato, N.; Bergamaschi, A.; Mustelin, T. *Int. J. Nanomed.* **2007**, *2*, 227-233.

(3) Gerion, D.; Herberg, J.; Bok, R.; Gjersing, E.; Ramon, E.; Maxwell, R.; Kurhanewicz, J.; Budinger, T. F.; Gray, J. W.; Shuman, M. A.; Chen, F. F. *J. Phys. Chem. C* **2007**, *111*, 12542-12551.

(4) Graf, C.; Dembski, S.; Hofmann, A.; Ruehl, E. *Langmuir* **2006**, *22*, 5604-5610.

(5) Zhu, M.-Q.; Han Jason, J.; Li Alexander, D. Q. *J. Nanosci. Nanotechnol.* **2007**, *7*, 2343-8.

(6) Lai, C.-Y.; Trewyn, B. G.; Jeftinija, D. M.; Jeftinija, K.; Xu, S.; Jeftinija, S.; Lin, V. S. Y. *J. Amer. Chem. Soc.* **2003**, *125*, 4451-4459.

(7) Areva, S.; Aeaeritalo, V.; Tuusa, S.; Jokinen, M.; Linden, M.; Peltola, T. *J. Mater. Sci.: Mater. Med.* **2007**, *18*, 1633-1642.

(8) Meseguer-Olmo, L.; Ros-Nicolas, M. J.; Vicente-Ortega, V.; Alcaraz-Banos, M.; Clavel-Sainz, M.; Arcos, D.; Ragel, C. V.; Vallet-Regi, M.; Meseguer-Ortiz, C. *J. Orthop. Res.* **2006**, *24*, 454-460.

(9) Radin, S.; El-Bassyouni, G.; Vresilovic, E. J.; Schepers, E.; Ducheyne, P. *Biomater.* **2004**, *26*, 1043-1052.

(10) Kortesuo, P.; Ahola, M.; Karlsson, S.; Kangasniemi, I.; Yli-Urpo, A.; Kiesvaara, J. *Biomater.* **1999**, *21*, 193-198.

(11) Dormer, K.; Seeney, C.; Lewelling, K.; Lian, G.; Gibson, D.; Johnson, M. *Biomaterials* **2005**, *26*, 2061-72.

(12) Arruebo, M.; Galan, M.; Navascues, N.; Tellez, C.; Marquina, C.; Ibarra, M. R.; Santamaria, J. *Chem. Mater.* **2006**, *18*, 1911-1919.

(13) Zhao, W.; Gu, J.; Zhang, L.; Chen, H.; Shi, J. *J. Amer. Chem. Soc.* **2005**, *127*, 8916-8917.

(14) Allouche, J.; Boissiere, M.; Helary, C.; Livage, J.; Coradin, T. *J.Mater. Chem.* **2006**, *16*, 3120-3125.

(15) Huo, Q.; Liu, J.; Wang, L.-Q.; Jiang, Y.; Lambert, T. N.; Fang, E. *J. Amer. Chem. Soc.* **2006**, *128*, 6447-6453.

(16) Kresge, C. T.; Leonowicz, M. E.; Roth, W. J.; Vartuli, J. C.; Beck, J. S. *Nature* **1992**, *359*, 710-12.

(17) Gruen, M.; Lauer, I.; Unger, K. K. *Adv. Mater.* **1997**, *9*, 254-257.

(18) Unger, K. K.; Kumar, D.; Grun, M.; Buchel, G.; Ludtke, S.; Adam, T.; Schumacher, K.; Renker, S. *J. Chromatogr., A* **2000**, *892*, 47-55.

(19) Huo, Q.; Feng, J.; Schueth, F.; Stucky, G. D. *Chem. Mater.* **1997**, *9*, 14-17.

(20) Qi, L.; Ma, J.; Cheng, H.; Zhao, Z. *Chem. Mater.* **1998**, *10*, 1623-1626.

(21) Kosuge, K.; Singh, P. S. *Microporous Mesoporous Mater.* **2001**, *44-45*, 139-145.

(22) Han, Y.; Ying, J. Y. *Angew. Chem., Int. Ed.* **2005**, *44*, 288-292.

(23) Huh, S.; Wiench, J. W.; Yoo, J.-C.; Pruski, M.; Lin, V. S. Y. *Chem. Mater.* **2003**, *15*, 4247-4256.

(24) Moeller, K.; Kobler, J.; Bein, T. *Adv. Funct. Mater.* **2007**, *17*, 605-612.

(25) Gu, J.; Fan, W.; Shimojima, A.; Okubo, T. *Small* **2007**, *3*, 1740-4.

(26) Slowing, I. I.; Trewyn, B. G.; Lin, V. S. Y. *J. Amer. Chem. Soc.* **2007**, *129*, 8845-8849.

(27) Bao, Y.-z.; Liao, J.-g.; Huang, Z.-m.; Weng, Z.-x. *J. Appl. Pol. Sci.* **2003**, *90*, 3848-3855.

(28) Teeguarden, J. G.; Hinderliter, P. M.; Orr, G.; Thrall, B. D.; Pounds, J. G. *Toxicol. Sci.***2007**, *95*, 300-312.

(29) Trewyn, B. G.; Whitman, C. M.; Lin, V. S. Y. *Nano Lett.* **2004**, *4*, 2139-2143.

(30) Che, S.; Liu, Z.; Ohsuna, T.; Sakamoto, K.; Terasaki, O.; Tatsumi, T. *Nature* **2004**, *429*, 281-284.

(31) Huh, S.; Wiench, J. W.; Trewyn, B. G.; Song, S.; Pruski, M.; Lin, V. S. Y. *Chem. Comm. (Cambridge, United Kingdom)* **2003**, 2364-2365.

(32) Burleigh, M. C.; Dai, S.; Hagaman, E. W.; Barnes, C. E.; Xue, Z. L. *ACS Symposium Series* **2001**, *778*, 146-158.

(33) Chen, H.-T.; Huh, S.; Lin, V. S. Y. *Catal. Prep.* **2007**, 45-73.

(34) Radu, D. R.; Lai, C.-Y.; Huang, J.; Shu, X.; Lin, V. S. Y. *Chem. Comm.* **2005**, 1264-1266.

(35) Huh, S.; Chen, H.-T.; Wiench, J. W.; Pruski, M.; Lin, V. S. Y. *Angew. Chem., Int. Ed.* **2005**, *44*, 1826-1830.

(36) Radu, D. R.; Lai, C.-Y.; Wiench, J. W.; Pruski, M.; Lin, V. S. Y. *J. Amer. Chem. Soc.* **2004**, *126*, 1640-1641.

(37) Lu, J.; Liong, M.; Zink, J. I.; Tammanoi, F. *Small* **2007**, *3*, 1341-1346.

(38) Feng, X.; Fryxell, G. E.; Wang, L. Q.; Kim, A. Y.; Liu, J.; Kemner, K. M. *Science* **1997**, *276*, 923-926.

(39) Mayor, S.; Pagano, R. E. *Nature Rev. Mol. Cell Biol.* **2007**, *8*, 603-612.

(40) Rejman, J.; Oberle, V.; Zuhorn, I. S.; Hoekstra, D. *Biochem. J.* **2004**, *377*, 159-169.

(41) Xing, X.; He, X.; Peng, J.; Wang, K.; Tan, W. *J. Nanosci. Nanotech.* **2005**, *5*, 1688-1693.

(42) Mornet, S.; Lambert, O.; Duguet, E.; Brisson, A. *Nano Lett.* **2005**, *5*, 281-285.

(43) Slowing, I.; Trewyn, B. G.; Lin, V. S. Y. *J. Amer. Chem. Soc.* **2006**, *128*, 14792-14793.

(44) Radu, D. R.; Lai, C.-Y.; Jeftinija, K.; Rowe, E. W.; Jeftinija, S.; Lin, V. S. Y. *J. Amer. Chem. Soc.* **2004**, *126*, 13216-13217.

(45) Chung, T.-H.; Wu, S.-H.; Yao, M.; Lu, C.-W.; Lin, Y.-S.; Hung, Y.; Mou, C.-Y.; Chen, Y.-C.; Huang, D.-M. *Biomater.* **2007**, *28*, 2959-2966.

(46) Giri, S.; Trewyn, B. G.; Stellmaker, M. P.; Lin, V. S. Y. *Angew. Chem., Int. Ed.* **2005**, *44*, 5038-5044.

(47) Huang, D.-M.; Hung, Y.; Ko, B.-S.; Hsu, S.-C.; Chen, W.-H.; Chien, C.-L.; Tsai, C.-P.; Kuo, C.-T.; Kang, J.-C.; Yang, C.-S.; Mou, C.-Y.; Chen, Y.-C. *FASEB J.* **2005**, *19*, 2014-2016.

(48) Kim, J.-S.; Yoon, T.-J.; Yu, K.-N.; Noh, M.-S.; Woo, M.; Kim, B.-G.; Lee, K.-H.; Sohn, B.-H.; Park, S.-B.; Lee, J.-K.; Cho, M.-H. *J. Vet. Sci.* **2006**, *7*, 321-6.

(49) Lu, C.-W.; Hung, Y.; Hsiao, J.-K.; Yao, M.; Chung, T.-H.; Lin, Y.-S.; Wu, S.-H.; Hsu, S.-C.; Liu, H.-M.; Mou, C.-Y.; Yang, C.-S.; Huang, D.-M.; Chen, Y.-C. *Nano Lett.* **2007**, *7*, 149-154.

(50) Daniel, M.-C.; Astruc, D. *Chemical Reviews (Washington, DC, United States)* **2004**, *104*, 293-346.

(51) Torney, F.; Trewyn, B. G.; Lin, V. S. Y.; Wang, K. *Nature Nanotech.* **2007**, *2*, 295-300.

(52) Mal, N. K.; Fujiwara, M.; Tanaka, Y. *Nature* **2003**, *421*, 350-353.

(53) Casasus, R.; Marcos, M. D.; Martinez-Manez, R.; Ros-Lis, J. V.; Soto, J.; Villaescusa, L. A.; Amoros, P.; Beltran, D.; Guillem, C.; Latorre, J. *J. Amer. Chem. Soc.* **2004**, *126*, 8612-8613.

(54) Gruenhagen, J. A.; Lai, C.-Y.; Radu, D. R.; Lin, V. S. Y.; Yeung, E. S. *Appl. Spectroscop.* **2005**, *59*, 424-431.

(55) Hernandez, R.; Tseng, H.-R.; Wong, J. W.; Stoddart, J. F.; Zink, J. I. *J. Amer. Chem. Soc.* **2004**, *126*, 3370-3371.

(56) Nguyen, T. D.; Tseng, H.-R.; Celestre, P. C.; Flood, A. H.; Liu, Y.; Stoddart, J. F.; Zink, J. I. *Proc. Nat. Acad. Sci. U. S. A.* **2005**, *102*, 10029-10034.

(57) Park, C.; Oh, K.; Lee, S. C.; Kim, C. *Angew. Chem., Int. Ed.* **2007**, *46*, 1455-1457.

(58) Vallet-Regi, M. *Chem. Eur. J.* **2006**, *12*, 5934-5943.

(59) Doadrio, J. C.; Sousa, E. M. B.; Izquierdo-Barba, I.; Doadrio, A. L.; Perez-Pariente, J.; Vallet-Regi, M. *J. Mater. Chem.* **2006**, *16*, 462-466.

(60) Balas, F.; Manzano, M.; Horcajada, P.; Vallet-Regi, M. *J. Amer. Chem. Soc.* **2006**, *128*, 8116-8117.

Table 1. Some functional groups introduced on the surface of MSN, and the methods employed to produce them.

Functional group	Method	Reference
Ureidoalkyl	co-condensation	[23,35]
Mercaptoalkyl	co-condensation, grafting	[23,34,38]
Cyanoalkyl	co-condensation, grafting	[23,34,35]
Aminoalkyl	co-condensation, grafting	[23,34,35]
Allyl	co-condensation, grafting	[23]
Isocyanatoalkyl	grafting	[34]
Epoxyalkyl	grafting	[36]
Phosphonatoalkyl	grafting	[37]
Metal-Aminoalkyl	Molecular imprinting	[32]

Table 2. Gatekeeping systems applied in the release of various molecules from MSN.

Gatekeeper	Stimulus	Trigger	Guest Molecule	Ref.
CdS-NP	Redox	Reducing Agent (DTT, ME)	ATP,Vancomycin	6
Fe_3O_4-NP	Redox	Reducing Agent (DTT, DHLA)	Fluorescein	46
Au-NP	Redox	Reducing Agent (DTT)	β-oestradiol,DNA	51
Coumarin	Photo	UV light (λ = 310 nm)	Cholestane, Phenanthrene	52
Diethylenetriamine	Ionic	pH, anions	"Blue squaraine"	53
PAMAM	Redox	Reducing Agent (DTT, TCEP)	ATP, DNA	44,54
[2] Pseudorotaxane [DNPD-CBPQT]$^{4+}$	Redox	$NaCNBH_3$	$Ir(ppy)_3$	55
[2] Rotaxane R^{4+}	Redox	$Fe(ClO_4)_3$, ascorbic acid	$Ir(ppy)_3$, Rhodamine B	56
[2] Pseudorotaxane PEI-CD	Ionic	pH	Calcein	57

Table 3. Comparison of the transfection efficiency of EGFP by PAMAM-GD-MSN with the one by three different commercial transfection agents (Reproduced with permission from[44], copyright by the American Chemical Society).

Transfection Reagent	% Cells Expressing Gene
G2-MSN	35 ± 5
PolyFect®	15 ± 2
SuperFect®	10 ± 2
Metafectene®	16 ± 2

Figure captions

Figure 1. TEM images of MSNs materials recording from the direction (a) parallel or (b) perpendicular to the long axis of the mesochannels.

Figure 2. Transmission electron microscopy images of HeLa cell with endocytosed MSN. (Reproduced with permission from[44], copyright by the American Chemical Society).

Figure 3. Confocal fluorescence images of fluorescein labeled MSN (green, panel a) endocytosed by HeLa cells co-stained with an endosome marker (FM 4-64, red, panel b) and nuclear dye (DAPI, blue, panel c). The merged images (panel d) show little coincidence of green and red spots (giving yellow) corresponding to MSN still inside of endosomes. As can be observed, some MSN (green) have already escaped from the (red) endosomes.

Figure 4. Representation of an MSN loaded with guest molecules and end-capped with a general gatekeeper.

Figure 5. (a) Images showing that application of ME on an astrocyte culture loaded with the intracellular Ca^{2+}-chelating fluorophore (Fura 2-AM) without the presence of MSN failed to produce any $[Ca^{2+}]_i$ response of astrocytes. (b) Pseudo-color image of astrocytes taken after the ME application showed no increase or decrease in $[Ca^{2+}]_i$ of the cells. (c) The same cells responded to the perfusion application of 100.0 μM ATP indicated by the increase of fluorescence intensity of the pseudo-color image of astrocytes, i.e., $[Ca^{2+}]_i$ increases. (Reproduced with permission from[6], copyright by the American Chemical Society)

Figure 6. Fluorescent microscopy images of HeLa cells treated with G2-MSN-DNA complexes that have first been exposed to *Bam*H I. (a) HeLa cells with green fluorescent proteins expressed in spite of the exposition to the endonuclease. (b) Phase contrast image of the same region of interest. (Reproduced with permission from[44], copyright by the American Chemical Society).

Figure 1.

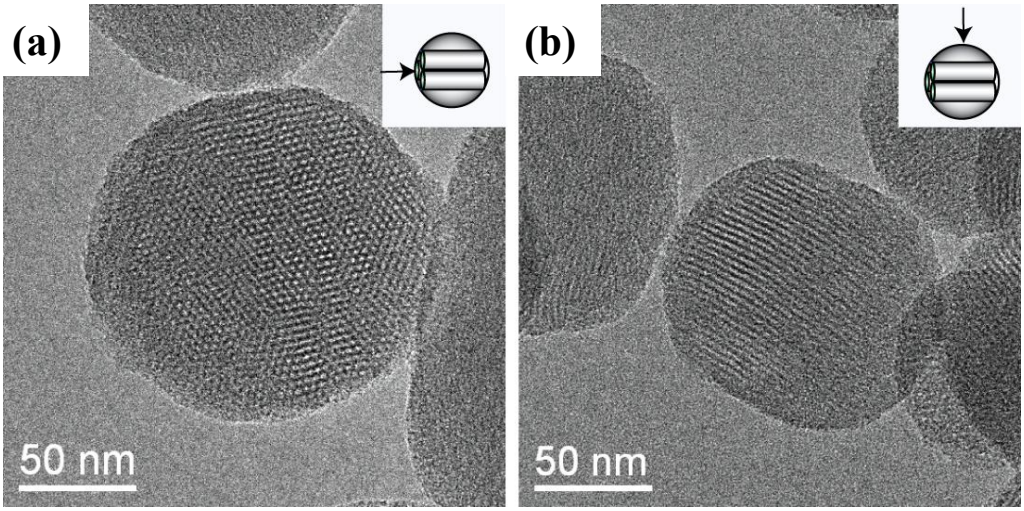

Figure 2.

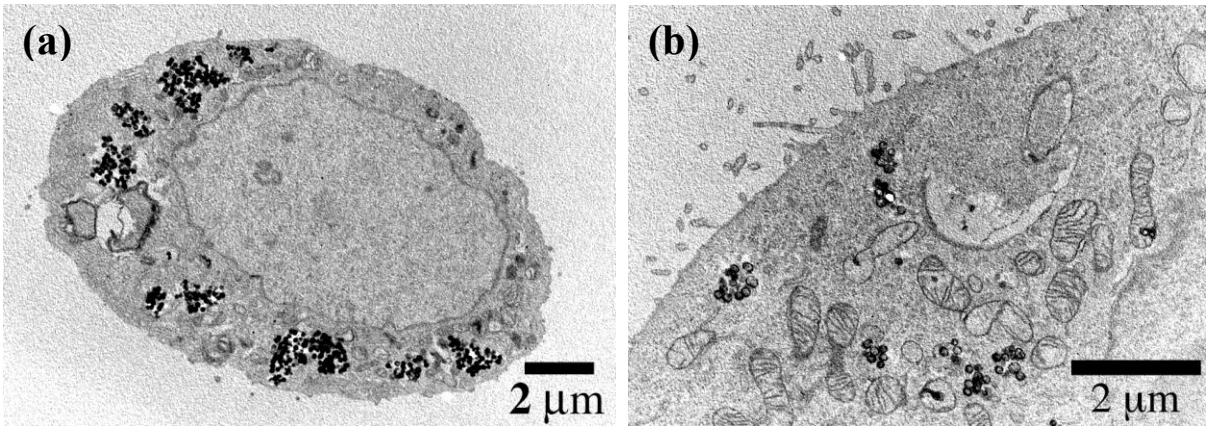

Figure 3.

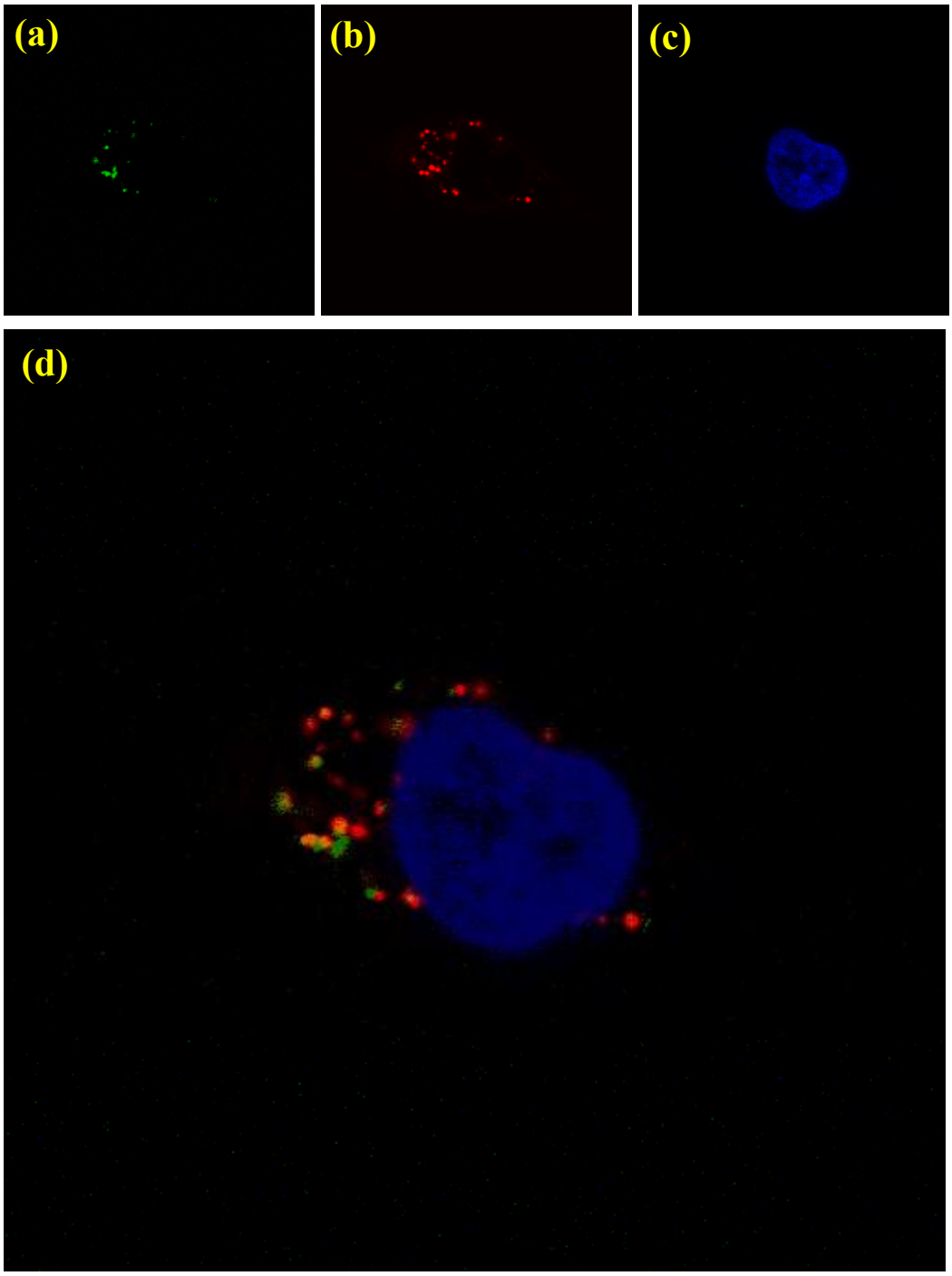

Figure 4.

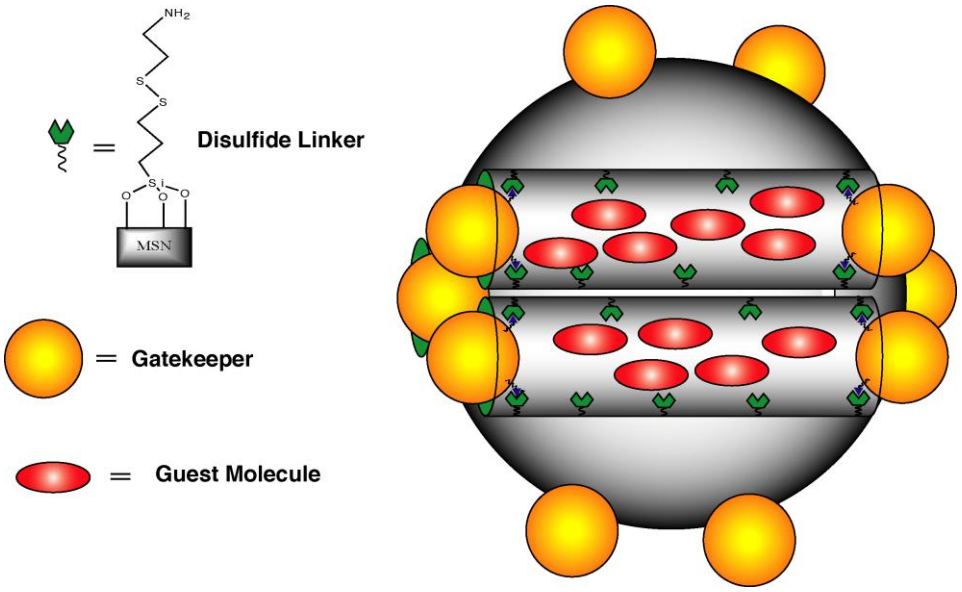

Figure 5.

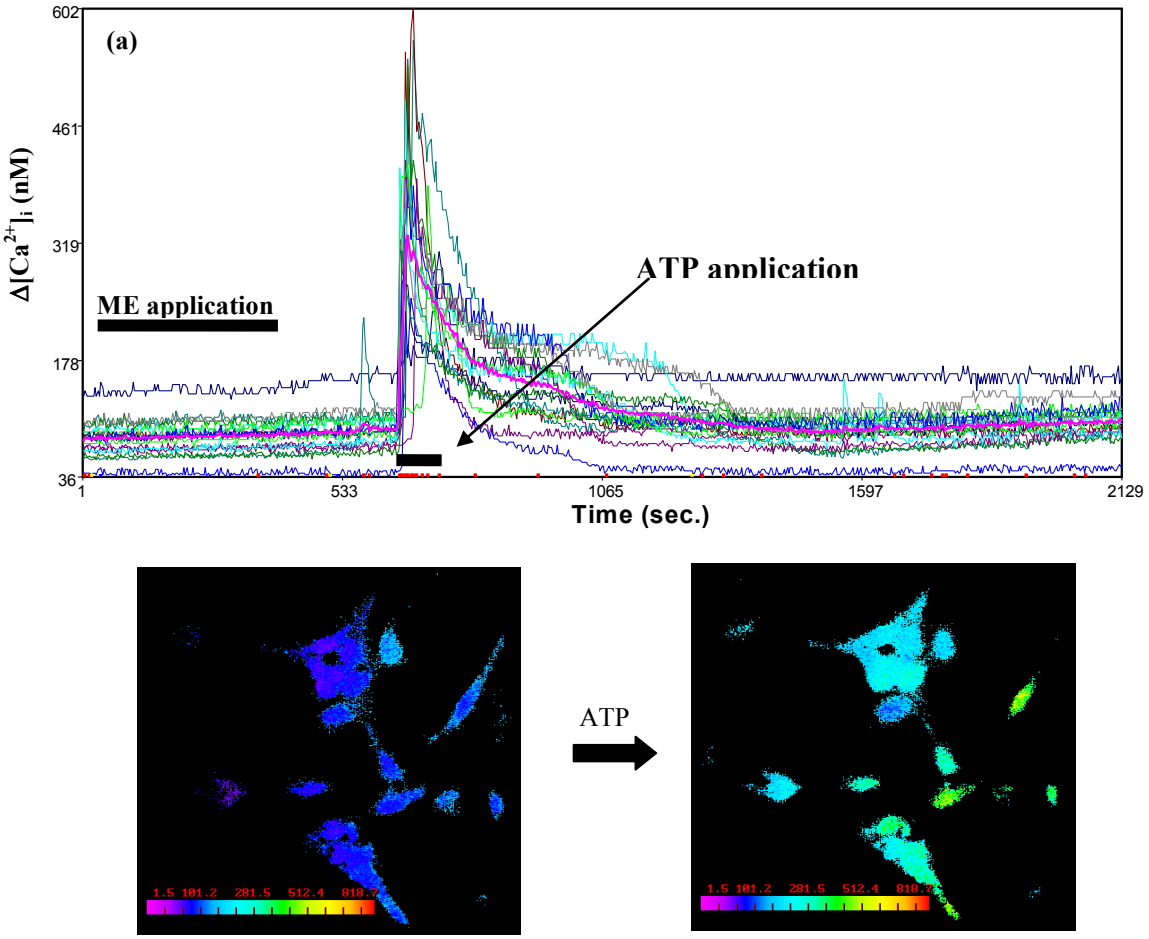

Figure 6.

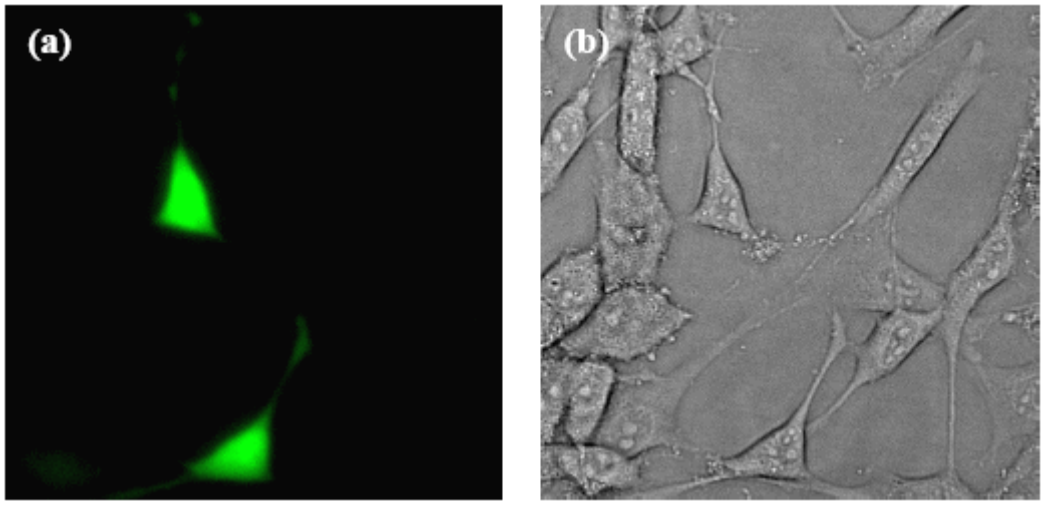

CHAPTER 3. EFFECT OF SURFACE FUNCTIONALIZATION OF MCM-41 TYPE MESOPOROUS SILICA NANOPARTICLES ON THE ENDOCYTOSIS BY HUMAN CANCER CELLS

A paper published in the ***Journal of the American Chemical Society***,

2006, *128*, 14792-14793.

Igor I. Slowing, Brian G. Trewyn and Victor S.-Y. Lin

Abstract

We have synthesized a series of MCM-41 type mesoporous silica nanoparticles (MSN). The surface of the MSNs are functionalized with 3-aminopropyl (AP), *N*-(2-aminoethyl)-3-aminopropyl (AEAP), and *N*-folate-3-aminopropyl (FAP). In contrast to the zeta potential of -18.4 mV of FITC-MSN, the values of ζ-potential for AP-, GP-, GEGP, and FAP-functionalized FITC-MSNs in 100 mM PBS buffer (pH 7.4) increased positively from -11.3, -10.6, -4.0, to +4.9 mV, respectively. The uptake efficiency, endocytosis mechanism, and biocompatibility of these organically functionalized MSNs were investigated with human cervical cancer cells (HeLa). Flow cytometry results suggested that the endocytosis of MSN could be manipulated by different surface functionalization. The immunocytochemistry study indicated that the uptake of these MSNs by HeLa cells was surface functional group dependent and involved several different mechanisms of endocytosis. Confocal fluorescence micrographs showed that the different surface functionalities of MSNs could also affect their ability to escape endosomal entrapment, which is a key factor in designing effective intracellular delivery vehicles.

Recent studies on the interaction between surface-functionalized inorganic nanoparticles and animal cells have shown great potential for utilizing these size-defined nanomaterials for various biomedical and biotechnological applications, such as cell type recognition, disease diagnosis, intracellular imaging, and drug/gene delivery. In particular, several recent reports,[1-5] including our own studies, have shown that mesoporous silica nanoparticles can be efficiently endocytosed by mammalian cells. The large surface areas and pore volumes of these materials offer the possibility of encapsulating and delivering large quantities of biogenic molecules through different cell membranes and to various intracellular targets. Furthermore, it has been demonstrated recently that the mesopores of these nanoparticles can be closed and opened at will by various capping/release strategies.[1,3,6] These new breakthroughs make the surface-functionalized MSNs excellent candidates for intracellular controlled release delivery. To realize this goal, an important prerequisite would be to understand the mechanism of cellular uptake of these surface-functionalized mesoporous silica nanoparticles, so that the uptake of MSNs by different cell types can be regulated. For example, to use these MSNs as efficient intracellular delivery vehicles, it would be important to use different surface functional groups to manipulate the rate of escape of MSNs from endosomes to cytosol and other intracellular organelles. To the best of our knowledge, no report has examined the effect of surface functional groups to the cell uptake properties of these mesoporous silica-based nanoparticles. Herein, we report on the synthesis of a series of organically functionalized MSNs and investigate the mechanism and efficiency of endocytosis of these materials with different charge profiles on human cervical cancer cells (HeLa).

First, we synthesized a fluorescein-functionalized, MCM-41 type mesoporous silica nanoparticle material (FITC-MSN).[7] As shown in Figure 1, FITC-MSN has an average particle diameter of 150 nm. The MCM-41 type mesoporous structure with a 2.4 nm average pore diameter and a surface area of 850 m^2/g was confirmed by powder x-ray diffraction (XRD), nitrogen sorption isotherms, and scanning and transmission electron microscopy (SEM and TEM, respectively) measurements.[7] Three functional groups, 3-aminopropyl (AP), *N*-(2-aminoethyl)-3-aminopropyl (AEAP), and *N*-folate-3-aminopropyl (FAP), were grafted onto the external surface of the FITC-MSN by refluxing 6 mmol of the corresponding trimethoxysilyl derivatives with 1 g of FITC-MSN in toluene for 20 h. The amino groups of the 3-aminopropyl and the N-(2-aminoethyl)-3-aminopropyl were transformed into guanidinopropyl (GP) and 3-[N-(2-guanidinoethyl)guanidinio]-propyl (GEGP) groups, respectively, via a literature procedure.[8] The amount of surface-anchored AP, GP, GEGP, and FAP groups were determined by solid-state direct polarization ^{29}Si NMR to be 1.5, 1.3, 0.97, and 0.89 mmol/g, respectively. After the grafting of these groups, the surfactant template (CTAB) molecules were removed from the MSNs by refluxing 1.0 g of the materials in 100 mL of methanol and 1 mL of concentrated HCl.

In contrast to the zeta potential (ζ-potential) of -34.73 mV of FITC-MSN, the values of ζ-potential for AP-, GP-, GEGP-, and FAP-functionalized FITC-MSNs in 100 mM PBS buffer (pH 7.4) increased positively from -4.68 to +12.81 mV, respectively, as outlined in Table 1.

To examine the biocompatibility of MSNs, we compared the cell growth profiles of HeLa cultures with and without MSNs (0.1 mg/mL) for four days. Our results showed no difference in growth with or without the MSNs.[7]

To investigate the uptake of these organically functionalized MSNs, different concentrations of MSNs were introduced to HeLa cell cultures seeded at 1.0×10^5 cells/mL for 10 h in serum-free media. The degree of endocytosis was determined by quantifying live cells that exhibited green fluorescence with flow cytometry. To ensure the fluorescence observed in the flow cytometry measurements was indeed from the MSNs that have been endocytosed, a fluorescence quencher, Trypan Blue, was included in the cell suspension. Since Trypan Blue cannot penetrate the membranes of living cells, it could only quench the fluorescence of those MSNs that are adsorbed on the exterior surface of cells.[9] The plots of the logarithms of the concentrations of MSNs versus the percentages of cells that took up the MSNs, showed a sigmoidal behavior, which is typical of dose-response endocytosis (Figure 2a). The degrees of uptake of these MSNs were determined by their ED_{50} values.

The uptake of non-functionalized, negatively charged silica materials by cells has been found to occur through a non-specific adsorptive endocytosis,[5] and that the resting potentials of cell membranes are normally negative (-50 mV for HeLa).[10] The relationship between the EC_{50} values and the ζ-potentials of these surface-functionalized MSNs was summarized in Table 1. Flow cytometry results suggested that the endocytosis of MSN could be manipulated by different surface functionalization. In addition to the surface charge effect, it is well known that the membranes of human cancer cells are abundant with folate receptors.[11] The folate groups on FAP-MSN could also play an active role in facilitating a receptor-mediated endocytosis.

To investigate the possible mechanism of endocytosis of the different MSNs, we tested the cellular uptake of these materials in presence of specific inhibitors. Our results indicated that

only the FITC- and FAP-MSNs are endocytosed via a clathrin-pitted mechanism, as the uptakes were inhibited by 450 mM sucrose (Figure 2b and c). In addition, the uptake of FAP-MSN was partially inhibited in presence of 1 mM folic acid, where the endocytosis of FITC-MSN was not perturbed (Figure 2b). This observation along with the higher uptake observed for FAP-MSN suggests that the mechanism of endocytosis for this material is mediated by folic acid receptors on the HeLa cell surface. In contrast, the endocytosis of AP- and GP-MSNs was affected by a caveola inhibitor, Genistein (Figure 2c) suggesting that these materials were endocytosed via a caveolae-mediated mechanism. The uptake mechanism of GEGP remains unclear because the endocytosis was not dramatically affected by any of the inhibitors.

To study the impact of surface functionality in endosome escape, we stained the endosomes with a red fluorescent endosome marker (FM 4-64) and monitored the confocal fluorescence micrographs (Figure 3)[7] of FITC-MSNs with different functional groups in HeLa cells. The green fluorescent spots observed in Figure 3a represent the FITC-MSNs that were able to escape endosomes, whereas those that were entrapped inside of the vesicles exhibited yellow in color, which is the result of overlapping red (endosome) and green (MSN) spots. We found that the more negatively charged FITC- and AP-MSNs appeared to be able to escape from endosomes within 6 h, while those with more positive ζ-potentials, such as GP-, GEGP- and FAP-MSNs, remained trapped within endosomes.[7] This behavior could be attributed to the proton-sponge effect,[12] where the more negatively charged materials would have a better buffering capacity, which is important for the endosome escape.[12]

In conclusion, we have demonstrated the uptake of MCM-41 type mesoporous silica nanoparticles by HeLa cells can be regulated by different surface functionalization. Our results indicated that these surface functionalities could also affect MSN's ability to escape endosomal entrapment, which is a key factor in designing effective intracellular delivery vehicles.

Acknowledgment. This research was supported by the NSF (CHE-0239570). The authors thank the cell and hybridoma facility of ISU for their assistance.

References

(1) Giri, S.; Trewyn, B. G.; Stellmaker, M. P.; Lin, V. S. Y. *Angew. Chem., Int. Ed. Engl.* **2005**, *44*, 5038-5044.

(2) Huang, D.-M.; Hung, Y.; Ko, B.-S.; Hsu, S.-C.; Chen, W.-H.; Chien, C.-L.; Tsai, C.-P.; Kuo, C.-T.; Kang, J.-C.; Yang, C.-S.; Mou, C.-Y.; Chen, Y.-C. *FASEB J.* **2005**, *19*, 2014-2016.

(3) Lai, C.-Y.; Trewyn, B. G.; Jeftinija, D. M.; Jeftinija, K.; Xu, S.; Jeftinija, S.; Lin, V. S. Y. *J. Am. Chem. Soc.* **2003**, *125*, 4451-4459.

(4) Lin, Y.-S.; Tsai, C.-P.; Huang, H.-Y.; Kuo, C.-T.; Hung, Y.; Huang, D.-M.; Chen, Y.-C.; Mou, C.-Y. *Chem. Mater.* **2005**, *17*, 4570-4573.

(5) Xing, X.; He, X.; Peng, J.; Wang, K.; Tan, W. *J. Nanosci. Nanotech.* **2005**, *5*, 1688-1693.

(6) Gruenhagen, J. A.; Lai, C.-Y.; Radu, D. R.; Lin, V. S. Y.; Yeung, E. S. *Appl. Spectrosc.* **2005**, *59*, 424-431.

(7) *See Supporting Information (Appendix)*.

(8) Bernatowicz, M. S. W., Youling; Matsueda, G. *J. Org. Chem.* **1992**, *57*, 2497-2502.

(9) Hed, J.; Hallden, G.; Johansson, S. G.; Larsson, P. *J. Immunol. Methods* **1987**, *101*, 119-25.

(10) Szabo, I.; Brutsche, S.; Tombola, F.; Moschioni, M.; Satin, B.; Telford, J. L.; Rappuoli, R.; Montecucco, C.; Papini, E.; Zoratti, M. *EMBO J.* **1999**, *18*, 5517-27.

(11) Ladino, C. A.; Chari, R. V. J.; Bourret, L. A.; Kedersha, N. L.; Goldmacher, V. S. *Int. J. Cancer* **1997**, *73*, 859-864.

(12) Boussif, O.; Lezoualc'h, F.; Zanta, M. A.; Mergny, M. D.; Scherman, D.; Demeneix, B.; Behr, J.-P. *Proc. Natl. Acad. Sci. U.S.A.* **1995**, *92*, 7297-301.

Table 1. Zeta potentials and EC_{50} for cellular uptake of the MSNs

Material	**ζ-Potential [mV]**	**EC_{50} (μg/mL)**
FITC-MSN	-34.73 ± 3.50	12.35
AP-MSN	-4.68 ± 1.54	10.95
GP-MSN	-3.25 ± 0.275	8.8
GEGP-MSN	+0.57 ± 0.095	6.39
FAP-MSN	+12.81 ±1.60	2.73

Figure captions.

Figure 1. Schematic representation of the endocytosis of organically functionalized mesoporous silica nanoparticles (MSN) by a human cervical cancer cell (HeLa). (a) TEM image of a fluorescein functionalized MSN (FITC-MSN).

Figure 2. (a) Uptake of the synthesized MSN as a function of their concentration: FITC- (black hollow circles), AP- (red triangles), GP- (green rhombi), GEGP- (blue circle), and FAP- (purple square) MSN. (b) and (c) Uptake of the materials in absence (blue bars), and presence of a series of inhibitors: 450 mM sucrose (prune); 1mM folic acid (gray); 200 mM genistein (cream).

Figure 3. Confocal fluorescence images of HeLa cells stained with FM 4-64 and 40 μg/mL suspensions of (a) FITC-MSN and (b) FAP-MSN after 6 h of introduction. The fluorescent images show the MSN (green, left) and FM 4-64-labeled endosomes (red, right). The merged images are shown in the center panel.

Figure 1.

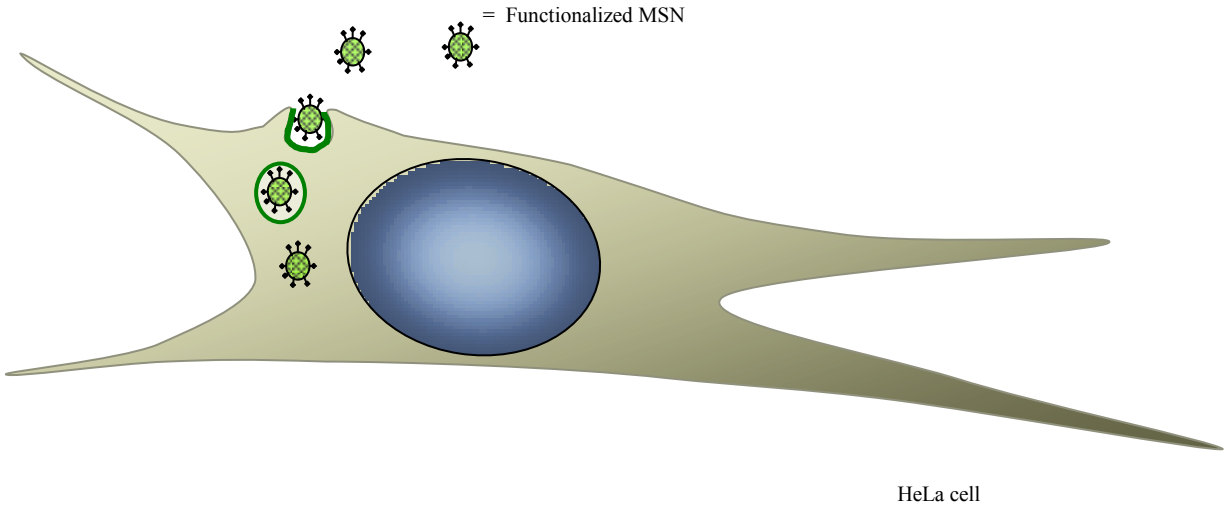

(a)

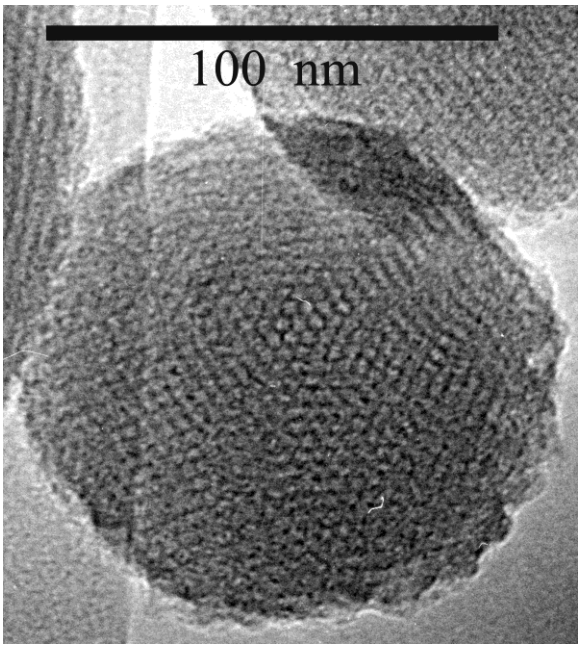

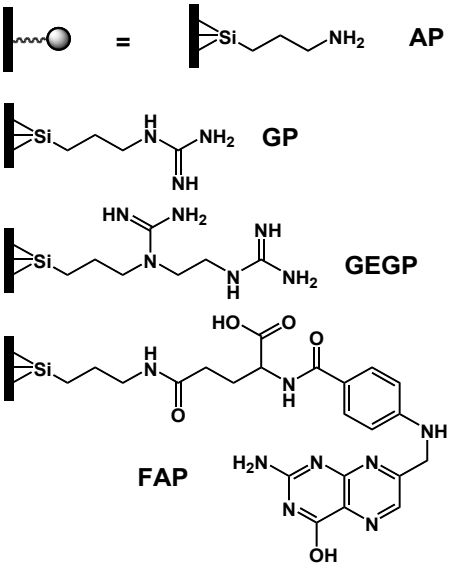

Figure 2.

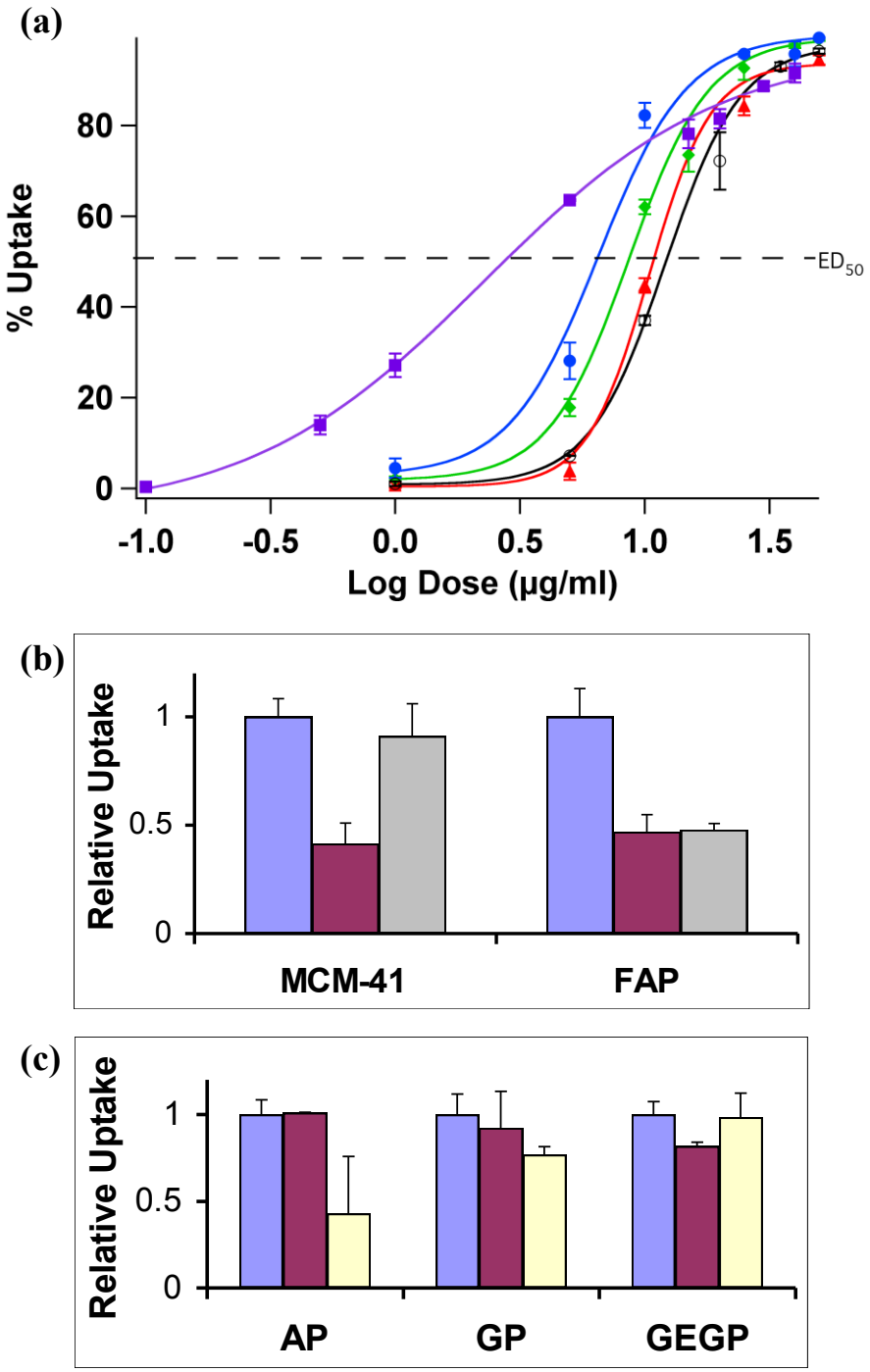

Figure 3.

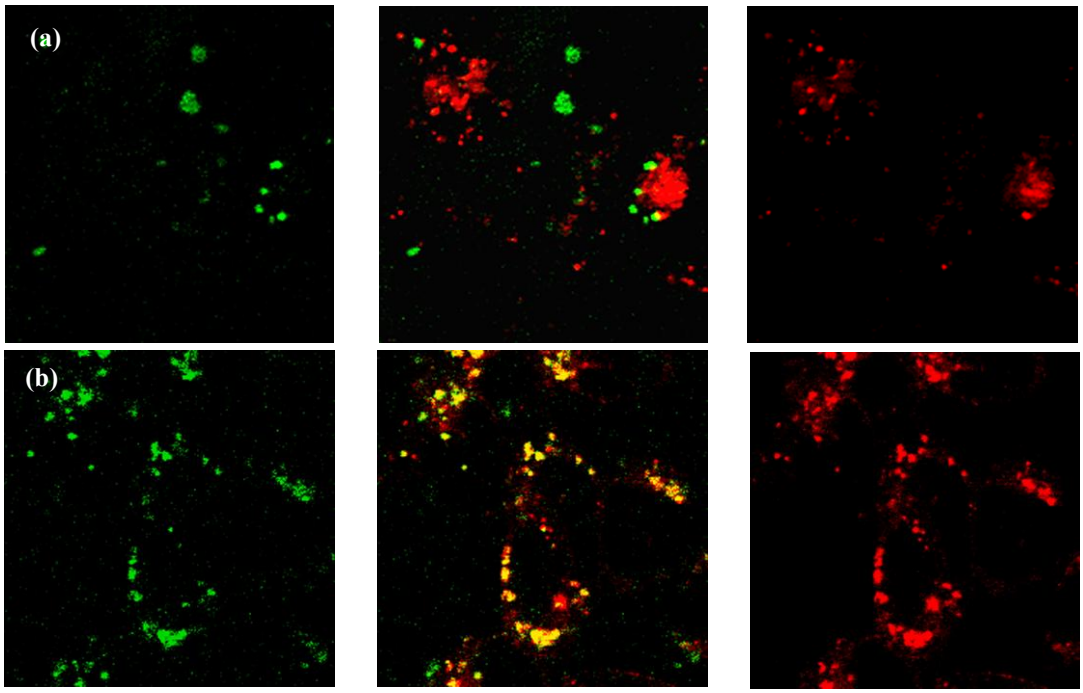

Appendix: Supporting information

1. Experimental:

1.1. Materials

Tetraethylorthosilicate was purchased from Gelest. 3-aminopropyltrimethoxysilane, 3-[*N*-(2-amino-ethyl)amino]propyltrimethoxysilane, fluorescein isothiocyanate isomer I, folic acid, 1-*H*-pyrazole carboxamidine hydrochloride, diisopropyl ethylamine, and *N*-ethyl-*N*-(3-dimethylaminopropyl)carbo-diimide hydrochloride were purchased from Aldrich. All chemicals were used as received.

1.2. Synthesis of fluorescein isothiocyanate-labeled mesoporous silica nanoparticles (FITC-MSNs)

FITC-MSN was prepared by reacting 500 mg (1.11 mmol) of fluorescein isothiocyanate with 0.2 mL (1.15 mmol) of (3-aminopropyl)trimethoxysilane (APTMS) for 2 h. The resulting product was introduced to a co-condensation reaction of 10.0 mL (43.9 mmol) tetraethylorthosilicate (TEOS), 2.04 g (5.32 mmol) cetyltrimethylammonium bromide (CTAB), 960 mL water, and 7.0 mL sodium hydroxide (2 M). The reaction mixture was heated at 80 ºC, under vigorous stirring for 2 h. The resulting orange colored solid was filtered, washed thoroughly with methanol and dried under vacuum for 20 h.

1.3. Synthesis of trimethoxysilylated FAP precursor (FAPTMS)

Following a literature procedure,[1] folic acid (66 mg, 0.15 mmol) was mixed with 150 mg (0.94 mmol) of *N*-ethyl-*N'*(3-dimethylaminopropyl)carbodiimide hydrochloride (EDC) in 10 mL of dimethylsulfoxide. After 30 minutes of stirring, APTMS (30 μL, 0.17 mmol) was added to the solution. The reaction was stirred at room temperature for 4 h. To avoid undesired hydrolysis of the FAPTMS, the DMSO solution was directly used for the grafting reaction described below without purification.

1.4. Synthesis of surface functionalized FITC-MSNs

3-Aminopropyl (AP), 3-[*N*-(2-aminoethyl)amino]propyl (AEAP), and 3-(*N*-folateamino)propyl (FAP) functionalized FITC-MSNs were prepared by grafting 6 mmol of the trimethoxysilylated precursors, APTMS, AEAPTMS (both were purchased from Aldrich), and the aforementioned FAPTMS, respectively, to the surface of FITC-MSN (1 g) in refluxing toluene (100 mL) for 20 h. The resulting materials were filtered, washed with methanol and dried under vacuum for 20 h. The success of the surface functionalization and the quantification of organic groups were examined by solid-state ^{13}C and ^{29}Si NMR spectroscopy (Section 2.4).

1.5. Removal of the CTAB surfactant from the organically functionalized FITC-MSNs

The CTAB surfactant was removed from each of the aforementioned materials by heating the mixture of 1.0 g of the MSN material in 100 mL of methanol and 1.0 mL of concentrated

[1]. Leamon, C.P.; Low, P.S. *Proc. Natl. Acad. Sci. USA* **1991**, *88*, 5572-5576.

hydrochloric acid for 6 h at 60 ºC. The surfactant-removed materials were centrifuged, washed several times with methanol and dried under vacuum for 20 h.

1.6. Synthesis of GP- and GEGP-functionalized FITC-MSNs

GP-functionalized FITC-MSN: 3-Guanidiniopropyl (GP) derivatized FITC-MSN was prepared by stirring 0.5 g of the surfactant-removed AP-MSN with 0.3 g (2.0 mmol) of 1-*H*-pyrazole carboxamidine hydrochloride (HPCA), 0.36 mL (2.1 mmol) diisopropyl ethylamine in 5 mL of dimethylformamide (DMF) for 24 h. The resulting material was centrifuged, washed with methanol and dried under vacuum for 20 h.

GEGP-functionalized FITC-MSN: 3-[*N*-(2-guanidinioethyl)guanidinio]propyl (GEGP) derivatized FITC-MSN was prepared by stirring 0.5 g of the surfactant-removed AEAP-MSN with 0.6g (4.0 mmol) of 1-*H*-pyrazole carboxamidine hydrochloride (HPCA), 0.72 mL (4.1 mmol) diisopropyl ethylamine in 5 mL of dimethylformamide (DMF) for 24 h. The resulting material was centrifuged, washed with methanol and dried under vacuum for 20 h.

2. Characterizations

2.1. Nitrogen adsorption/desorption isotherms

Surface analysis of the materials was performed by nitrogen sorption isotherms in a Micromeritics ASAP2000 sorptometer. The surface areas were calculated by the Brunauer-Emmett-Teller (BET) and the pore size distribution were calculated by the Barrett-Joyner-Halenda method.

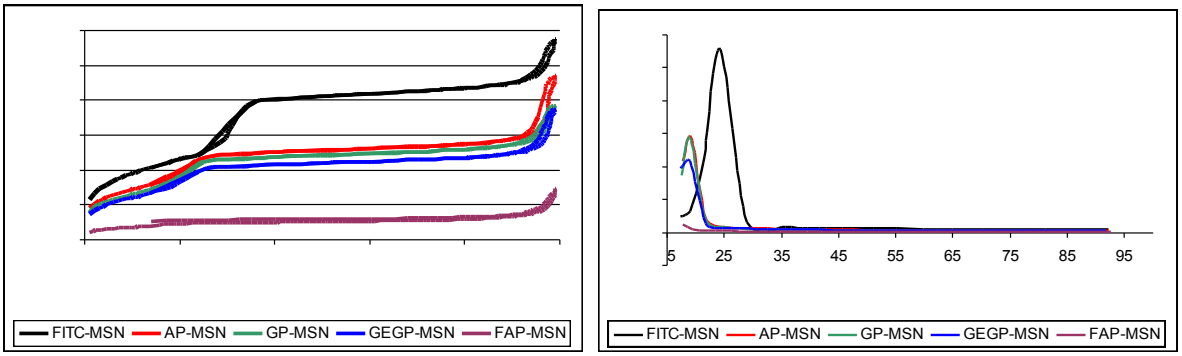

Figure S1. BET nitrogen adsorption/desorption isotherms (left), and BJH pore size distribution (right) of the MSN materials.

Table S1. Surface properties of the MSN materials

Material	BET Surface Area [m^2/g]	Average Pore Width [Å]	Pore Volume [cm^3/g]
FITC-MSN	850	24	0.799
AP-MSN	706	19	0.636
GP-MSN	645	19	0.570
GEGP-MSN	623	19	0.522
FAP-MSN	177	<17	0.195

2.2. Powder X-ray diffraction

X-ray diffraction patterns were obtained in a Scintag XDS-2000 powder diffractometer using Cu Kα irradiation. All of the materials exhibit the hexagonal mesoporous structure, which is typical of MCM-41 with the characteristic (100) peak between 2.10 and 2.20 degrees (2θ). The high ordered (110) and (200) peaks are also observed in these organically functionalized FITC-MSNs.

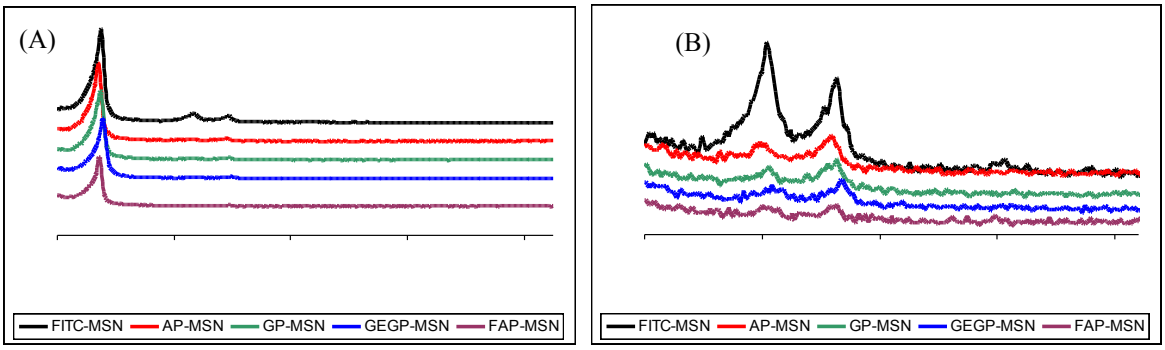

Figure S2. **(A)** The X-Ray diffraction patterns of the prepared materials from 1.5 to 10 degrees (2θ). **(B)** Enlarged view of the (110) and (200) peaks between 2.7 and 7.0 degrees (2θ).

2.3. ζ-Potential measurement

The ζ-potentials of these MSN materials were measured in a Malvern Nano HT Zetasizer. Each material was tested in triplicate. Suspensions (200 μg/mL) of each material in PBS buffer were prepared. The pH of the PBS buffer was 7.69 (40 mg KCl, 40 mg KH_2PO_4, 1.600g NaCl and 0.432g $Na_2HPO_4 \cdot 7H_2O$ per liter of nanopure water.) The ζ-potential was measured immediately after ultrasonication for 15 min. For the ζ-potential measurements of FITC-, AP- and FAP-MSN, 30 scans were taken per sample, while for the ζ-potential measurement of GP- and GEGP-MSN, the number of scans was reduced to 10 to avoid any

deposition of the GP- and GEGP-MSNs on the surface of electrodes. Figure S3 shows zeta-potential graphs.

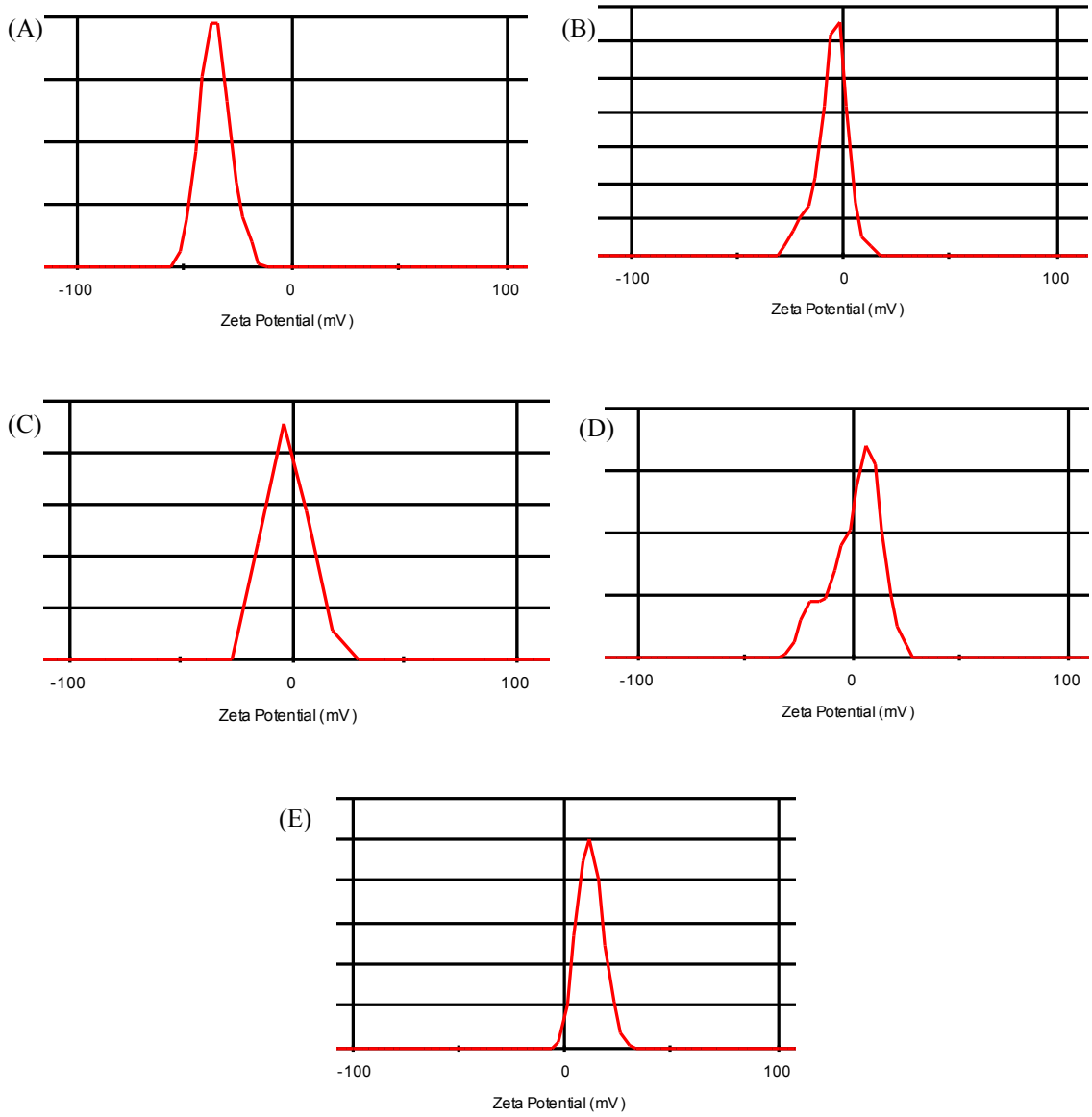

Figure S3. ζ-potential graphs of **(A)** FITC-MSN, **(B)** AP-MSN, **(C)** GP-MSN, **(D)** GEGP-MSN, and **(E)** FAP-MSN in 10 mM PBS buffer pH 7.69.

2.4. Solid state NMR

Solid-state ^{13}C and ^{29}Si crossed polarization and direct polarization magic angle spinning NMR (CP- and DP-MAS NMR) measurements of MSNs were conducted by using a Bruker MSL-300 spectrometer with a Bruker 4 mm rotor MAS probe.

2.4.1. MAS ^{13}C-NMR

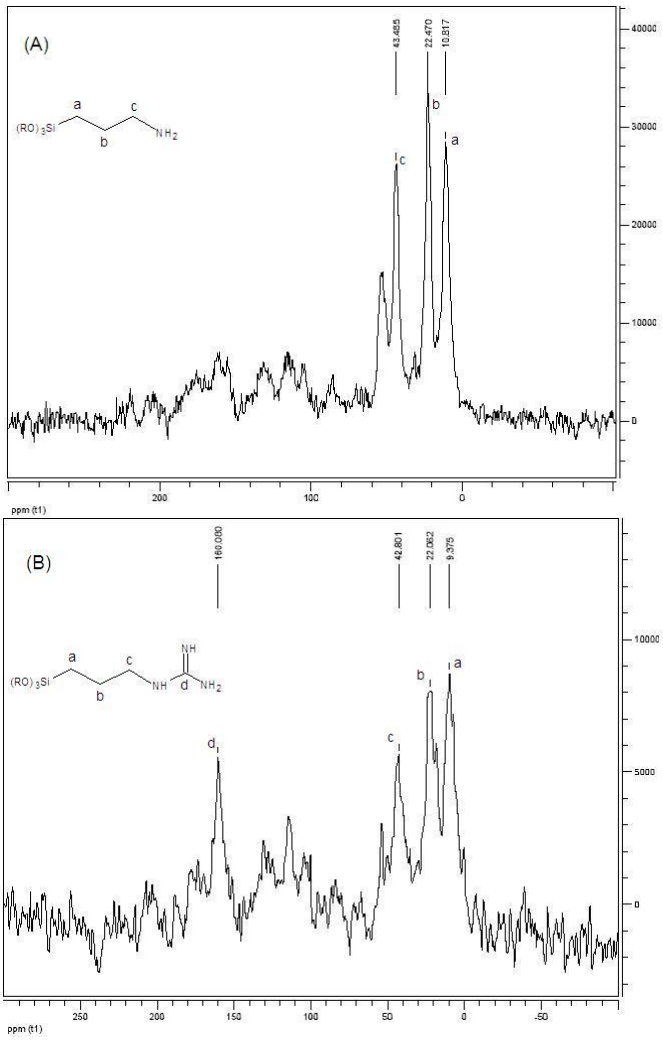

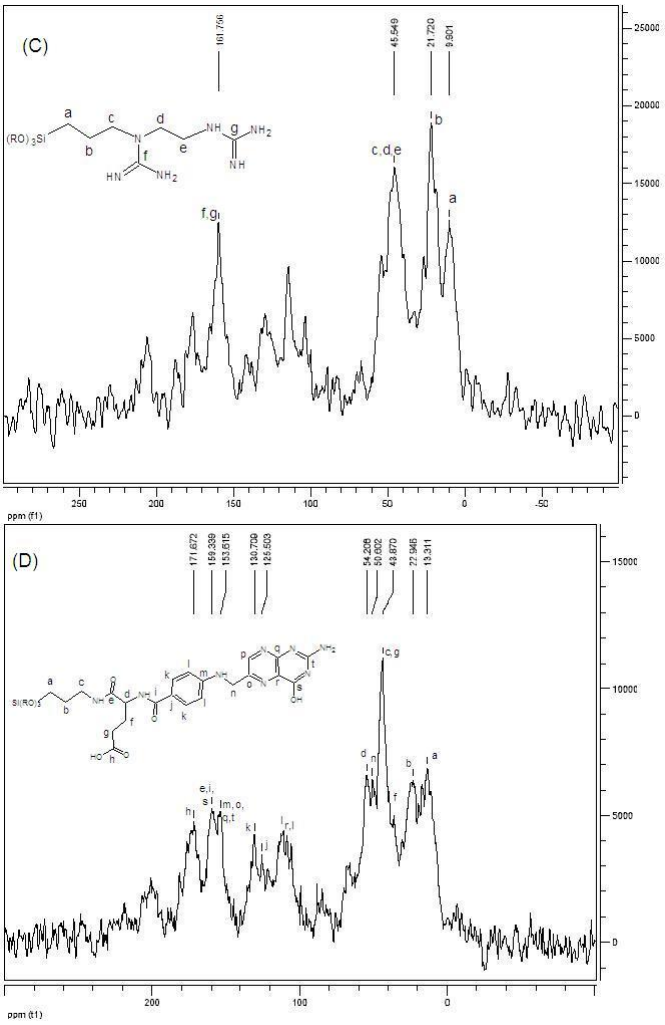

Figure S4. $^{1}H \rightarrow ^{13}C$ cross polarization (CP) solid-state NMR spectra of the functionalized materials: (A) AP-MSN, (B) GP-MSN, (C) GEGP-MSN and (D) FAP-MSN.

All spectra showed a small signal around 50 ppm, which is due to surface-adsorbed methanol from the washings. The smaller signals between 80 and 160 ppm correspond to the co-condensed FITC-APTMS. The signals at 160 and 161 ppm in (B) and (C), respectively, correspond to the guanidine carbons. No peaks of residual CTAB surfactant were observed in these measurements.

2.4.2. MAS DP ^{29}Si-NMR

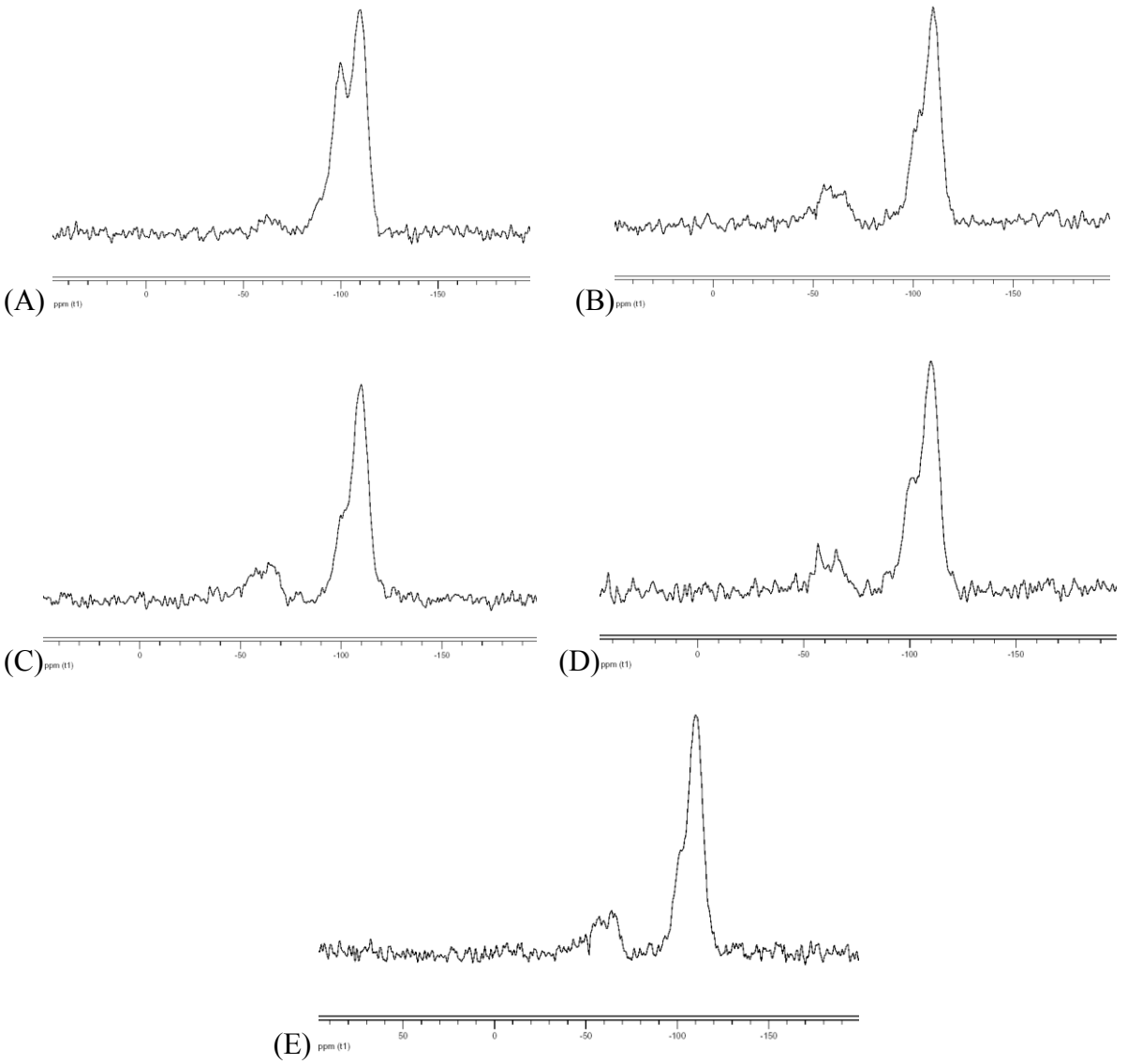

Figure S5. Direct polarization (DP) solid-state ^{29}Si-NMR spectra of all the materials: (A) FITC-MSN, (B) AP-MSN, (C) GP-MSN, (D) GEGP-MSN and (E) FAP-MSN.

Table S2. Composition of the materials as calculated from the DP ^{29}Si-NMR analysis.

Material	Formula	Loading [mmol/g]
FITC-MSN	$(SiO_2)_{100}(H_2O)_{25}(FITC^*)_5$	0.575
AP-MSN	$(SiO_2)_{100}(H_2O)_{13}(FITC)_5(C_3H_6NH_2)_{14}$	1.507
GP-MSN	$(SiO_2)_{100}(H_2O)_7(FITC)_5(C_3H_6NHC(NH)NH_2)_{13}$	1.344
GEGP-MSN	$(SiO_2)_{100}(H_2O)_{12}(FITC)_5(C_3H_6N(CNHNH_2)C_2H_4NHC(NH)NH_2)_{10}$	0.970
FAP-MSN	$(SiO_2)_{100}(H_2O)_5(FITC)_5(C_3H_6NHC_{19}H_{18}N_7O_5)_{13}$	0.891

* FITC = $C_3H_6NHSC_{21}H_{11}NO_5$

2.5. Scanning electron microscopy

Particle morphology was investigated by using a JEOL 840A scanning electron microscope with a 10 kV acceleration voltage.

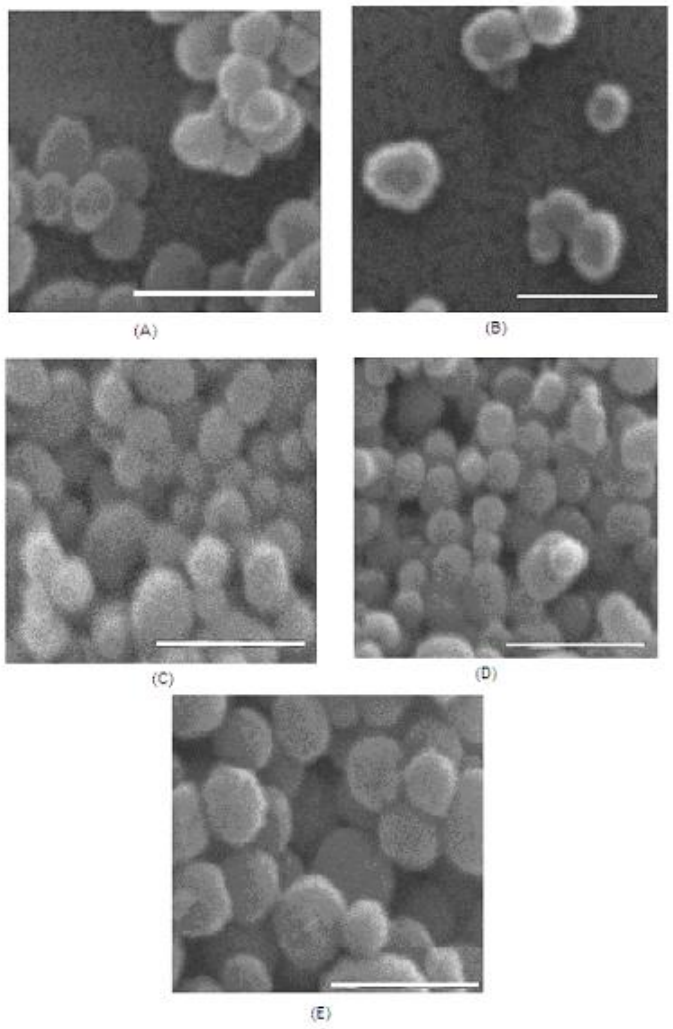

Figure S6. Scanning electron micrographs (SEMs) of (A) FITC-MSN, (B) AP-MSN, (C) GP-MSN, (D) GEGP-MSN, and (E) FAP-MSN. The scale bars are 500 nm. These materials are spherical particles ranging from 100 to 250 nm in diameter.

3. Measurement of uptake of the materials by HeLa cells

The cellular uptake profiles of all MSNs were examined by FACS flow cytometry and fluorescence confocal microscopy.

3.1. Flow cytometry

For the flow cytometry assays, HeLa cells were seeded in six well plates with a density of 1 × 10^5 cells/mL in 3 mL of D-10 medium. The D-10 medium is a Dubelcco modified Eagle's medium (DMEM) containing 10% equine serum, *L*-alanylglutamine, gentamicin, and penicillin/streptomycin. After 34 h incubation, the D-10 medium was replaced by 3 mL of MSN suspensions at different concentrations ranging from 0.1 to 40 μg/mL in the serum-free DMEM medium for 10 h. Different concentrations of MSN suspensions were tested. All the tests were run in triplicate. The cells were washed then with medium and harvested by trypsinization. After centrifugation the cell pellets were resuspended in 0.4 % trypan blue PBS solution, and analyzed by flow cytometry with a Becton-Dickinson FACSCanto cytometer and BD-FACS Diva software.

To distinguish the true fluorescence generated by the FITC-MSN from the natural autofluorescence of cells, a threshold of fluorescence intensity was established by performing the flow cytometry analysis on HeLa cells incubated without any MSN. The threshold was set at a fluorescence intensity slightly above the highest value observed for control samples (HeLa Cells only). The number of cells with encytosed MSNs was determined by counting the cells showing fluorescence intensity higher than the threshold.

3.2. Inhibition and competition assays

HeLa cells were seeded at the density of 1×10^5 cells/mL in 6 well plates and allowed to attach for 48 h in 3 mL of D-10 medium. The D-10 medium was then replaced by 3 mL of: (a) DMEM medium for the wells used as control, (b) 1 mM folic acid in DMEM medium for the wells used in the competition assay, and (c) 450 mM sucrose in DMEM medium for the wells used in the clathrin inhibition assay. The cells were left in contact with the media for 30 min. The media were then replaced with 3 mL of MSN (40 μg/mL) in: (a) DMEM medium for the control, (b) 1 mM folic acid in DMEM medium for the competition assay, and (c) 450 mM sucrose in DMEM medium for the clathrin inhibition assay. After 1 h, the cells were washed with DMEM medium and harvested by trypsinization. After centrifugation, the cell pellets were resuspended in 0.4% trypan blue PBS solution, and analyzed by flow cytometry with a Becton-Dickinson FACSCanto cytometer and BD-FACS Diva software.

3.3 Cell growth and viability assays

Cell growth and viability of the HeLa cells in the presence and absence of MSN were studied by Guava ViaCount assay (Guava Technologies, Inc.; Hayward, CA). For that purpose HeLa cells were seeded in four six well plates with a density of 1×10^5 cells/mL in 3 mL of D-10 medium containing (a) no MSNs, (b) FITC-MSN, (c) AP-MSN, (d) GP-MSN, (e) GEGP-MSN and (f) FAP-MSN. The concentration of the MSNs in the culture media was 40 μg/mL. After seeding them the plates were set in an incubator at 37°C and 5% CO_2 and every other day, for a lapse of four days, one plate was removed from the incubator, the

media of each well was discarded, each well was washed with fresh D-10 medium and the cells trypsinized, centrifuged and resuspended in D-10 medium. The cells in the resuspended media were then counted and their viability determined by the Guava ViaCount cytometry assay. Figure S7 shows the results of the cell counts at every day, the viability was found to be between 90 and 100 %.

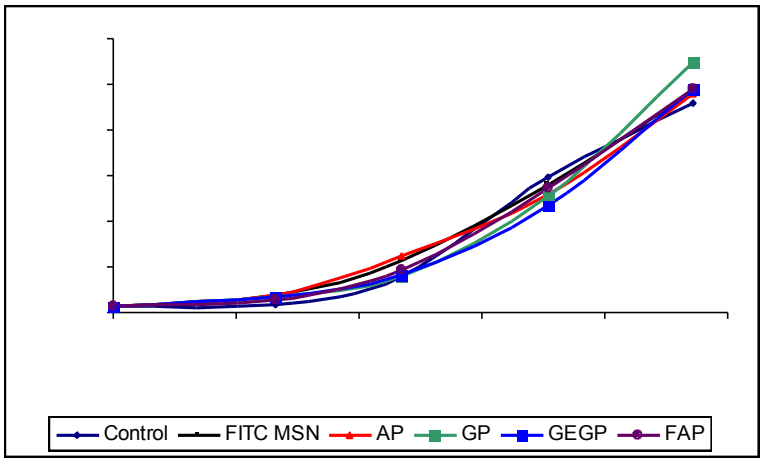

Figure S7. Cell counts performed with Guava ViaCount assay after incubation at different times in absence and in presence of 40 μg/mL of the MSNs in D-10 media.

3.4. Confocal fluorescence microscopy

3.4.1. Localization of the MSNs inside the cells

For confocal fluorescence microscopy measurements, HeLa cells were seeded at the density of 1×10^5 cells per well in 6 well plates in 3 mL D-10 medium with coverslips at the bottom of the wells. After 34 h incubation, the D-10 medium was replaced by 3 mL of MSNs (40 μg/mL) in the serum-free DMEM medium for 10 h. The cell-plated coverslips were then washed with medium and soaked for 30 min in 3 mL of 0.4 % trypan blue in 100 mM PBS buffer (pH 7.4). The trypan blue solution was then replaced by a solution of 5.7 μM 4',6-Diamidino-2-phenyindole (DAPI) and 3.7 % formaldehyde in 100 mM PBS buffer pH 7.44. The DAPI-stained coverslips were placed in microscope slides and examined under a Leica TCS NT confocal fluorescence microscope system using a 100x oil immersion objective. As depicted in Figure S8, the blue fluorescent, DAPI-stained nuclei (right images) were clearly observed by exciting the cells with a UV laser at wavelengths from 340 to 458 nm. The green fluorescent FITC-MSN particles inside of the HeLa cells (middle images) were visualized by excitation at 488nm with an Argon Laser and the phase contrast images of the cells (left images) were obtained with a 568nm Krypton laser.

Figure S8. (See next page) Confocal fluorescence images of HeLa cells loaded with the different organically functionalized MSNs: (A) FITC-MSN, (B) AP-MSN, (C) GP-MSN, (D) GEGP-MSN, and (E) FAP-MSN. The left images were taken with a Krypton laser source, the ones in the middle showed the endocytosed green fluorescent FITC-labeled MSN particles (Argon laser) and the right images exhibited the blue fluorescent, DAPI-stained nuclei (UV laser).

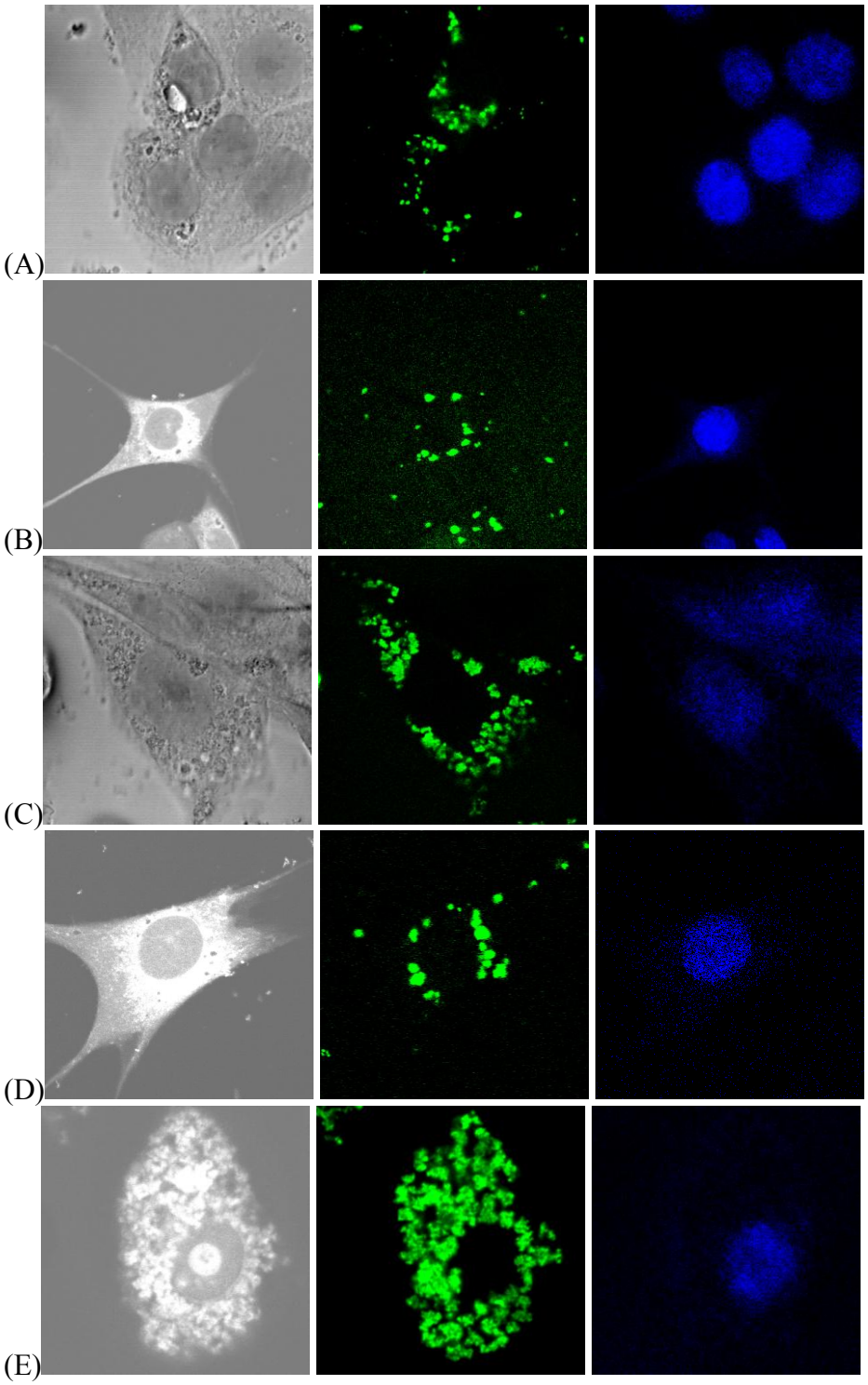

3.4.2. Localization of the MSNs inside the cells in presence of an endosome marker

HeLa cells were seeded at the density of 1×10^5 cells per well in 6 well plates in 3 mL D-10 medium with coverslips at the bottom of the wells. After 38 h incubation, the D-10 medium was replaced by 3 mL serum-free DMEM medium containing MSNs (40 µg/mL) and the endosome marker FM 4-64 (10µg/mL) and incubated for 6 h. The cell-plated coverslips were then washed with medium and soaked for 30 min in 3 mL of 0.4 % trypan blue in 100 mM PBS buffer (pH 7.4). The trypan blue solution was then replaced by a solution of 5.7 µM 4',6-Diamidino-2-phenyindole (DAPI) and 3.7 % formaldehyde in 100 mM PBS buffer pH 7.44. The DAPI-stained coverslips were placed in microscope slides and examined under a Leica TCS NT confocal fluorescence microscope system using a 100x oil immersion objective. Both, the MSNs and the endosome marker were excited at 488 nm with an Argon Laser, the MSNs were detected at wavelengths in the 515 to 590 nm range (observed green) while the endosome marker was detected at wavelengths in the 590 to 750 nm range (observed red). MSNs are considered to be inside of the endosomes in the spots where the green and the red spots are co-localized to give a yellow color. The phase contrast images of the cells (right images) were obtained with a 568nm Krypton laser.

Figure S9. (See next page) Confocal fluorescence images of HeLa cells loaded with the different organically functionalized MSNs: (A) FITC-MSN, (B) AP-MSN, (C) GP-MSN, (D) GEGP-MSN, and (E) FAP-MSN, and stained with the endosome marker FM 4-64. The images to the right were taken with a Krypton laser source, and the ones to the left show the Argon laser excited endocytosed green fluorescent FITC-labeled MSNs, the red fluorescent marked endosomes, and the yellow spots where the MSNs and endosomes are colocalized.

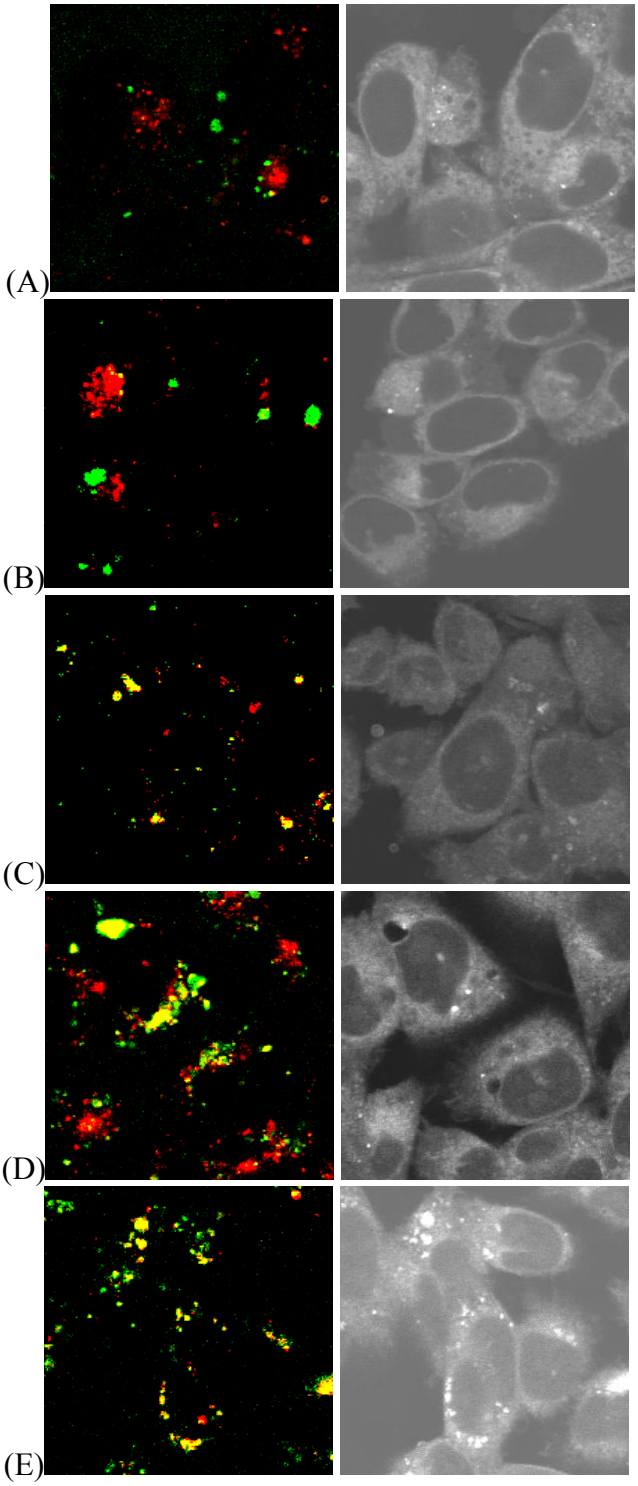

CHAPTER 4. MESOPOROUS SILICA NANOPARTICLES FOR INTRACELLULAR DELIVERY OF MEMBRANE-IMPERMEABLE PROTEINS

A paper published in the ***Journal of the American Chemical Society***,

2007, *129*, 8845-8849.

Igor I. Slowing, Brian G. Trewyn and Victor S.-Y. Lin

Abstract

A MCM-41 type mesoporous silica nanoparticle (MSN) material with a large average pore diameter (5.4 nm) is synthesized and characterized. The *in vitro* uptake and release profiles of cytochrome *c* by the MSN were investigated. The enzymatic activity of the released protein was quantitatively analyzed and compared with that of the native cytochrome *c* in physiological buffer solutions. We found that the enzymes released from the MSNs are still functional and highly active in catalyzing the oxidation of 2,2'-azino-bis(3-ethylbenzthiazoline-6-sulfonate) (ABTS) by hydrogen peroxide. In contrast to the fact that cytochrome *c* is a cell-membrane impermeable protein, we discovered that the cytochrome *c* encapsulated MSNs could be internalized by live human cervical cancer cells (HeLa) and the protein could be released into the cytoplasm. We envision that these MSNs with large pores could serve as a transmembrane delivery vehicle for controlled release of membrane impermeable proteins in live cells, which may lead to many important biotechnological applications including therapeutics and metabolic manipulation of cells.

Introduction

Recent breakthroughs in the synthesis of mesoporous silica materials with high surface areas (> 800 m^2/g) and tunable pore diameter (2-10 nm) have led to the developments of a series of new delivery systems, where various guest molecules, such as pharmaceutical drugs, fluorescent imaging agents, and other molecules, could be adsorbed into the mesopores and later released into various solutions.[1-4] Furthermore, recent reports on the design of functional mesoporous silica materials by decorating the pore surface with organic or inorganic moieties that could serve as gating devices to regulate the release of guest molecules under the control of several different external stimuli, such as chemicals,[5-9] temperature,[10] redox reactions,[11,12] and photo-irradiation,[13,14] have highlighted the potential of utilizing this kind of nanodevices for many controlled release applications.

To further advance this burgeoning field of research and to use these mesoporous materials in practical biotechnological and biomedical applications, one key step would be to gain control of the particle morphology and the surface properties of these inorganic oxides, so that the compatibility with biological macromolecules, such as polynucleotides (DNA and RNA), proteins, and live cells can be enhanced. We and others have demonstrated that, by controlling the particle size, shape, and surface functionality of the mesoporous silicas, these structurally defined materials can be efficiently endocytosed by live cells with high biocompatibility *in vitro* and serve as delivery vehicles for the controlled release of genes and membrane impermeable chemicals.[3,5-7]

Also, several enzymes have been shown to be functional without being denatured inside the frameworks of mesoporous silicas, such as MCM-41 and SBA-15 silicas.[15-23] However, to

the best of our knowledge, there were only two prior reports on the controlled release of proteins from SBA-15 type mesoporous silica materials under non-physiological conditions.[24,25] Since the intracellular delivery of membrane impermeable proteins is an important research topic for understanding metabolic pathways of different cell types as well as for therapeutic applications, different cell penetrating molecular agents and materials, such as peptides,[26,27] polymers,[28] and carbon nanotubes,[29-31] have been employed as carriers for this purpose with different degrees of success. For example, single wall carbon nanotubes have been demonstrated recently to be able to deliver a cell-membrane impermeable protein, cytochrome *c*, into cells. However, the protein-nanotube composites were unable to escape endosomal entrapment without the introduction of an endosome-disrupting agent, chloroquine, to the cells.[29] In contrast to these prior systems, there are several advantages of using mesoporous silicas for intracellular protein delivery: (1) The large pore volumes (> 1 cm^3/g) of mesoporous silicas allow for loading vast, yet quantifiable, amounts of proteins into the particles. (2) The chemically and mechanically stable inorganic oxide framework of mesoporous silicas shelters the protein molecules from exposure to harmful species, such as proteases and denaturation chemicals. (3) It has been previously observed that mesoporous silica nanoparticles are able to escape the endo-lysosomal entrapment.[32-34] Therefore, the particles could serve not only as vehicles for introducing the proteins into the cells, but also to enable their release into the cytoplasm.

Herein, we report on the synthesis and characterization of a MCM-41 type mesoporous silica nanoparticle (MSN) material with a large pore diameter (5.4 nm). The uptake and release profiles of cytochrome *c* by the MSN were investigated. To examine whether the

encapsulation causes any harmful effect to cytochrome *c*, we analyzed the enzymatic activity of the pore-released protein and compared with that of the native cytochrome *c* in physiological buffer solutions. In addition, we discovered that the cytochrome *c* encapsulated MSNs could be internalized by living human cervical cancer cells (HeLa) and the protein could be released into the cytoplasm as depicted in Figure 1.

Results and discussion

As detailed in the supporting information, we synthesized MSN with large pores by adding a pore-expanding agent (mesitylene) to a CTAB-templated, base-catalyzed condensation reaction of silicate that we have previously reported.[35] The template-removed mesoporous silica nanoparticle material is comprised of a MCM-41 type, hexagonal array of mesoporous channels as shown in the transmission electron micrographs (Figure 2 and Figure SI 1). The powder X-ray diffraction pattern (XRD) further confirmed the hexagonal mesoporous structure (Figure SI 2a) with the d_{100} value of 71.8 Å, d_{110} of 40.8 Å, d_{200} of 35.1 Å and d_{210} of 26.2 Å. The nitrogen surface sorption analysis of the material exhibited a Type IV isotherm with a BET surface area of 1061 m^2/g and a pore volume of 1.82 cm^3/g (Figure SI 2b). The BJH method gave two pore size distributions centered on 5.4 nm (major peak) and 14.5 nm (minor) (Figure SI 2c). Of both pore distributions, the wider ones (> 10 nm) appear to correspond to incomplete wall formation in the outermost layer of some particles, as observed by TEM imaging (Figures 2b and SI 1). Thus, the wider pores seem to be entrances shared by two or more of the smaller channel-type pores that run along the particles. The particle size of MSN in PBS suspension was measured by dynamic light scattering. Two

different particle size distributions (265 and 933 nm) were observed (Figure SI 3). These particles are spherical and oval-shaped as shown in Figure 2.

We found that the loading of cytochrome *c* (molecular dimensions 2.6 × 3.2 × 3.3 nm)[17,36] into the MSN was dependent to the solution concentrations of cytochrome *c*, which indicated that the encapsulation is a diffusion driven process. As described in the supporting information, the amount of protein entrapped inside the MSN was determined by measuring the difference in concentration of cytochrome *c* in the supernatant before and after the loading of MSN. The maximum loading was determined to be 415.0 mg of cytochrome *c* per 1.0 gram of MSN at the conditions studied. The XRD of a cytochrome *c* encapsulated MSN with a loading of 95.0 mg/g MSN could still exhibit the hexagonal symmetry of the porous structure with a lower contrast because of the pore-filling effect (Figure SI 4a). Also, the entrapment of cytochrome *c* inside the mesopores was observed in the nitrogen sorption analysis, where the BET surface area decreased from 1061 to 290 m^2/g and the pore volume reduced from 1.82 to 0.19 cm^3/g upon loading with cytochrome *c* at 95 mg/g (Figure SI 4b).

The release of cytochrome *c* from the MSN material at room temperature was studied by measuring the UV-Vis absorption profile of the Soret band (412 nm) of cytochrome *c* in supernatant after separation of the solid MSNs by centrifuge. Two suspensions of cytochrome *c*-loaded MSN (100 μg/mL) were prepared in PBS buffer at two different pH values (7.4 and 5.2). These numbers were chosen to mimic the normal pH values in the cytoplasm and inside endosomes.[37,38] In both cases, a sigmoidal release curve was observed over a period of 25 h, which is characteristic of an energy-dependent release process. The total percent of loaded proteins that were released were 45% and 55% at pH 7.4 and 5.2,

respectively (Figure 3). Given that the pI of cytochrome *c* is 10.5 and that the surface of MSN is rich in silanol groups (pK_a around 3), the protein is expected to be positively charged, while the MSN would be negatively charged at both pH values. Therefore, for cytochrome *c* molecules to be released from the mesopores, the favorable electrostatic interactions between the protein and the pore-surface silicates need to be replaced by other ionic species in the solution similar to what has been observed in the literature.[15,16,24] The observed difference in the rates of release (Figure 3) at these two pH values could be attributed to the different amount of negative charges on the MSN surface. To test this hypothesis, we measured the change of the ζ-potential of both MSN and cytochrome *c* as a function of pH (Figure SI 5). As expected, the ζ-potential of the protein remained almost constant, with very little change (between +15 and + 17 mV) between pH 5.5 to 8.0, whereas the ζ-potential of MSN dropped dramatically from -25.5 mV at pH 7.35 to -1.81 mV at pH 5.22. This confirmed the surface charge property of MSN was indeed affected by the change in pH.

As shown in Figure 3, no significant release of cytochrome *c* from MSN was observed at pH 7.4 even after 4 h, while some release was observed immediately at pH 5.2. This difference in the rate of release of cytochrome *c* allows us to introduce the protein-loaded MSN to cell cultures under the physiological condition without losing a large amount of protein in the first 4 h. Based on the previous studies by us and others,[32-34] human cancer and other animal cells are able to internalize MSN materials within 1 h. The resulting endosome-entrapped protein-MSN material could then release cytochrome *c* molecules inside the cell.

To examine whether the MSN-released cytochrome *c* can still function as an active enzyme, we collected proteins that were released at pH 7.4 and tested the catalytic reactivity for the oxidation of 2,2'-azino-bis(3-ethylbenzthiazoline-6-sulfonate) (ABTS) by hydrogen peroxide. We compared the enzymatic activity of the MSN-released cytochrome *c* with that of the native protein at the same concentration and under the same conditions as described in the supporting information. As depicted in Figure 4, the kinetics of the two enzyme-catalyzed reactions are essentially identical, indicating that the MSN-released cytochrome *c* could serve as an active enzyme in aqueous solutions.

To exploit MSN as a transmembrane delivery carrier for intracellular controlled release of cytochrome *c*, we first covalently attached a fluorescent dye, fluorescein isothiocyanate (FITC), to the protein via a literature reported procedure.[39] The labeling efficiency was determined to be 1.8 moles of FITC per mole of cytochrome *c* by UV-Vis absorption spectroscopy. The fluorescein-labeled cytochrome c was then encapsulated inside the MSN by the aforementioned method described in the supporting information. The resulting cytochrome *c*-loaded MSNs were introduced to HeLa cell cultures with the cell density of 1×10^5 cells/mL in D-10 growth medium. The uptake of the protein-MSN material by HeLa cancer cells was analyzed by flow cytometry. As shown in Figure 5, the flow cytometry result exhibited an efficient uptake with an EC_{50} of 33.6 μg/mL. The cellular uptake of the material was also confirmed by confocal fluorescence microscopy. The uptake of MSN observed in this work is lower than the one we observed previously for MSN of smaller pore size (EC_{50} of 12.4 μg/mL).[34] This difference in uptake efficiency can be attributed mainly to the difference in particle size, for the smaller pore MSN has an average size around 150 nm,

while the pore enlarged MSN are larger than that. It has been previously reported that an increase in the size of sub-micron particles usually leads to a decrease in the ability of cells to take them up.[40] To determine whether or not the cytochrome *c*-loaded MSNs could escape the endosomal entrapment, we stained the endosomes with a red fluorescent endosome marker (FM 4-64)[41] and monitored the confocal fluorescence micrographs (Figure 6) of FITC-cytochrome *c*-loaded MSNs in HeLa cells. The green fluorescent spots observed in Figure 6 represent the FITC-cytochrome *c*-loaded MSNs that were able to escape endosomes, whereas those that were entrapped inside of the vesicles exhibited yellow in color, which is the result of overlapping red (endosome) and green (FITC-cytochrome *c* loaded MSN) spots. As depicted in Figure 6a, there were a few FITC-cytochrome *c*-loaded MSNs trapped inside of endosomes within the first 2 h. However, as shown in Figures 6b and c no yellow spots could be observed in the micrographs indicating that there was no overlap between the green fluorescent FITC-cytochrome *c* and the red fluorescent endosomes. Our results clearly show that the FITC-cytochrome *c* could escape from the endosomes efficiently within a few hours of endocytosis. Interestingly, after 18 h of incubation, we observed an increasing number of HeLa cells displaying green fluorescence throughout their entire cell bodies (Figure 7) in addition to others that showed only isolated spots of green fluorescence inside the cytoplasm. Also, as depicted in Figure 7a, several spots with higher fluorescence intensities (FITC-cytochrome *c* loaded MSN) could be observed inside the cell that displayed green fluorescence in the whole body. These spots faded away with time as the green fluorescence intensified throughout the whole cell body (Figure 7b). These results suggested that the

fluorescein-labeled cytochrome *c* molecules were gradually released from the conglomerates of MSNs and were able to diffuse throughout the entire cytoplasm.

Conclusion

In summary, we have demonstrated that the mesoporous silica nanoparticles with large pores can host small membrane impermeable proteins, such as cytochrome *c*, and release them under physiological conditions. Like the native cytochrome *c*, the protein released from MSNs could also function as an active enzyme for oxidation reactions in aqueous solutions. These MSNs could serve as efficient transmembrane carriers to deliver cytochrome *c* into the cytoplasm of human cervical cancer cells (HeLa), while avoiding the endosomal entrapment. The intracellular release of the fluorescein-labeled cytochrome *c* was also observed by confocal fluorescence microscopy. Further development of these MSN-based controlled release systems for protein delivery may lead to breakthroughs for many therapeutics and metabolic manipulation applications.

Acknowledgment. The authors thank the financial support for this research from the U.S. National Science Foundation (CHE-0239570) and from the U.S. DOE Ames Laboratory through the office of Basic Energy Sciences under Contract No. DE-AC02-07CH11358.

References

(1) Gruenhagen, J. A.; Lai, C.-Y.; Radu, D. R.; Lin, V. S. Y.; Yeung, E. S. *Appl. Spectrosc.* **2005**, *59*, 424-431.

(2) Horcajada, P.; Ramila, A.; Perez-Pariente, J.; Vallet-Regi, M. *Microporous Mesoporous Mater.* **2004**, *68*, 105-109.

(3) Trewyn, B. G.; Whitman, C. M.; Lin, V. S. Y. *Nano Lett.* **2004**, *4*, 2139-2143.

(4) Balas, F.; Manzano, M.; Horcajada, P.; Vallet-Regi, M. *J. Am. Chem. Soc.* **2006**, *128*, 8116-8117.

(5) Giri, S.; Trewyn, B. G.; Stellmaker, M. P.; Lin, V. S. Y. *Angew. Chem., Int. Ed. Engl.* **2005**, *44*, 5038-5044.

(6) Lai, C.-Y.; Trewyn, B. G.; Jeftinija, D. M.; Jeftinija, K.; Xu, S.; Jeftinija, S.; Lin, V. S. Y. *J. Am. Chem. Soc.* **2003**, *125*, 4451-4459.

(7) Radu, D. R.; Lai, C.-Y.; Jeftinija, K.; Rowe, E. W.; Jeftinija, S.; Lin, V. S. Y. *J. Am. Chem. Soc.* **2004**, *126*, 13216-13217.

(8) Leung, K. C. F.; Nguyen, T. D.; Stoddart, J. F.; Zink, J. I. *Chem. Mater.* **2006**, *18*, 5919-5928.

(9) Nguyen, T. D.; Leung, K. C. F.; Liong, M.; Pentecost, C. D.; Stoddart, J. F.; Zink, J. I. *Org. Lett.* **2006**, *8*, 3363-3366.

(10) Fu, Q.; Rao, G. V. R.; Ista, L. K.; Wu, Y.; Andrzejewski, B. P.; Sklar, L. A.; Ward, T. L.; Lopez, G. P. *Adv. Mater. (Weinheim, Ger.)* **2003**, *15*, 1262-1266.

(11) Hernandez, R.; Tseng, H.-R.; Wong, J. W.; Stoddart, J. F.; Zink, J. I. *J. Am. Chem. Soc.* **2004**, *126*, 3370-3371.

(12) Nguyen, T. D.; Tseng, H.-R.; Celestre, P. C.; Flood, A. H.; Liu, Y.; Stoddart, J. F.; Zink, J. I. *Proc. Natl. Acad. Sci. U. S. A.* **2005**, *102*, 10029-10034.

(13) Mal, N. K.; Fujiwara, M.; Tanaka, Y. *Nature (London)* **2003**, *421*, 350-353.

(14) Mal, N. K.; Fujiwara, M.; Tanaka, Y.; Taguchi, T.; Matsukata, M. *Chem. Mater.* **2003**, *15*, 3385-3394.

(15) Deere, J.; Magner, E.; Wall, J. G.; Hodnett, B. K. *J. Phys. Chem. B* **2002**, *106*, 7340-7347.

(16) Diaz, J. F.; Balkus, K. J., Jr. *J. Mol. Catal. B: Enzymatic* **1996**, *2*, 115-126.

(17) Hartmann, M. *Chem. Mater.* **2005**, *17*, 4577-4593.

(18) Vinu, A.; Murugesan, V.; Tangermann, O.; Hartmann, M. *Chem. Mater.* **2004**, *16*, 3056-3065.

(19) Lee, C.-H.; Mou, C.-Y.; Ke, S.-C.; Lin, T.-S. *Mol. Phys.* **2006**, *104*, 1635-1641.

(20) Cheng, Y. Y.; Lin, S. H.; Chang, H. C.; Su, M. C. *J. Phys. Chem. A* **2003**, *107*, 10687-10694.

(21) Katiyar, A.; Ji, L.; Smirniotis, P.; Pinto, N. G. *J. Chromatogr., A* **2005**, *1069*, 119-126.

(22) Lei, J.; Fan, J.; Yu, C.; Zhang, L.; Jiang, S.; Tu, B.; Zhao, D. *Microporous Mesoporous Mater.* **2004**, *73*, 121-128.

(23) Yiu, H. H. P.; Wright, P. A. *J. Mater. Chem.* **2005**, *15*, 3690-3700.

(24) Han, Y.-J.; Stucky, G. D.; Butler, A. *J. Am. Chem. Soc.* **1999**, *121*, 9897-9898.

(25) Song, S. W.; Hidajat, K.; Kawi, S. *Langmuir* **2005**, *21*, 9568-9575.

(26) Ye, D.; Xu, D.; Singer, A. U.; Juliano, R. L. *Pharm. Res.* **2002**, *19*, 1302-1309.

(27) Gros, E.; Deshayes, S.; Morris, M. C.; Aldrian-Herrada, G.; Depollier, J.; Heitz, F.; Divita, G. *Biochim. Biophys. Acta, Biomembranes* **2006**, *1758*, 384-393.

(28) Vicent, M. J.; Duncan, R. *Trends Biotechnol.* **2006**, *24*, 39-47.

(29) Kam, N. W. S.; Dai, H. *J. Am. Chem. Soc.* **2005**, *127*, 6021-6026.

(30) Kam, N. W. S.; Jessop, T. C.; Wender, P. A.; Dai, H. *J. Am. Chem. Soc.* **2004**, *126*, 6850-6851.

(31) Kam, N. W. S.; Liu, Z.; Dai, H. *Angew. Chem., Int. Ed. Engl.* **2006**, *45*, 577-581.

(32) Lin, Y.-S.; Tsai, C.-P.; Huang, H.-Y.; Kuo, C.-T.; Hung, Y.; Huang, D.-M.; Chen, Y.-C.; Mou, C.-Y. *Chem. Mater.* **2005**, *17*, 4570-4573.

(33) Huang, D.-M.; Hung, Y.; Ko, B.-S.; Hsu, S.-C.; Chen, W.-H.; Chien, C.-L.; Tsai, C.-P.; Kuo, C.-T.; Kang, J.-C.; Yang, C.-S.; Mou, C.-Y.; Chen, Y.-C. *FASEB J.* **2005**, *19*, 2014-2016.

(34) Slowing, I.; Trewyn, B. G.; Lin, V. S. Y. *J. Am. Chem. Soc.* **2006**, *128*, 14792-14793.

(35) Huh, S.; Wiench, J. W.; Yoo, J.-C.; Pruski, M.; Lin, V. S. Y. *Chem. Mater.* **2003**, *15*, 4247-4256.

(36) Berman, H. M.; Westbrook, J.; Feng, Z.; Gilliland, G.; Bhat, T. N.; Weissig, H.; Shindyalov, I. N.; Bourne, P. E. *Nucleic Acids Res.* **2000**, *28*, 235-42.

(37) Simoes, S.; Moreira, J. N.; Fonseca, C.; Duzgunes, N.; Pedroso de Lima, M. C. *Adv. Drug Delivery Rev.* **2004**, *56*, 947-965.

(38) Tafani, M.; Cohn, J. A.; Karpinich, N. O.; Rothman, R. J.; Russo, M. A.; Farber, J. L. *J. Biol. Chem.* **2002**, *277*, 49569-49576.

(39) Goding, J. W. *J. Immunol. Methods* **1976**, *13*, 215-26.

(40) Rejman, J.; Oberle, V.; Zuhorn, I. S.; Hoekstra, D. *Biochem. J.* **2004**, *377*, 159-169.

(41) Vida, T. A.; Emr, S. D. *J. Cell Biol.* **1995**, *128*, 779-92.

Figure captions

Figure 1. Schematic representation of the MSN transporting cytochrome *c* through the cell membrane and releasing the protein into the cytoplasm.

Figure 2. Transmission electron micrograph of large-pore MSN.

Figure 3. Release profiles of cytochrome *c* from MSN at pH 7.4 (blue rhombi) and 5.2 (red squares).

Figure 4. Oxidation of 2,2'-azino-bis(3-ethylbenzthiazoline-6-sulfonate) (ABTS) catalyzed by cytochrome *c*. The blue line and markers correspond to a solution of native protein and the red ones to the protein released from the MSN.

Figure 5. Uptake profile of FITC-cytochrome *c* loaded MSN by HeLa cancer cells.

Figure 6. Uptake of FITC-cytochrome *c* loaded MSN by HeLa cancer cells as observed by confocal fluorescence microscopy at the following incubation times: **(a)** 2, **(b)** 14 and **(c)** 24 hours. For each set of pictures the upper left image is the autofluorescence image of the cells, the lower left corresponds to the green fluorescent protein taken up by the cells, the lower right shows the red fluorescent FM 4-64 labeled endosomes, and the upper right image is the merging of the green and red fluorescent images.

Figure 7. Confocal fluorescence images of HeLa cells displaying green fluorescence on their whole cell bodies, after incubation with FITC-cytochrome *c* loaded MSN for: **(a)** 18 and **(b)** 26 hours. The left pictures correspond to the autofluorescence image of the cells when excited at 568 nm, the middle ones to the green fluorescent labeled protein (excitation at 488 nm) and the right ones to the merge of the first two.

Figure 1.

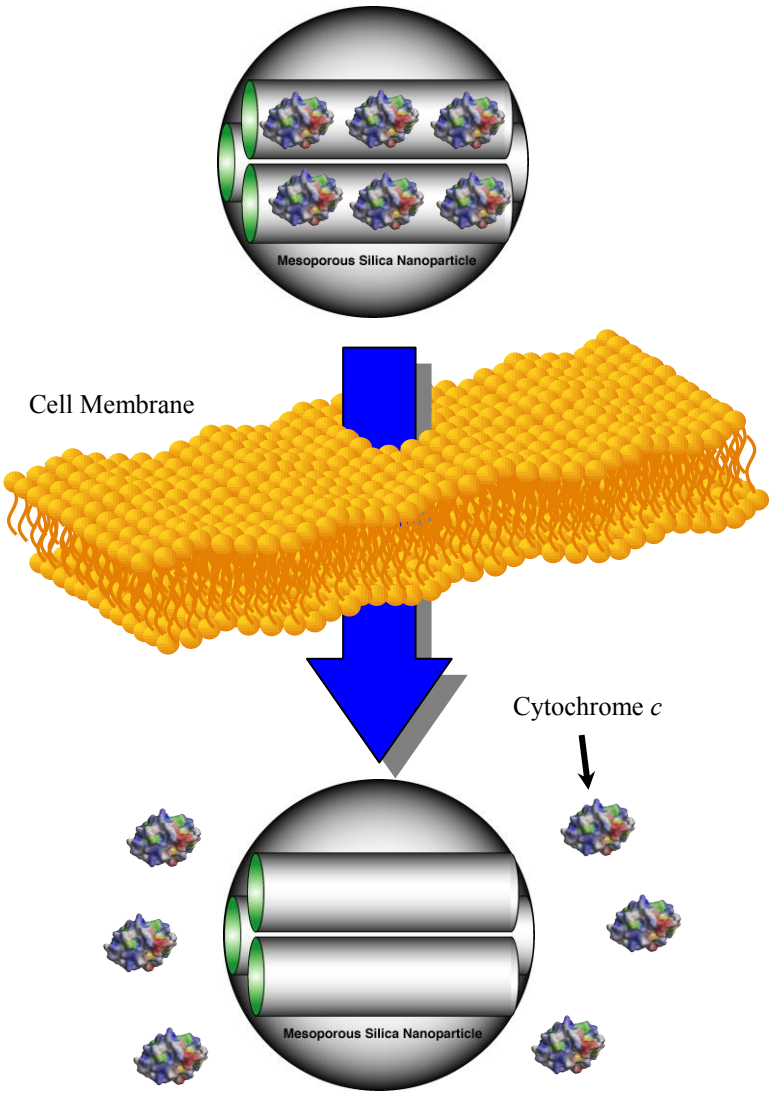

Intracellular Controlled Release

Figure 2.

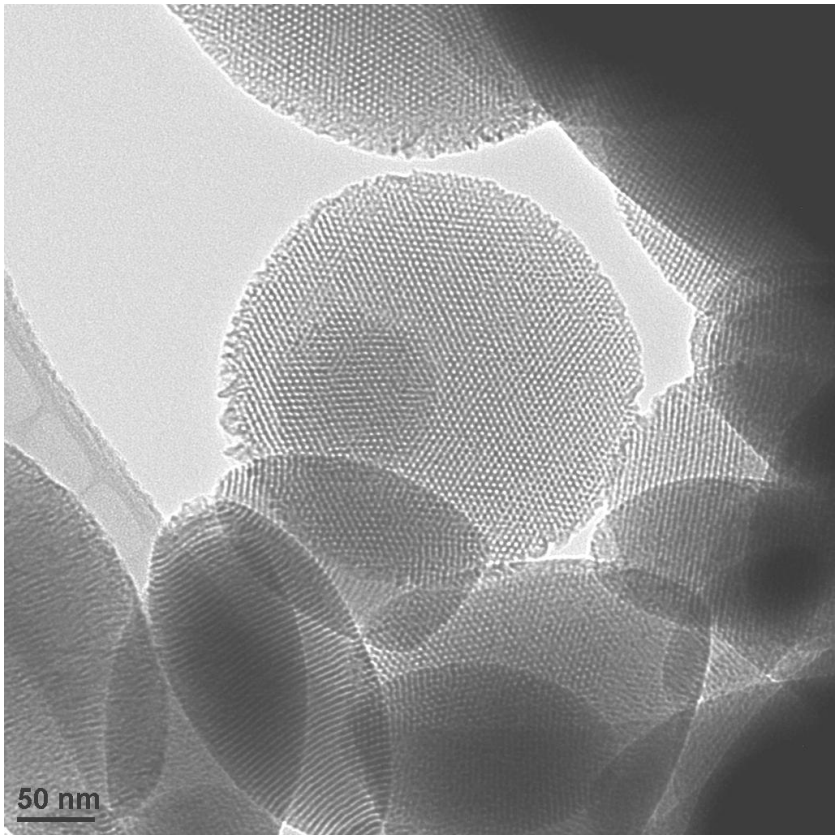

Figure 3.

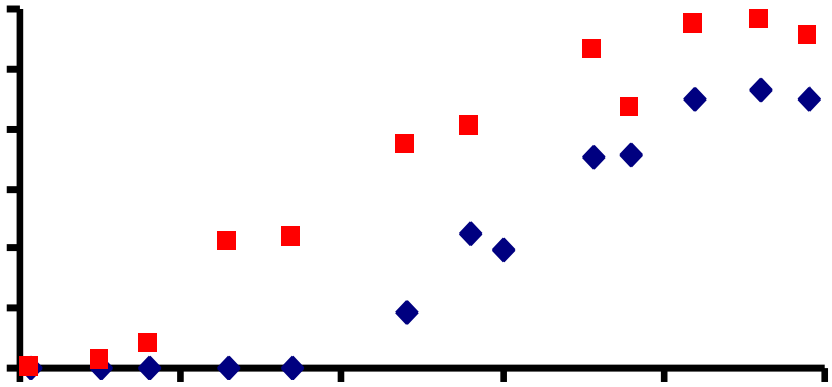

Figure 4.

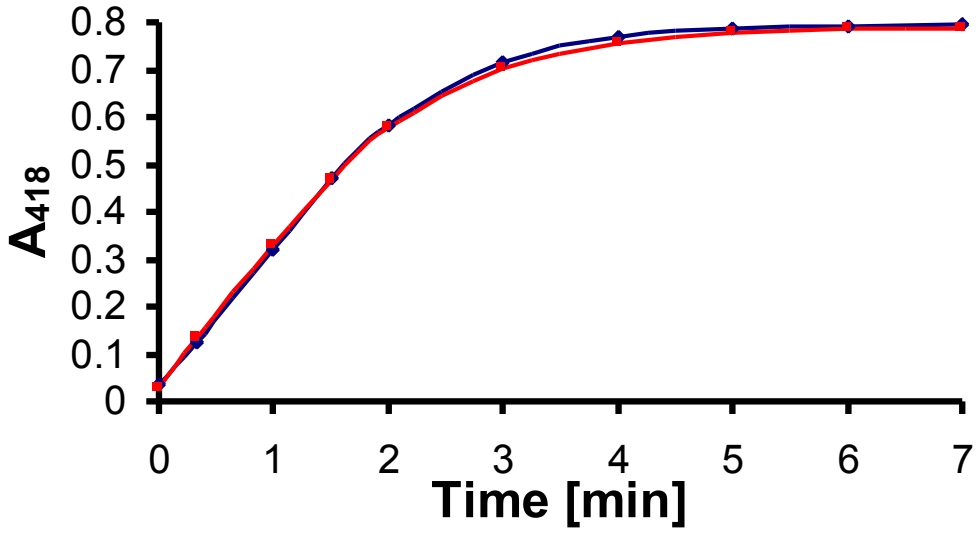

Figure 5.

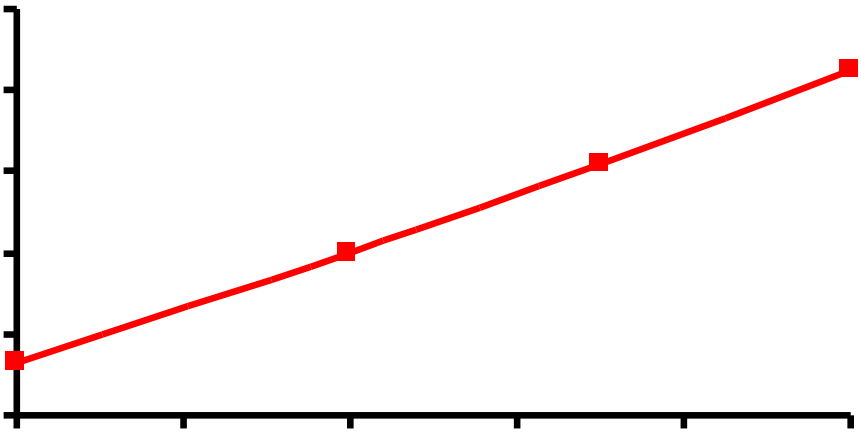

Figure 6.

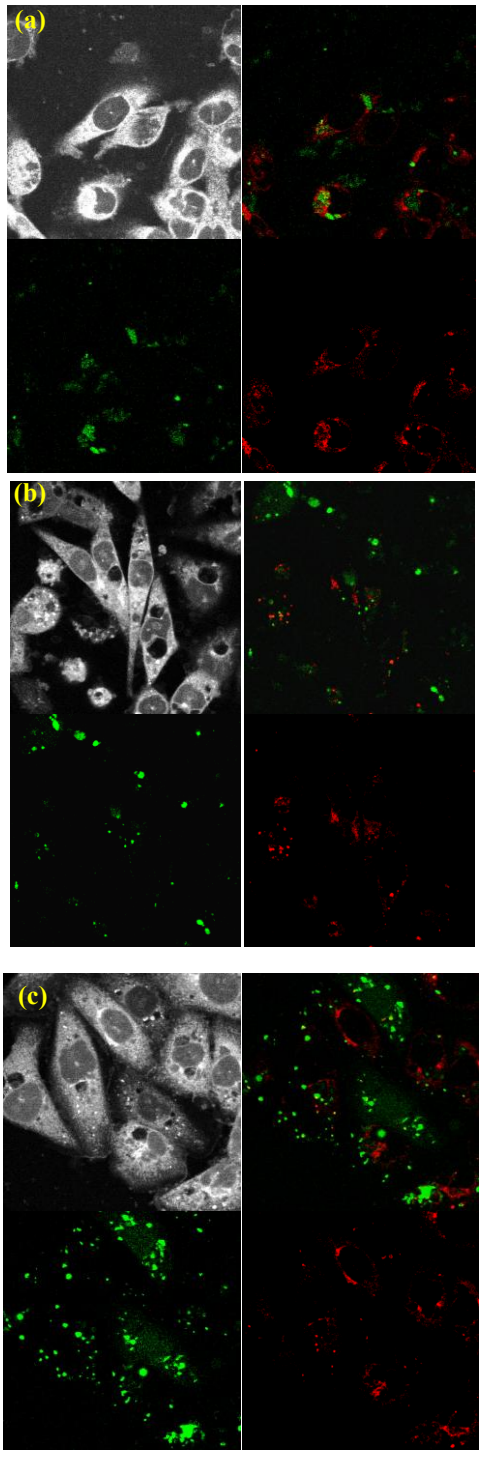

Figure 7.

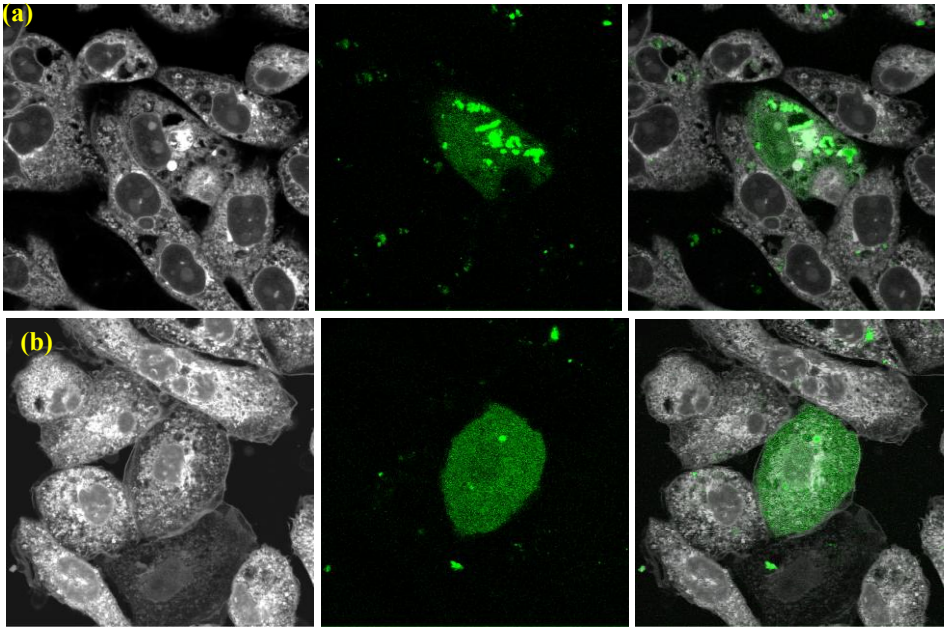

Appendix: Supporting information

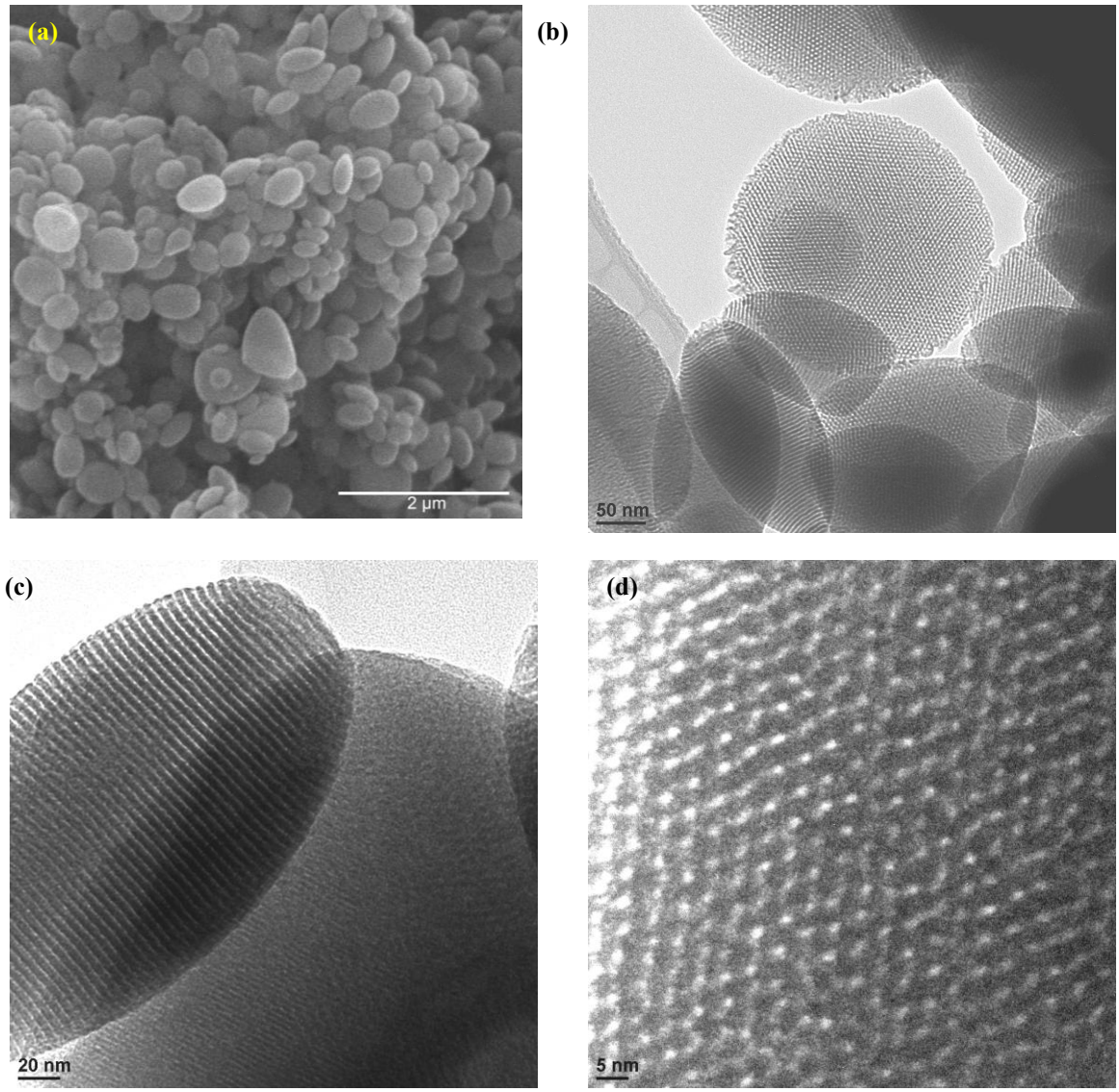

Figure SI 1. (a) Scanning and (b), (c) and (d) transmission electron micrographs of large-pore MSN.

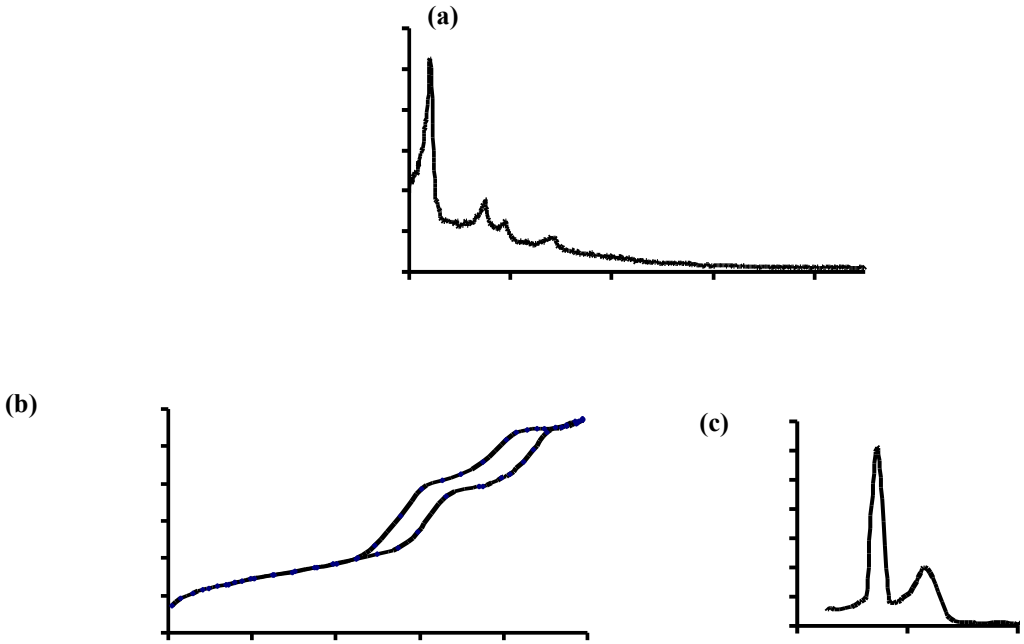

Figure SI 2. (a) Small angle X-ray diffraction, (b) BET nitrogen sorption isotherms, and (c) BJH pore size distribution of MSN.

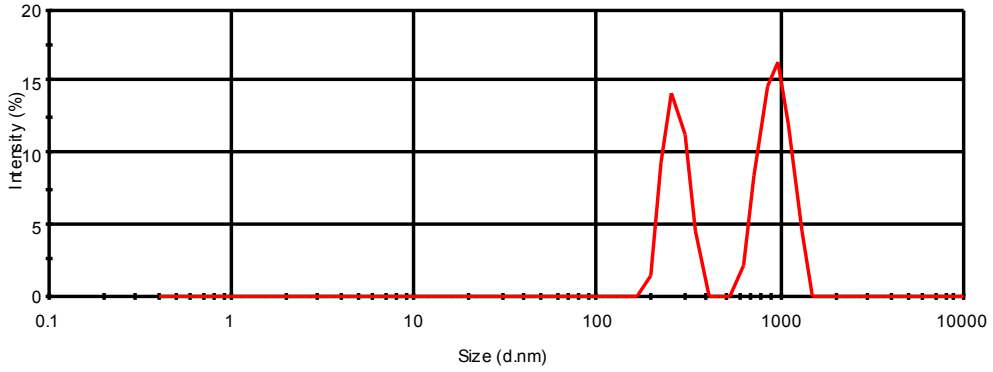

Figure SI 3. Particle size distribution of large-pore MSN suspended in 10 mM PBS pH 7.4 measured by dynamic light scattering.

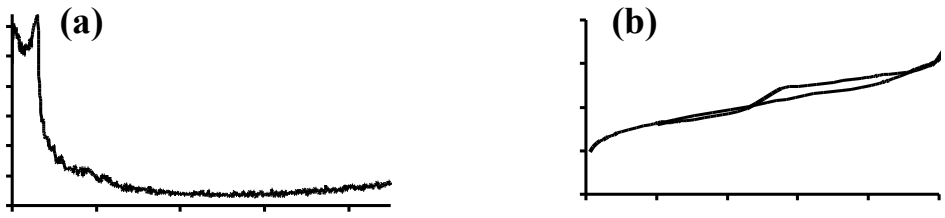

Figure SI 4. (a) X-ray diffraction pattern and (b) nitrogen sorption isotherm of MSN loaded with cytochrome c (95 mg/g).

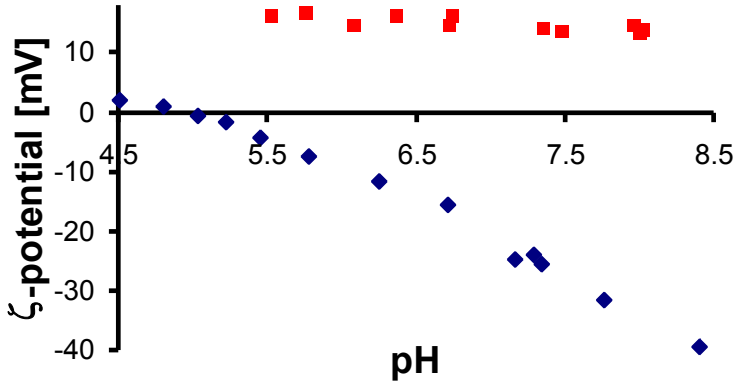

Figure SI 5. Variation of the ζ-potential of MSN (blue rhombi) and cytochrome c (red squares) as a function of pH.

Experimental Section

1. Materials

Horse heart cytochrome c, fluorescein isothiocyanate isomer I, mesitylene, cetyltrimethylammonium bromide, and 2,2'-azino-bis(3-ethylbenzthiazoline-6-sulfonate) were purchased from Sigma-Aldrich. Tetraethyl orthosilicate was purchased from Gelest. FM 4-64 endosome marker was purchased from Molecular Probes, Inc. All chemicals were used as received.

2. Synthesis of mesoporous silica nanoparticle (MSN) with large pores.

Cetyltrimethylammonium bromide (CTAB, 1.0 g, 2.7 mmol) was dissolved in a solution of 480 mL water and 3.5 mL of 2M NaOH (aq). Mesitylene (7.0 mL, 48.8 mmol) was then added to the solution. The mixture was stirred vigorously at 80 °C for 2 h. Tetraethyl orthosilicate (5.0 mL, 21.9 mmol) was then added dropwise at a rate of 1 mL per min to the solution. The reaction mixture was stirred vigorously at 80 °C for another 2 h. The resulting white precipitate was isolated by filtration, washed with abundant methanol, and dried under vacuum at 100 °C for 12 h. The structure-templating CTAB and mesitylene molecules were removed from the composite material via acidic extraction. A suspension of 1.0 g of the as synthesized material was stirred for 6 h at 50 °C in a 100 mL methanolic solution with 0.75 mL concentrated hydrochloric acid. The template-removed solid product was then isolated via filtration and dried under vacuum at room temperature for 12 h.

3. Characterization of the MSN material.

Surface analysis of the MSN materials was performed by nitrogen sorption isotherms at 77 K with a Micromeritics ASAP2000 sorptometer. The surface areas were calculated by the Brunauer-Emmett-Teller (BET) method and the pore size distribution were calculated by the Barrett-Joyner-Halenda (BJH) method. Small angle X-ray diffraction patterns were obtained with a Scintag XDS-2000 powder diffractometer using Cu Kα irradiation. For transmission electron microscopy measurements, an aliquot of the powder was sonicated in nanopure water for 15 min. A single drop of this suspension was placed on a lacey carbon coated copper TEM grid and dried in air. The TEM examination was completed on a Tecnai G2 F20 electron microscope operated at 200 kV to examine at electron optical magnification of 64,000 to 550,000. Particle size was measured in a Malvern Zetasizer Nano Series HT. For the analysis the MSN were suspended in phosphate buffer saline solution (PBS, 10 mM phosphate and 75 mM sodium chloride) pH 7.4 at a concentration of 0.75 mg/ml and sonicated for 40 minutes. The suspension was then transferred to a polystyrene cuvette and its particle size was measured, and the results were processed with DTS software version 4.20.

4. Labeling of cytochrome *c*.

Cytochrome *c* (5.4 mg) was dissolved in 2.0 mL 0.1 M sodium bicarbonate solution pH 8.98. Fluorescein isothiocyanate isomer I (FITC) was dissolved in dimethyl sulfoxide at a concentration of 4 mg/mL, and 500 μL of this solution were added dropwise to the protein solution. The mixture was stirred at room temperature for 2 h and then stirred for 12 h at 4

°C, followed by the addition of ammonium chloride (21 mg). The solution mixture was stirred for 2 h at room temperature. The resulting FITC-labeled protein was then isolated by size exclusion chromatography with Sephadex G-25 as stationary phase and PBS as mobile phase. The isolated FITC-cytochrome c was then characterized by ultraviolet-visible absorption spectroscopy, and the labeling efficiency was determined to be 1.8 moles FITC per mole of protein.

5. Loading of cytochrome *c* into MSN.

For the loading of FITC-cytochrome *c* to MSN, 5 mL of solutions of different concentrations of the protein ranging from 0.4 to 8 mg/mL in PBS were stirred for 6 h at room temperature in the presence of 20 mg of MSN in each solution. The suspensions were then centrifuged and the loading was determined by measuring the difference in absorption of the Soret band of cytochrome c (410 nm) in the supernatant before and after the loading. The isolated protein-MSN composites were dried in the dark at room temperature and under vacuum for 12 h.

6. Release of cytochrome *c* from MSN.

The release of FITC-cytochrome *c* from MSN was measured by preparing suspensions of the FITC-cytochrome c-loaded MSNs in PBS at the concentration of 100 µg/mL. The suspensions were kept at room temperature and the release was determined by taking an aliquot of the suspension at different times. The aliquots were centrifuged and the UV-Vis

absorbance of the Soret band of cytochrome c in the supernatant was measured to give information on the quantity of released protein.

7. Measurement of the ζ-potential variation of cytochrome *c* and MSN.

The variation of the ζ-potentials of cytochrome *c* and MSN induced by different pH values of the aqueous solutions were measured by a Malvern Nano HT Zetasizer equipped with an MPT-2 autotitrator. The ζ-potentials of cytochrome c and MSN were measured separately in non-buffered aqueous media at pH 4.5 of HCl(aq). A specific amount of 0.135 M solution of sodium hydroxide was added by the titrator to obtain a stable pH and ζ-potential reading for all of the samples. This process was repeated until the pH reached a value of 8.5.

8. Measurement of the enzymatic activity of cytochrome *c*.

The enzymatic activity of cytochrome *c* was measured by examining the catalytic conversion of the oxidation of 2,2'-azino-bis(3-ethylbenzthiazoline-6-sulfonate) (ABTS) in a PBS solution of cytochrome c that was released from MSN overnight. The cytochrome c employed for this assay was not labeled with FITC. The concentration of cytochrome c in this solution was determined to be 21 μg/mL by the UV-Vis absorption of the Soret Band of the protein. The enzymatic activity of the MSN-released cytochrome c was compared with that of a solution of the protein directly dissolved in PBS solution. This solution of cytochrome c was kept at room temperature overnight before measuring the catalytic performance, and its concentration was adjusted to be the same as the one of the cytochrome c released from the MSN. Hydrogen peroxide (500 μL, 25 mM) was then added to 500 μL of

the cytochrome c solution in a polystyrene cuvette, followed by the addition of 300 μL of ABTS. The absorbance at 418 nm of the oxidized product was monitored every 30 sec for 7 min. A control experiment was performed by using an enzyme-free 500 μL PBS solution.

9. Measurement of the internalization of FITC-cytochrome *c* loaded MSN by HeLa cells.

The cellular uptake profile of the protein-loaded MSN was examined by FACS flow cytometry. For the assay, HeLa cells were seeded in 6-well plates with a density of 1 × 105 cells/mL in 3 mL of D-10 medium. The D-10 medium is a Dubelcco modified Eagle's medium (DMEM) containing 10% equine serum, L-alanylglutamine, gentamicin, and penicillin/streptomycin. After incubation for 34 h, the D-10 medium was replaced by 3 mL of MSN suspensions at concentrations 10, 25, 50, and 100 μg/mL in the D-10 medium for 12 h. All of the tests were run in triplicate. The cells were washed with medium and harvested by trypsinization. After centrifugation, the cell pellets were resuspended in 0.4 % trypan blue PBS solution, and analyzed by flow cytometry with a Becton-Dickinson FACSCanto cytometer and BD-FACS Diva software.

To distinguish the true fluorescence generated by the loaded MSN from the natural autofluorescence of cells, a threshold of fluorescence intensity was established by performing the flow cytometry analysis on HeLa cells incubated without any MSN. The threshold was set at an intensity of fluorescence slightly above the highest value observed for control

samples (HeLa cells only). The number of cells with encytosed MSNs was determined by counting the cells showing fluorescence intensity higher than the threshold.

10. Confocal fluorescence microscopy of HeLa cells with the FITC-cytochrome *c* loaded MSNs.

For confocal fluorescence microscopy measurements, HeLa cells were seeded at a density of 1 × 105 cells per well in 6-well plates in 3 mL D-10 medium with coverslips at the bottom of the wells. Three samples were prepared for the microscopy study. The first sample was prepared by incubating the cells for 24 h, followed by the replacement of the D-10 medium with 3 mL of the FITC-cytochrome c-loaded MSN (100 μg/mL) in the D-10 medium and allowed to grow for additional 50 h. The second sample was prepared by an initial incubation in the D-10 medium for 50 h, followed by the replacement of medium with 3 mL of the FITC-cytochrome c-loaded MSN (100 μg/mL) in the D-10 medium and allowed to grow for 24 h. The third sample was prepared by first incubating in the D-10 medium for 56 h, followed by the replacement of medium with 3 mL of the FITC-cytochrome c-loaded MSN (100 μg/mL) in the D-10 medium and allowed to grow for 18 h.

The cell-plated coverslips of these three samples were isolated, washed with medium, and fixed with 3.7 % formaldehyde in 100 mM PBS buffer pH 7.44 for 30 min. The coverslips were then placed in microscope slides and examined under a Leica TCS NT confocal fluorescence microscope system using a 100x oil immersion objective. The green fluorescent FITC-cytochrome c-loaded MSN particles inside of the HeLa cells were visualized by

excitation at 488nm with an Argon Laser and the autofluorescence images of the cells were obtained with a 568nm Krypton laser.

11. Determination of endosomal escape of the FITC-cytochrome *c* loaded MSN.

HeLa cells were seeded at the density of 1 × 105 cells per well in 6-well plates in 3 mL D-10 medium with coverslips at the bottom of the wells. Again, three samples were prepared for the microscopy study. The first sample was prepared by incubating the cells for 24 h, followed by the replacement of the D-10 medium with 3 mL of the FITC-cytochrome c-loaded MSN (100 μg/mL) and an endosome marker34 (FM 4-64; 10μg/mL) in the D-10 medium and allowed to grow for additional 24 h. The second sample was prepared by an initial incubation in the D-10 medium for 34 h, followed by the replacement of medium with the same MSN and endosome marker mixture in the D-10 medium and allowed to grow for 14 h. The third sample was prepared by first incubating in the D-10 medium for 46 h, followed by the replacement of medium with the same MSN and endosome marker mixture in the D-10 medium and allowed to grow for 2 h.

The cell-plated coverslips of these samples were isolated and washed with medium, followed by a fixation with 3.7 % formaldehyde in 100 mM PBS buffer pH 7.4. The coverslips were placed in microscope slides and examined under a Leica TCS NT confocal fluorescence microscope system using a 100x oil immersion objective. Both, the FITC-cytochrome *c*-loaded MSNs and the endosome marker were excited at 488 nm with an Argon Laser, the FITC-cytochrome *c* were detected at wavelengths between 515-590 nm (observed green),

while the endosome marker was detected at wavelengths between 590-750 nm (observed red). The FITC-labeled proteins are considered to be inside of the endosomes, where the green and the red spots are overlapped to give a yellow/orange color. The autofluorescence images of the cells were obtained with a 568 nm Krypton laser.

CHAPTER 5. BIOCOMPATIBILITY STUDY OF MESOPOROUS SILICA NANOPARTICLES WITH RED BLOOD CELLS

A paper submitted to ***Nano Letters***

Igor I. Slowing and Victor S.-Y. Lin

Abstract

Amorphous silica particles are toxic to red blood cells. We studied the biocompatibility of mesoporous silica nanoparticles (MSN) with rabbit red blood cells. The source of the hemolytic properties of amorphous silica and the effect of functionalization on those properties were analyzed. We demonstrated that the unique structural characteristics of MSN prevent them from displaying hemolytic activity at the tested concentrations. Based on these results, we envision MSN as safe candidates for in vivo drug delivery applications.

Different forms of silica, including amorphous silica nanoparticles and mesoporous silica nanoparticles (MSN) have been proposed recently as candidates for drug delivery applications.[1, 2] Such proposals are based, besides of a series of advantageous properties, on the observed biocompatibility of these materials with a variety of cell types.[3-7] The low in vitro cytotoxicity of silica nanoparticles towards many kinds of mammalian cells is, however, no guarantee of their safety for in vivo applications. In fact, amorphous silica has been long known to cause hemolysis when set in contact with red blood cells (RBC).[8] Such a behavior draws serious concerns regarding the safe use of unmodified amorphous silica for drug

delivery applications involving intravenous administration and transport. Many research groups have studied the hemolytic effects of amorphous silica and proposed a variety of explanations for such a property. Among the causes believed to be responsible for that undesirable behavior we can mention the generation of reactive oxygen species by the surface of silica,[9] denaturation of membrane proteins through electrostatic interactions with silica,[10] and the high affinity of silica for tetraalkylammonium groups that are abundant in the membranes of RBC.[11] It has been recently demonstrated that the hemolytic properties of amorphous silica are proportional to the concentration of silanol in its surface.[12] It is surprising that even if the hemolytical properties of amorphous silica have been so well documented, there is, to the best of our knowledge, no report on the biocompatibility of MSN with RBC.

MSN synthesized by our previously reported method,[3] are spherical particles with diameters of ranging from 100 to 200 nm. Their structure consists of a series of approximately 3 nm wide parallel channels arranged in a 2D hexagonal geometry (Figure 1). The high degree of order of the mesopores is reflected by their typical signals observed in powder X-ray diffraction. These properties along with the large surface areas and pore volumes of MSN (close to 1,000 m^2/g and 1 cm^3/g respectively, see Supporting Information), make them highly convenient carriers for small and medium sized molecules.[3, 4, 7, 13-15]

Considering that in our previous studies of endocytosis of MSN, efficient cellular uptake of the material was achieved at concentrations below 50 μg/mL and no cytotoxic effects were observed but at concentrations above 100 μg/mL, we decided to set a threshold concentration of 100 μg/mL to evaluate the compatibility of the material with RBC.[3, 5, 13] As a control to

our experiments we used commercially available amorphous silica nanoparticles (Sigma Aldrich, Co., St. Louis, MO). The hemolytic properties of the materials were evaluated on rabbit RBC, which were isolated from EDTA stabilized blood, by centrifugation and five successive washes with sterile isotonic phosphate saline buffered solution (PBS). After the final wash the RBC were diluted to one tenth with PBS. The diluted RBC suspension (300 μL) was mixed with a suspension of the silica material to be tested (750 μL, 200 μg/mL) and the total volume was adjusted to 1500 μL with PBS. Positive and negative controls were made by mixing the 300 μL of RBC suspensions with 1200 μL of nanopure water and PBS respectively. After vortexing the samples, they were let to rest for 2 hours at room temperature. The samples were then centrifuged for 10 min at 14,000 rpm and the absorption of the hemoglobin released in the supernatant was measured at 541 nm. Amorphous silica, as expected, showed hemolytic properties. However, surprisingly, MSN did not produce any hemolysis (Figures 2, 3, and Supporting Information).

In order to determine if the hemolytic activity was related to the abundance of silanol groups, as it had been previously reported,[12] solid state ^{29}SiNMR spectra were taken for both materials. Surprisingly, the hemolytic amorphous silica showed a lower amount of silanol groups than the non-hemolytic MSN (Figure 4). This result is even more puzzling considering the fact that upon measuring the ζ-potential of both materials, amorphous silica resulted being more negative (-49 mV) than MSN (-35 mV). This apparent contradiction was solved upon considering the unique structural properties of MSN. As can be noted in Figures 1 and 5(b) the surface of MSN can be divided into two types, namely: an external and an internal surface. It is easy to see that the internal surface, constituted by the mesopores, is by

far larger than the external one, which is limited mainly to the borders of the pore openings. This makes the number of silanol groups available to contact the surface of RBC significantly smaller than the amount of silanol groups present in the external surface of the amorphous silica particles. The difference between the external surfaces of both materials is analogous to the comparison of the surface of a solid sphere with the one of a spherical net. Therefore, even if MSN has a larger number of silanol groups than amorphous silica, most of these groups are unable to lead to the hemolysis of RBC, for they are "hidden" in the inside of the mesopores, and are consequently unable to get in contact with the cells (Figure 5). These results suggest that it is less likely that the hemolytic properties of silica arise from the generation of reactive oxygen species by the silanol groups as previously proposed,[9] than from the direct interaction of the silanol groups with the cell membrane surface.

To further test the hypothesis of an electrostatic interaction of silica as the possible cause of the hemolysis of RBC, we functionalized the surfaces of the materials with groups that were expected to modify their surface charges. As can be observed in Table 1, upon grafting 3-aminopropyltrimethoxysilane on the surface of amorphous silica, its ζ-potential is completely inverted and this results in a dramatic decrease of the hemolytic property of the material. Furthermore, upon functionalizing MSN with a benzenesulfonic moiety its ζ-potential is shifted to a value even more negative than the one of amorphous silica, and the resulting material clearly displayed hemolytic activity.

The conclusion, however, is not as straightforward as it appears to be. The hemolytic properties of silica seem to involve more than a simple electrostatic interaction. To further test if particle charge is the only property required to produce hemolysis, we functionalized

MSN with carboxylic acid terminated chains, in a quantity enough to achieve a ζ-potential comparable to the one of amorphous silica. Surprisingly, despite its highly negative ζ-potential (-50 mV), the resulting material did not show significant hemolytic activity (less than 4%). This result shows the hemolytic activity of silica has a more subtle origin, probably related to a special affinity existing between silica and the membrane lipids. The lipids of the external leaflet of the membranes of RBC are particularly abundant in sphingomyelin and posphatidylcholine, whose polar heads end in a trimethylammonium group.[16] The affinity between silica and lipids containing trimethylammonium head groups, is well known.[17-19] A good example of this affinity is precisely the use of alkyltrimethylammonium surfactants as templates for the polymerization of silica to yield ordered mesoporous materials.[20] A measure of this interaction is given by the negative value of the heat of displacement of water from the surface of silica by hexadecyltrimethylammonium ions at low concentrations.[21] Furthermore, benzenesulfonates have been shown also to have stronger affinities for alkyltrimethylammonium ions than carboxylates: the enthalpies of transfer from water to a cetyltrimethylammonium solution were found to be negative for sodium benzenesulfonate, but positive for sodium acetate.[22, 23] The affinities of anions for alkyltrimethylammonium species have been shown to correlate well with the Hofmeister series.[22] It has been also reported that following the Hofmeister series, anions are increasingly able to penetrate a lipid layer and disrupt the packing of the hydrophobic chains.[24] Based on this information we believe it is plausible that silica and benzenesulfonate functionalized silica are able to produce the hemolysis of RBC because of their high affinity for trimethylammonium headgroups of the membrane lipids. This explains

also why in spite of its highly negative ζ-potential, MSN functionalized with carboxy groups, which have low affinity for trimethylammonium ions, display little hemolytic activity.

In conclusion, we have demonstrated that contrary to the known cytotoxicity that silica displays towards RBC, MSN are biocompatible with this type of cells at concentrations adequate for potential pharmacological applications. We have shown that the unexpected compatibility of MSN arises from the little amount of silanol groups available for interaction with the RBC membranes, which is a unique structural characteristic of the material. We have demonstrated that the hemolytic property of silica is related only to the amount of silanol groups accessible to the cell membrane, and that the cytotoxic effect is probably related to the disruption of the membrane through attractive interactions with trimethylammonium head groups of the membrane lipids. This study provides a contribution to the understanding of a health problem that has been debated for a long time. Based on these results we envision MSN as a safe candidate for in vivo drug delivery applications.

Acknowledgment The authors thank the Hybridoma Facility and the Laboratory Animal Resources office of Iowa State University for providing the blood samples. This work was supported by NSF Career Award (CHE-02239570), CMS-0409625 and US DOE (AL-03380-011 and W-7405-Eng-82).

References

1. Slowing, I. I.; Trewyn, B. G.; Giri, S.; Lin, V. S. Y. *Adv. Funct. Mater.* 2007, 17, (8), 1225-1236.

2. Barbe, C.; Bartlett, J.; Kong, L.; Finnie, K.; Lin, H. Q.; Larkin, M.; Calleja, S.; Bush, A.; Calleja, G. *Adv. Mater.* 2004, 16, (21), 1959-1966.

3. Radu, D. R.; Lai, C.-Y.; Jeftinija, K.; Rowe, E. W.; Jeftinija, S.; Lin, V. S. Y. *J. Amer. Chem. Soc.* 2004, 126, (41), 13216-13217.

4. Torney, F.; Trewyn, B. G.; Lin, V. S. Y.; Wang, K. *Nature Nanotech.* 2007, 2, (5), 295-300.

5. Slowing, I.; Trewyn, B. G.; Lin, V. S. Y. *J. Amer. Chem. Soc.* 2006, 128, (46), 14792-14793.

6. Huang, D.-M.; Hung, Y.; Ko, B.-S.; Hsu, S.-C.; Chen, W.-H.; Chien, C.-L.; Tsai, C.-P.; Kuo, C.-T.; Kang, J.-C.; Yang, C.-S.; Mou, C.-Y.; Chen, Y.-C. *FASEB J.* 2005, 19, (14), 2014-2016.

7. Lu, J.; Liong, M.; Zink Jeffrey, I.; Tamanoi, F. *Small* 2007, 3, (8), 1341-6.

8. Nash, T.; Allison, A. C.; Harington, J. S. *Nature* 1966, 210, (5033), 259-61.

9. Razzaboni, B. L.; Bolsaitis, P. *Environ. Health Perspect.* 1990, 87, 337-41.

10. Diociaiuti, M.; Bordi, F.; Gataleta, L.; Baldo, G.; Crateri, P.; Paoletti, L. *Environ. Res.* 1999, 80, (3), 197-207.

11. Depasse, J.; Warlus, J. *J. Coll. Interf. Sci.* 1976, 56, (3), 618-21.

12. Murashov, V.; Harper, M.; Demchuk, E. *J. Occup. Environ. Hygiene* 2006, 3, (12), 718-723.

13. Slowing, I. I.; Trewyn, B. G.; Lin, V. S. Y. *J. Amer. Chem. Soc.* 2007, 129, (28), 8845-8849.

14. Giri, S.; Trewyn, B. G.; Stellmaker, M. P.; Lin, V. S. Y. *Angew. Chem., Int. Ed.* 2005, 44, (32), 5038-5044.

15. Lai, C.-Y.; Trewyn, B. G.; Jeftinija, D. M.; Jeftinija, K.; Xu, S.; Jeftinija, S.; Lin, V. S. Y. *J. Amer. Chem. Soc.* 2003, 125, (15), 4451-4459.

16. Yawata, Y., *Cell Membrane: The Red Blood Cell as a Model.* 1 ed.; Wiley-VCH Verlag: Darmstadt, 2003; p 439.

17. Rapuano, R.; Carmona-Ribeiro, A. M. *J. Coll. Interf. Sci.* 2000, 226, (2), 299-307.

18. Mornet, S.; Lambert, O.; Duguet, E.; Brisson, A. *Nano Letters* 2005, 5, (2), 281-285.

19. Chen, C.-S.; Yao, J.; Durst, R. A. *J. Nanopart. Res.* 2006, 8, (6), 1033-1038.

20. Kresge, C. T.; Leonowicz, M. E.; Roth, W. J.; Vartuli, J. C.; Beck, J. S. *Nature* 1992, 359, (6397), 710-12.

21. Stodghill, S. P.; Smith, A. E.; O'Haver, J. H. *Langmuir* 2004, 20, (26), 11387-11392.

22. Larsen, J. W.; Magid, L. J. *J. Amer. Chem. Soc.* 1974, 96, (18), 5774-82.

23. Larsen, J. W.; Magid, L. J. *J. Phys. Chem.* 1974, 78, (8), 834-9.

24. Zhang, Y.; Cremer, P. S. *Curr. Op. Chem. Biol.* 2006, 10, (6), 658-663.

Table 1. Relationship between ζ-potential of the materials and their ability to produce hemolysis of RBC.

	ζ-potential [mV]	% Hemolysis
Amorphous silica	- 49	90
MSN	- 35	0.3
Aminopropyl grafted amorphous silica	+ 27	1
Ethylbenzenesulfonato functionalized MSN	- 90	61

Materials at a concentration of 100 μg/mL.

Figure captions.

Figure 1. Transmission electron micrograph of MSN.

Figure 2. Mixtures of RBC with (a) amorphous silica, (b) PBS (negative control) and (c) MSN. The mixtures were centrifuged to detect the presence of red color in the supernatants, which corresponds to hemoglobin released from the RBC.

Figure 3. Phase contrast images of RBC after 24 hours in contact with 100 μg/mL suspensions of (a) amorphous silica, and (b) MSN.

Figure 4. DP MAS ^{29}Si NMR of (a) amorphous silica, and (b) MSN. CP MAS ^{29}Si NMR of (c) amorphous silica, and (d) MSN. It can be noted that amorphous silica has a large Q^4 and a hardly identifiable Q^3 signal, while in MSN both peaks do have similar intensities.

Figure 5. Representation of (a) amorphous silica, and (b) MSN. The cartoons show the expected differences between the locations of the silanol groups in the surfaces of both materials.

Figure 1.

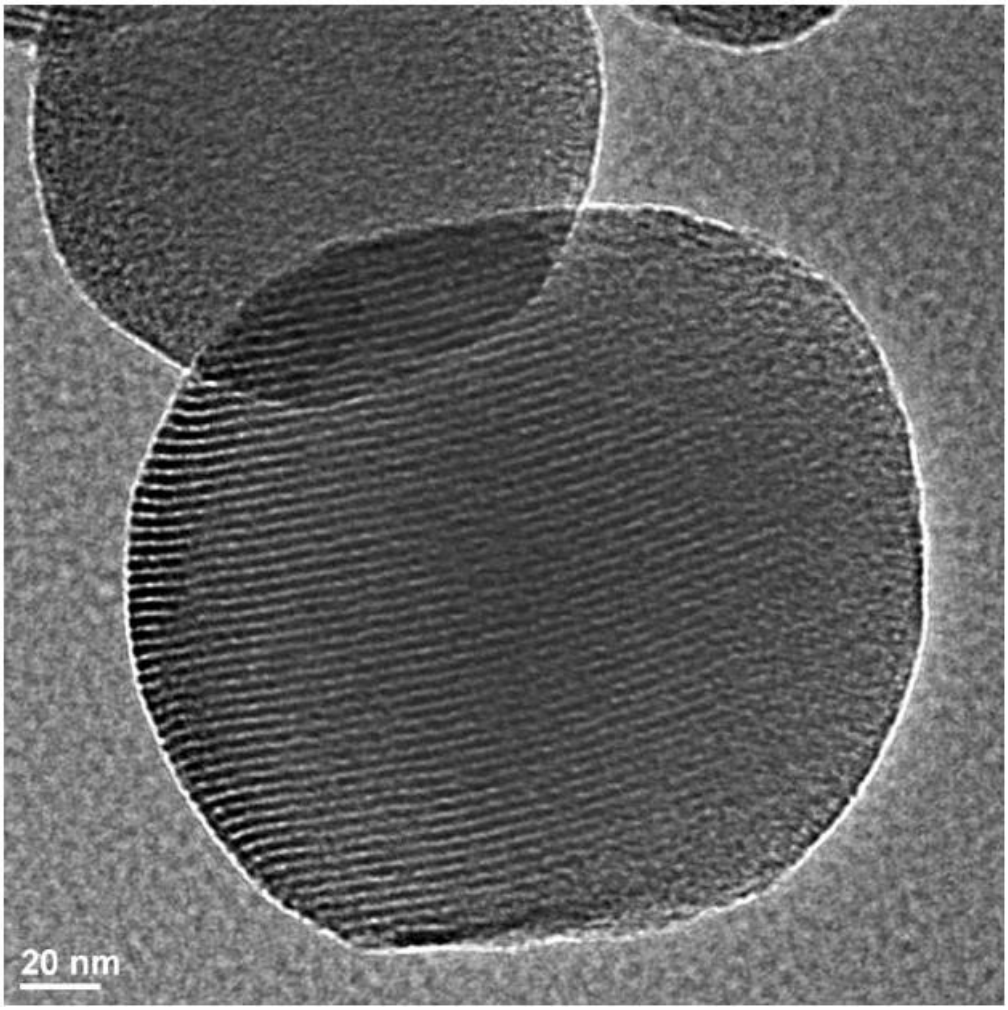

Figure 2.

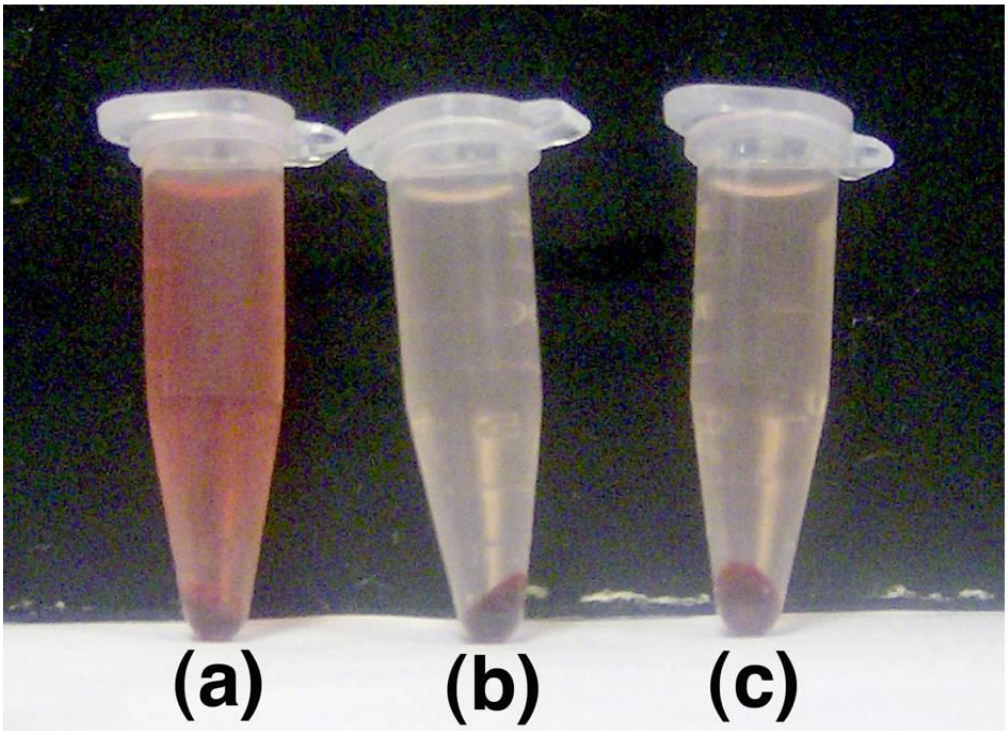

Figure 3.

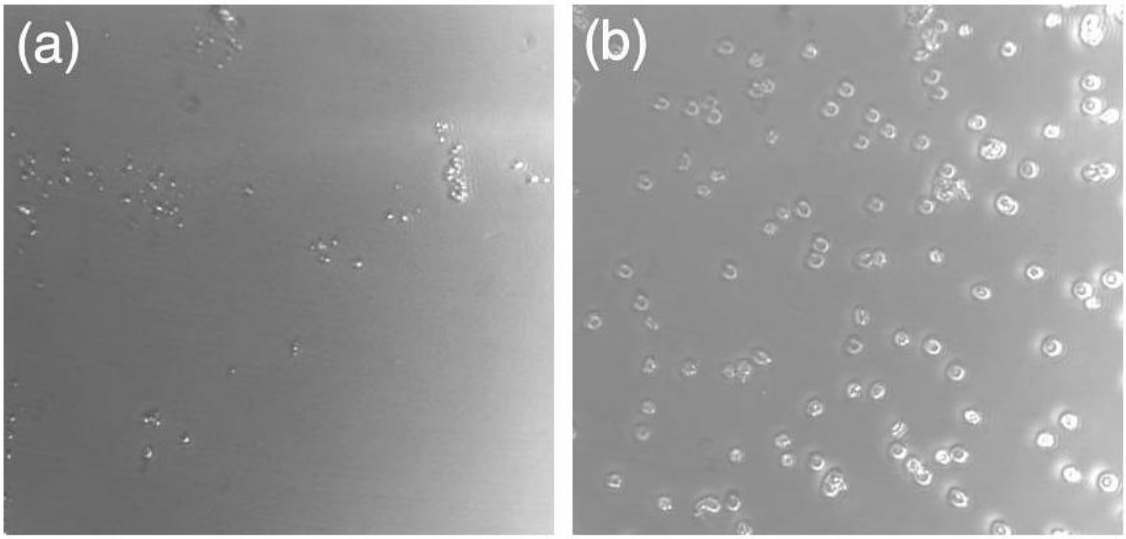

Figure 4.

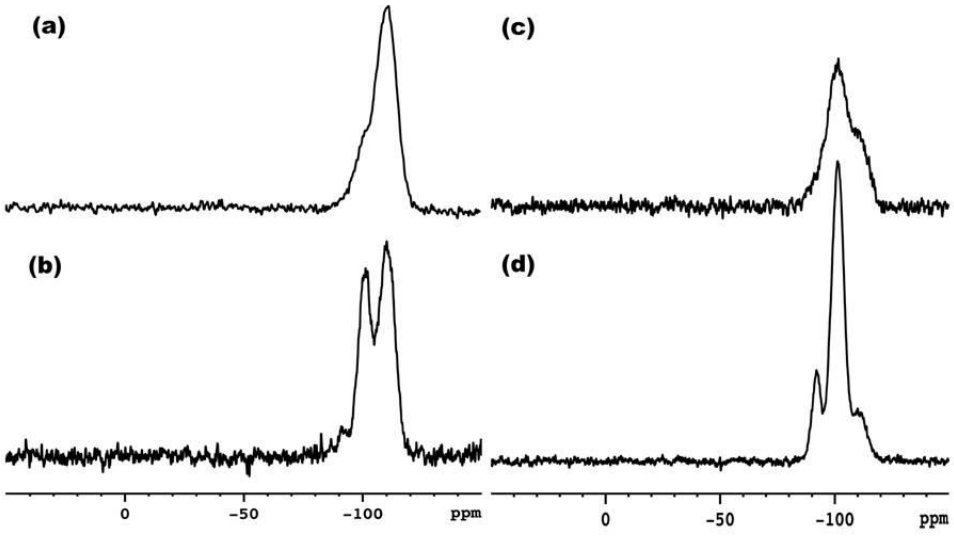

Figure 5.

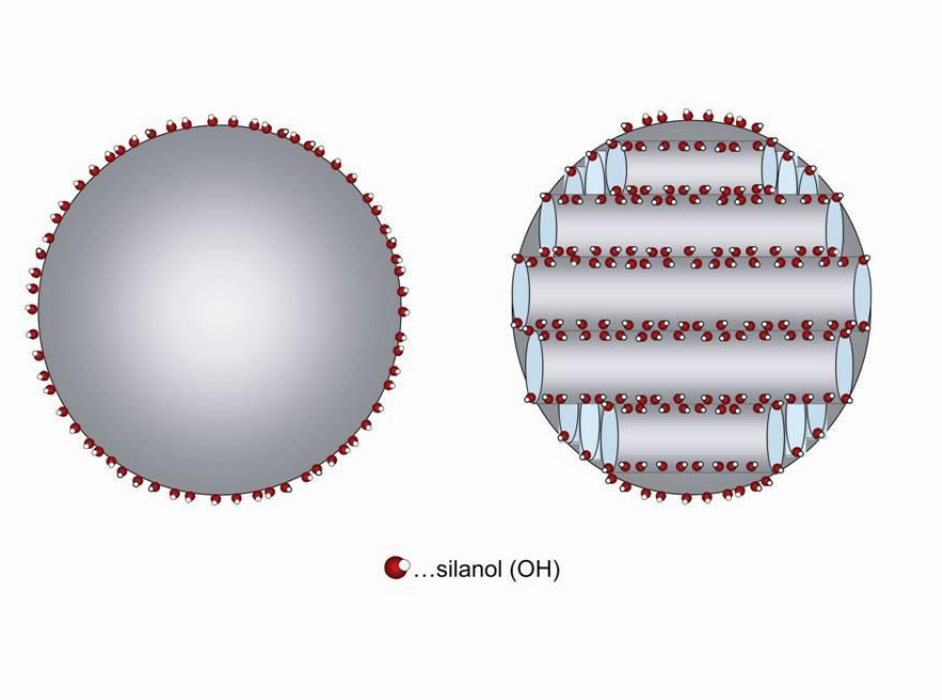

Appendix: Supporting Information

1. Synthesis or the materials

Tetraethylorthosilicate (TEOS), 2-(4-chlorosulfonylphenyl)ethyltrimethoxysilane were purchased from Gelest. 3-aminopropyltrimethoxysilane, 3-mercaptopropyl-trimethoxysilane, cetyltrimethylammonium bromide (CTAB), Aldrithiol-2®, 3-mercaptopropionic acid were purchased from Sigma-Aldrich. All chemicals were used as received.

1.1 Synthesis of Mesoporous Silica Nanoparticles (MSN).

A mixture of CTAB (1.02 g, 2.66 mmol), water (480 mL) and sodium hydroxide (2 M, 3.5 mL), was heated at 80^{o}C under vigorous stirring. TEOS (5.0 mL, 22 mmol) was then added dropwise to the reaction mixture, the temperature was maintained at 80^{o}C for 2 h, after which the resulting white colored solid was filtered, washed with abundant methanol and dried under vacuum overnight.

1.2 Synthesis of 2-(4-sulfonatophenyl)ethyl-MSN.

For the synthesis of the sulfonic acid functionalized MSN, the procedure described in 1.1 was slightly modified by adding mesitylene (7 mL) to the original CTAB mixture and 2-(4-chlorosulfonylphenyl)ethyltrimethoxysilane (1.5 mL, 3.0 mmol) dropwise immediately after the addition of TEOS.

1.3 Grafting of functional groups on amorphous silica and MSN.

The functionalization of amorphous silica with 3-aminopropyl groups and of MSN with 3-mercaptopropyl groups was performed by refluxing a suspension of the silica material (1 g of amorphous silica or MSN prepared as indicated in section 1.1) with the trialkoxysilane precursors of the corresponding functional group (5 mmol) in 100 mL Toluene for 20 h. After that time the products were filtered, washed with methanol and dried under vacuum overnight.

1.4 Preparation of carboxylate functionalized MSN.

A solution of Aldrithiol-2® (99.0 mg, 0.44 mmol) in 5.0 mL methanol was added to a suspension of 3-mercaptopropyl functionalized MSN (300 mg, prepared from procedure 1.3) suspended in 15.0 mL methanol. The resulting suspension, which was changing from white to light yellow as the reaction was progressing, was stirred at room temperature for 24 h. After that time the resulting white solid was recovered by filtration, and was washed with abundant methanol. The yellow filtrate was discarded with the washes. The amount of aldrithiol reacted was determined to be 0.191 mmol by absorption of the by product in the supernatant and the combined washes at 354 nm.

The washed solid was resuspended in 5 mL methanol. 3-mercaptopropionic acid (100 μL, 1.13 mmol) was then added to the suspension under stirring at room temperature. The mixture that turned almost immediately from white to light yellow was kept stirring at room temperature for further 24 h. After that time the product was filtered and washed with abundant methanol. The amount of mercaptopropionic acid reacted was determined to be

0.0738 mmol by absorption of the by product in the supernatant and the combined washes at 354 nm. The resulting white solid was then dried under vacuum overnight.

1.5 Removal of the template surfactant from MSN and from functionalized MSN.

The CTAB surfactant was removed from the MSN obtained from the procedures 1.1, 1.2 and 1.4, by refluxing a suspension of the corresponding solid (1.0 g) in 100 mL methanol for 6 h. Following the reflux the resulting solid was filtered, washed with abundant methanol and dried under vacuum overnight.

2. Characterization of the materials.

2.1 X-ray diffraction analysis.

Powder X-ray diffraction patterns were obtained in a Scintag XDS-2000 diffractometer using Cu Kα irradiation. All of the MSN materials do possess the hexagonal structure typical of MCM-41 with the characteristic (100), (110) and (200) signals.

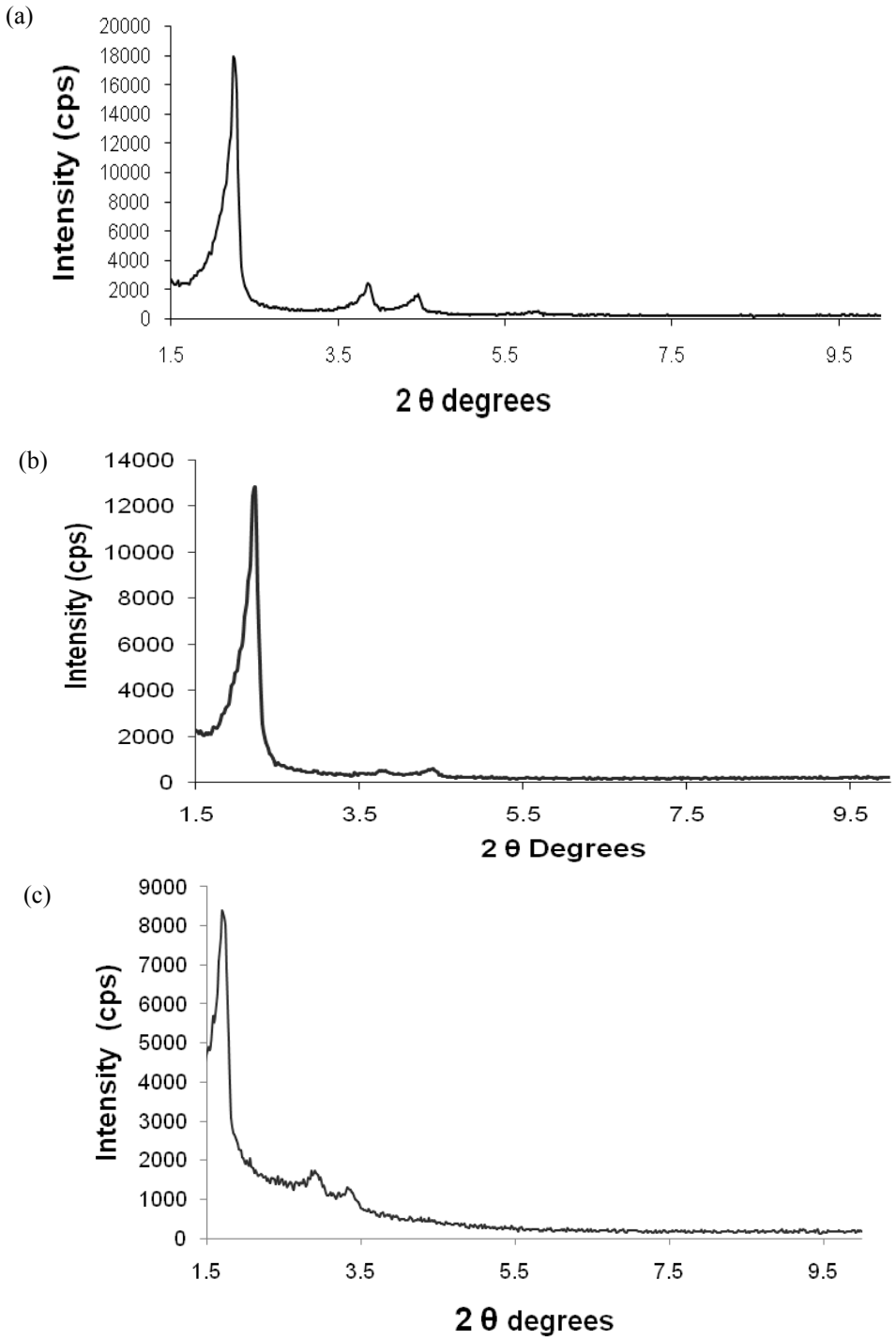

Figure SI 1. X-ray diffraction patterns of (a) MSN, (b) 3-aminopropyl-MSN and (c) (4-sulfonatophenyl)ethyl-MSN.

2.2 Nitrogen sorption analysis of MSN.

The surface properties of the MSN materials were analyzed in a Micromeritics Tristar surface area and porosity analyzer, with analysis software Tristar 3000 version 6.05.

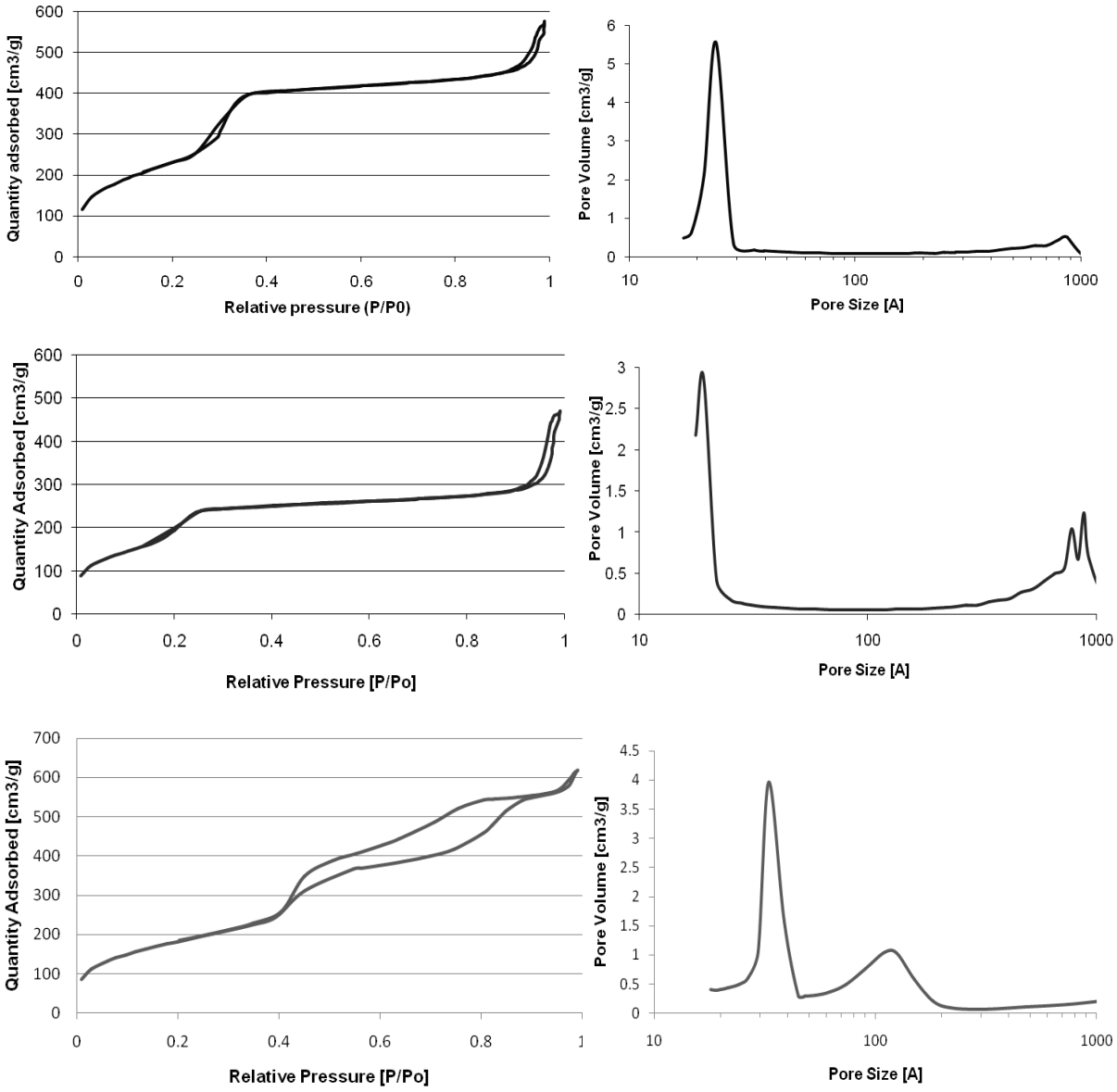

Figure SI 2. Nitrogen sorption isotherm and pore size distribution plots of (a) MSN, (b) 3-aminopropyl-MSN and (c) 4-(sulfonatophenyl)ethyl-MSN.

2.3 ζ-potential measurements.

The surface charge of the materials was measured in a Malvern Nano HT Zetasizer ZS90, processed with Dispersion Technology Software version 4.20. The measurements were performed on 1 mg/mL suspensions of each material in buffer solution containing sodium phosphates (1 mM) and sodium chloride (15.4 mM) set at pH 7.4.

2.4 Hemolysis assay.

Rabbit blood stabilized with EDTA was obtained from the Laboratory Animal Resources office of Iowa State University. The serum was removed from the blood by centrifugation and suction, and the red blood cells were then washed five times with sterile isotonic PBS solution. Following the last wash the cells were diluted to 1/10 of their volume with sterile isotonic PBS solution.

The diluted RBC suspension (200 µL) was then mixed with: a) 1300 µL of PBS as a negative control; b) 1300 µL nanopure water as a positive control; c) 1300 µL of a suspension of the silica materials of interest at a concentration of 115 µg/mL. The mixtures were then vortexed and then let to rest for two hours at room temperature. After that time the samples were centrifuged and the absorbances of the supernatants at 541 nm were measured in a HP 845x UV-Visible station. The percent hemolysis of each sample was calculated by dividing the difference of absorptions of the sample and the negative control, by the difference of absorptions of the positive and the negative controls, and multiplying the resulting ratio by 100.

CHAPTER 6. GENERAL CONCLUSIONS

In view of the growing interest in the development of smart vehicles for intracellular delivery of drugs or biologically active molecules, a series of materials have been recently synthesized, such materials include among others, quantum dots, carbon nanotubes and silica nanoparticles. Joining these efforts Victor Lin's group at Iowa State University has developed mesoporous silica nanoparticles (MSN) and has provided initial results for their use as intracellular delivery vehicles. This dissertation has provided a deeper analysis of the interactions of MSN with animal cells and has shown how functionalization and structure modification can regulate and control their membrane transport capabilities.

In order to optimize the properties of MSN for applying them as intracellular molecular cargos it is necessary to understand the mechanism of their internalization into cells. It has been demonstrated in this work that even if the uptake of MSN by cells is not receptor-mediated, it is an energy dependent process involving clathrin coated pits. The modification of the surface of MSN however, was shown to induce changes in the uptake mechanism, either by invoking the response of specific receptors or by shifting the internalization to a non-clathrin dependent pathway. Furthermore this work demonstrated that surface functionalization of the material is able to induce differences in the efficiency of the uptake either through electrostatic matching or through the participation of groups for which the cells do have receptors. It was also found that an increase in uptake efficiency does not necessarily imply improved cytosolic delivery, for the intracellular fate of the material is also dependent on the nature of its surface. It was observed that materials with

surface properties that enabled them to be up taken in high degree by the cells were less able to reach the cytoplasm, remaining trapped in intracellular vesicles. It was thus demonstrated that in order to prepare an efficient intracellular delivery agent, the surface properties have to be fine tuned so as to enable not only internalization but also endosomal escape.

Besides of the capability of modifying the surface of MSN, it is desirable to be able to tune their structure so as to provide a reservoir with a size that matches the size requirements of the guest molecules. It was demonstrated in this work that it is possible to adjust the pore size of MSN so that it is able to host biomolecules such as proteins. Pore enlarged MSN were shown to be able to adsorb up to 40% of their mass with cytochrome *c*, and were able to slowly release the protein upon resuspension in buffered medium. The protein released from the MSN was shown to completely retain its enzymatic activity. The introduction of the fluorescently labeled protein into living cells by means of MSN was evidenced by flow cytometry and confocal microscopy, and the release of the pro-apoptotic protein cytochrome *c* into the cytosol was observed by the spreading of the dyed molecules throughout the whole cell body and through the observation of large intracellular vacuoles, characteristic of apoptotic cells. This work demonstrated that pore enlarged MSN can be efficiently employed to deliver membrane impermeable proteins into living cells.

Since silica particles have been long known to be cytotoxic to red blood cells, the possibility of using MSN for *in vivo* delivery applications was in question. In this work it was demonstrated that as opposed to non-porous silica, and because of their unique structure, MSN are not able to expose a continuous surface for disruptive interaction with the

membrane of red blood cells. The work demonstrated that only upon functionalizing MSN with the highly negative benzenesulfonate groups, did they acquire hemolytic properties.

This dissertation represents a significant contribution to establish the chemical and structural characteristics that are prerequisites for the application of MSN as safe intracellular delivery agents, and thus opens the doors for the future *in vivo* studies of the material. Further work is required to understand the mechanism of endosomal escape by the material, as well as its long term fate. Future developments of the material are expected which may include the achievement of cell type selectivity both in terms of uptake and release, and the use of the material for interfering with intracellular processes through the sequestration of bioactive molecules.